CAVITATION IN HYDRAULIC MACHINERY : ITS INFLUENCE ON THE DESIGN OF IMPELLERS FOR CENTRIFUGAL AND AXIAL-FLOW PUMPS.

by

William Powell Lewis,
B. Mech. E., A.M.I.E. Aust.

Thesis presented for the degree

of

Master of Engineering.

C O N T E N T S

N O T A T I O N

Symbol		First Used in Equation
a	acoustic velocity	(3.6)
a	area	(3.8)
A	area	(5.20)
A	a constant	(3.20)
b	width of impeller passage at blade inlet	(4.9)
B	a constant	(3.20)
c	chord length of impeller blade	
c_D	drag coefficient	
c_L	lift coefficient	
c_P	pressure coefficient	(2.8)
c_H	heat transfer coefficient	(3.11)
c_Q	volume entrainment coefficient	(3.11)
c_l	specific heat of liquid	(3.8)
C	a constant	(2.2)
d	diameter of cavitation bubble	(2.4)
d	average diameter of impeller passage at blade inlet	(4.9)
D	diameter of runner (pump or turbine)	(3.21)
D	diameter of impeller eye (pump)	(4.9)
D_h	diameter of impeller hub	(4.9)
f_1	velocity ratio, v_m / v_a	(4.10)
f_2	velocity ratio, v_m' / v_a	(4.36)
Fr	Froude number	(3.5)
g	acceleration due to gravity	
h	height of surface roughness	(3.7)
h	height of cavity wake	(5.1)
h	static head	(2.4)
h_1	static head at impeller entry	(5.11)
h_a	atmospheric pressure	
h_s	suction pressure	
H	total head of pump or turbine	(3.1)

Symbol		First Used in Equation
H_{sv}	net positive suction head of pump or turbine	(3.1)
k	thermal conductivity	
k_a k_m	cavitation coefficients	(Appendix
K	cavitation number	(2.8)
K_o	coefficient	(4.13)
K_{1a}	coefficient (used with ϕ_a)	(4.14)
K_{1m}	coefficient (used with ϕ_m)	(4.14)
K_a	impeller cavitation coefficient (based on v_a)	(4.8),
K_m	impeller cavitation coefficient (based on v_m)	(4.8)
K_m'	impeller cavitation coefficient (based on v_m')	(4.34)
K_u	impeller cavitation coefficient (based on u)	(4.8)
l	length of cavity	(5.19)
L	typical length	(3.4)
M	Mach number	(3.6)
M	Factor in equations (4.38) and (4.39)	(4.38)
n	exponent	(3.10)
n	number of nuclei	(3.16)
N	number of nuclei per unit volume	(3.16)
N	rotational speed	(4.6)
N_s	specific speed	(4.12)
p	pitch of helical inducer	
p	static pressure	(2.6)
P	power	
P	ratio of suction specific speeds	(4.32)
Pe	Peclet number	(3.9)
Pr	Prandtl number	
Q	capacity, rate of flow	(4.6)
Q_o	capacity at maximum efficiency	
Q_1	unit capacity	(3.20)
r	radius of cavitation bubble	(2.1)
r	radius at impeller eye	(4.25)
r_{LE}	radius of curvature of leading edge of inducer	
r_s	radius of front shroud at impeller eye	
R	radius	(2.9)

Symbol		First Used in Equation
R	factor in equation (4.35)	(4.35)
R	ratio of relative velocities entering and leaving cascade	(5.6)
Re	Reynolds number	(3.4)
s	blade spacing in cascade	(5.1)
S	suction specific speed	(4.7)
S'	adjusted suction specific speed	(4.7)
t	thickness of impeller blade	(4.9)
t	time	(2.10)
T	temperature	(3.8)
u	peripheral velocity at impeller eye	(4.9)
u_p	peripheral component of the absolute velocity of the liquid entering the impeller	(4.1)
V	typical velocity	(2.6)
v	specific volume	(3.8)
v	absolute velocity of liquid entering impeller	
v_a	axial velocity of liquid at impeller eye	(4.9)
v_m	meridional velocity of liquid at blade inlet	(4.9)
v_m'	meridional velocity of liquid at blade inlet, ignoring effect of blade thickness	(4.34)
v_w	whirl component of velocity	(5.31)
w	relative velocity	
w_1	relative velocity of flow entering cascade	(5.1)
w_2	relative velocity of flow leaving cascade	(5.1)
W	Weber number	(3.14)
X	correction factor	(5.20)
z	complex variable	(5.17)
z	number of impeller blades	(4.9)
z	vertical elevation	
α	angle of incidence	(5.1)
α	air content of liquid	(3.19)
α_s	air content of liquid when saturated	(3.19)
β	blade angle at entry to impeller	(4.1)
β	blade angle of cascade	(5.1)
γ	specific weight	(2.4)

Symbol		First Used in Equation
δ	surface tension	(2.1)
δ	angle of stagger of cascade	(5.17)
Δ	size of cavitation nucleus	(3.15)
ϵ	velocity ratio, u_p/u	(4.21)
ζ	hodograph variable	(5.17)
η	efficiency	
θ	camber angle of hydrofoil	
Θ	angle of flow leaving cascade	(5.7)
Θ	$\phi\left(\frac{\sin\beta}{1+\cos\beta}\right)$, parameter	(5.28)
λ	latent heat of vapourization	(3.8)
λ	velocity ratio, u_{p_o}/v_{a_o}	(4.26)
μ	viscosity	(3.4)
ν	kinematic viscosity	(3.21)
ξ	hub-tip ratio at impeller eye D_h/D	(4.7)
ρ	density	(2.6)
σ	Thoma cavitation parameter	(3.1)
ϕ	inlet flow coefficient	
ϕ_a	inlet flow coefficient (based on v_a)	(4.8)
ϕ_m	inlet flow coefficient (based on v_m)	(4.8)
ϕ_m'	inlet flow coefficient (based on v_m')	(4.35)

Suffixes:

ave	average value	(4.9)
bd.	condition at cavitation breakdown	
g	gas	(2.1)
i	condition at cavitation inception	(2.7)
l	liquid	(3.8)
max	maximum value	(4.19)
min	minimum value	(2.8)
opt	optimum value	(4.18)
v	vapour	(2.1)

Notes:

Where quantities refer to conditions at impeller inlet it is understood that they apply to the blade tips unless otherwise stated. In equations (4.26) and (4.27) the suffix "o" is used to distinguish conditions at the

outer radius of the impeller eye.

Where equations are derived in a general form it is assumed that a consistent set of units is used throughout. The units used in any detailed calculations in the thesis are stated in the text.

P R E F A C E

This thesis considers aspects of rotating hydraulic machinery of the centrifugal, mixed-flow, and axial-flow types; wherever the word "pump" is used without any qualifying adjective it is understood that it is a generic term which includes all these types. The objective is to present and discuss the methods available for the design of pump impellers for cavitating or near-cavitating conditions.

In order to give an orderly and logical account of this subject the thesis opens with a description of cavitation in hydrodynamics, and this is followed by an examination of its mechanism and of the physical factors which affect it. Model experiments are an important tool in assisting the designer predict performance and one chapter is therefore devoted to a discussion of model laws and scale effects in cavitation. Chapters 4 and 5 deal with the detailed design of impellers for non-cavitating and cavitating flows, while the final ohapter evaluates this work and draws some general conclusions.

CHAPTER 1.

INTRODUCTION - CAVITATION IN HYDRODYNAMICS

1.1 DEFINITION

In most engineering applications cavitation consists of the formation of the vapour phase of a liquid when it is subject to reduced pressure at constant ambient temperature. In general a liquid is said to cavitate when vapour bubbles are observed to form and grow as a consequence of pressure reduction. In hydraulic machinery the phase transition is a result of pressure changes brought about by hydrodynamic means, that is pressure changes within the moving liquid caused by changes in the velocity of flow.

In a cavitating flow there is a continuous process of formation and collapse of cavities within the liquid stream. There are three stages in this process :-

(1) Inception
(2) Growth
(3) Collapse

and each of these will be studied.

1.2 FIELDS OF INTEREST

Cavitation has long been of interest and importance in the fields of hydraulic structures, hydraulic machinery, shipbuilding, underwater signalling, and underwater weapons. In recent years cavitation has become of increasing interest in other applications. These include : lubrication of journal bearings, chemical processing (acceleration of reactions, industrial cleaning), medicine (bullet wounds, speculations on brain concussion under blows), nuclear physics (use of bubble chambers for research on high energy particles), and the handling of highly volatile liquid rocket fuels and cryogenic liquids.

1.3 EFFECTS OF CAVITATION

1.3.1 General

The effects of cavitation are predominantly undesirable and often destructive. In a few applications its characteristics are deliberately employed for a constructive purpose; for example, as a means of limiting the capacity of special centrifugal pumps, in particular of condensate extraction pumps in power stations. These pumps are sited as near to the condenser as possible and are often allowed to operate under cavitating conditions, the static head at pump inlet being reduced to a low value in order to minimise the cost of foundations.

Another example of the constructive use of cavitation is the design of "super-cavitating" propellers which seek to exploit the promise of high efficiency super-cavitating flows about lifting surfaces.

The bad effects of cavitation are numerous, so numerous in fact that a catalogue of them would be practically endless. In general they may be grouped under four headings : (1) Material Damage, (2) Performance, (3) Vibration, (4) Noise.

1.3.2 Cavitation Damage

Cavitation damage is so common and so serious that by many people it is thought of as the phenomenon itself rather than as an effect of which cavitation is the cause.

Hydraulic structures: a flood passing over a spillway or through the outlet works of a dam may leave in its wake cavitation damage costing thousands of pounds to repair. Concrete surfaces, needle valves, spillway gates and seats have all been badly damaged as a result of cavitation. Hydraulic machinery: damage to hydraulic turbines may occur in the low pressure regions at the discharge end of the runner passages and in the draft tube, but may also be found in the relief valve and associated energy dissipation devices. In centrifugal and axial flow pumps cavitation damage can take the form of erosion of the impeller blades near inlet and also of the inlet portions of the volute tongue or diffuser vanes. Fig. (1.1) and (1.2) show typical examples of damaged runners.

With large pump or turbine installations the plant designer is constantly urged to keep the initial cost as low as possible. That tends to keep the margin of safety against cavitation to a minimum. The present knowledge of the factors controlling cavitation is still incomplete, and that has led on occasion to the designed margin of safety being found insufficient when the plant is put into operation.

Marine propellers are another type of hydraulic machine in which cavitation damage is commonly encountered, particularly in high-speed ships. Another example which has received a lot of investigation recently is the damage to liners of diesel engines.

1.3.3 Performance

The effect of cavitation on the performance characteristics of hydraulic equipment is of great importance. Broadly speaking it can be said that hydraulic equipment consists of combinations of surfaces or passages which guide and constrain liquids to flow in specified directions at desired speeds. One effect of cavitation on such a surface or passage is to alter the effective size of the passage and the direction of the guidance. The flow no longer conforms to the designer's intentions, and is, in general, degraded: the changes in direction are less than those specified and the resistance to flow is increased. In centrifugal pumps these effects generally result in loss of head and often a simultaneous increase in power consumption; in hydraulic turbines the power output is lowered. In both cases the efficiency is reduced. It is of interest to note that at one stage of the development of a modern fighter aircraft its ceiling was limited

not by aerodynamic considerations but by the onset of cavitation in its fuel pumps.

On ships' propellers cavitation causes a reduction of thrust and efficiency and hence of the speed of the ship. Cavitation on fins and rudders of surface craft causes loss of control and decrease in stabilising effect.

1.3.4 Vibration

The production of vibration in all types of hydraulic equipment is another effect resulting from cavitation. The cavitation process is an unsteady one and usually is associated with relatively large hydrodynamic forces. This produces vibration of the equipment in which the cavitation is occurring. The amplitude of vibration may vary from very small values to values large enough to cause major damage or even destruction.

It is pertinent to interpolate here that pump vibrations are sometimes falsely attributed to cavitation when in fact they result from the presence of air in the liquid passing through the impeller. Air entraining vortices can form in the liquid from which the pump is drawing its supply if this liquid has a free surface whose level is too low in relation to the impeller. These vortices can be long thin filaments persisting for some distance into the liquid. If they are long enough to extend to the impeller itself the rotating blades experience varying forces as they impinge on the mixture of air and liquid, and hence vibrations are set up. To prevent this happening care must be taken in the design of the installation and in important cases model experiments should be carried out.

1.3.5 Noise.

The cavitation process is essentially noisy. The importance of this noise varies tremendously with the use of the equipment. A given amount of cavitation noise in hydraulic turbines in a large power house may be hardly detectable, whereas the same amount of noise produced by a cavitating propeller on a submarine may destroy completely the usefulness of the vessel.

1.4 DETERMINATION OF INCEPTION OF CAVITATION

The various effects produced by cavitation have been used to determine its inception. In experiments with hydraulic machinery the following methods have been used.

(1) Visual - viewing through a window in the apparatus to determine either when the vapour bubbles appear as the system pressure is lowered, or when they disappear as the pressure is increased from a value sufficiently low to have already caused cavitation. This method supplemented with special high-speed photographic equipment is commonly used in research work.

(2) Acoustic - using either the human ear or hydrophones to detect the onset of cavitation. It is widely believed that this is the most accurate method as in the first phase of cavitation the bubble size is very small, and may escape detection by visible means.

(3) Vibrational - detecting cavitation by attaching a pick-up to the item being tested to measure its amplitude of vibration.

(4) Performance - In the field of centrifugal and axial-flow pumps it is common practice to define the point of cavitation inception as that condition when the head (H) generated by the pump first departs by a measurable amount from its value under non-cavitating conditions. This definition will be used later in the detailed discussion of pumping equipment. Careful experiment has shown that cavitation starts before any reduction in performance is observed, and that in this initial phase the amount occurring is so small that there are no deleterious effects either on performance or due to damage or vibration.

After this brief survey of cavitation and its effects it is now proposed to look at some fundamental considerations before moving on to an account of its influence on the design of hydraulic machinery.

CHAPTER 2.

NECHANICS OF CAVITATION

2.1 GENERAL

In this chapter the inception of cavitation is examined and the process of bubble growth and collapse discussed. This leads to a study of cavitation damage and means of protection against it.

Fundamental investigations into cavitation phenomena are difficult and costly, because the cavities themselves are very small and because their formation, growth and collapse takes place at high frequencies. Knowledge of the subject is therefore incomplete; the account which follows is intended to provide an appreciation of the salient features of cavitation and to outline current theories concerning its nature.

2.2 INCEPTION OF CAVITATION

2.2.1 Role of Nuclei

The formation of a cavity within a liquid obviously involves a rupture of the liquid. Intuitively it might appear that a liquid has no rupture strength whereas in fact many specially constructed experiments have shown conclusively that liquids such as water can withstand tensions even if only for short periods. Measurements made under static conditions when a steady tension is applied to undisturbed water have given a wide range of values for its tensile strength, from several atmospheres to estimates as high as a thousand atmospheres. Measurements made by the centrifuge method in which a steady tension is created at the centre of a rotating column of water have yielded tensile strengths up to three hundred atmospheres, Briggs (1). Moreover, the Kinetic theory of liquids predicts high tensile strengths.

It is common experience that ordinary liquids usually cavitate whenever the local pressure reaches the vapour pressure. Since this is the condition when there is no longer an external force to hold the liquid together, it appears that these liquids have no effective tensile strength. To explain this great discrepancy it has been postulated that ordinary liquids always contain impurities or "nuclei" which are weak spots that rupture or tear at vanishingly small tensions thus producing cavities.

These impurities are not dissolved in the liquid since the theory of solutions indicates that a dissolved impurity should have very little effect on the tensile strength of the base liquid. This class of impurity is thus eliminated from consideration, leaving undissolved solids, immiscible liquids and free gas as the possible sources of weak spots in ordinary liquids. Immiscible liquids can be eliminated because they are not universally present in common liquids and because experiments have demonstrated that the interface between immiscible liquids is not weak enough to explain the observed lack of effective tensile strength

of normal liquids. With regard to undissolved solids there is ample evidence to show that with a high degree of wetting of the solid matter by the liquid the adhesive force across the interface is very high and even for a low degree of wetting it is probably higher than the effective tensile strengths observed in normal liquids. This reasoning reduces the range of impurities responsible for the weak spots in liquids to undissolved gases, and unwetted, that is, hydrophobic solids.

It is now generally accepted that the inception of cavitation in ordinary liquids is associated with the growth of nuclei (submicroscopic in size) containing vapour, undissolved gas or both, which are present either within the liquid or in crevices on suspended solid particles or on bounding walls.

The wide discrepancies in the measurements of the tensile strength of water are attributed to variations in the nuclei content of the specimens; these measurements may also have been affected by the interfacial properties of the liquid container system, the treatment of the liquid before testing, and the experimental methods used. In most cases of practical interest in hydrodynamics (e.g. ship propulsion, hydraulic machinery) inception of cavitation occurs at pressures of the order of the vapour pressure, and is associated with the growth of nuclei with diameters ranging from 10^{-5} to 10^{-3}cm.

The smaller the size of these nuclei and the fewer they are in number, the higher will be the fracture strength of the liquid. Thus it has been demonstrated by Harvey et al. (2), Knapp (3) and others that ordinary water saturated with air when "denucleated" by the prior application of large pressure exhibits fracture strengths of the order of hundreds of atmospheres, in line with the Kinetic theory predictions. (This theory incidentally postulates the existence of very small nuclei of the order of molecular dimensions which are assumed to form statistically as a result of thermal fluctuations in the interior of the liquid. After the application of pressure these ultra-small nuclei will remain although larger ones will be forced into solution). The existence of nuclei of the sizes required for inception near the vapour pressure (i.e. about 10^{-3}cm has also been demonstrated experimentally by techniques based on the absorption of ultrasonic vibrations by nuclei bubbles in resonance with the applied frequencies, Strasberg (4), Richardson (5). Work is proceeding in an endeavour to develop these techniques to the point where they can be used to give information on the number of nuclei of different sizes in a liquid specimen.

It has been suggested that some of the scatter in cavitation measurements may be due to the action of cosmic rays, as it is known that the passage of highly energized cosmic rays through a superheated liquid can give rise to the formation of bubbles of vapour within the liquid. If this suggestion is correct, the longer a liquid is exposed to high energy radiation the more nuclei it should contain, its tensile strength should be lower and its susceptibility to cavitation increased. However, no such

time-dependent effects have been observed, and this implies that cavity formation in liquids cannot be explained by nucleation resulting from cosmic or other high-energy radiation.

2.2.2 Stability and Growth of Nuclei.

In water and other liquids the nuclei present will consist of small, undissolved bubbles of air and/or vapour; it is usually postulated that the nuclei consist of air or other non-condensable gas and may contain some vapour due to evaporation of the liquid from the walls of the bubbles. Now diffusion theory clearly shows that such nuclei cannot persist but should dissolve spontaneously in the water. To resolve this dilemma, an explanation must be found for the failure of the nuclei to dissolve even if the water is undersaturated. The most common suggestion to account for the presence of nuclei in undersaturated liquids is that microscopic dust particles are present on which the nuclei are stabilised, possibly by being trapped in cracks on their surfaces. Another suggestion is that solution does not occur because the bubbles are surrounded by a thin protective skin formed from organic impurities existing in the water. Since the growth behaviour of nuclei stabilized in crevices and stabilized by organic skins would be functionally the same, Strasberg (4), it is difficult to differentiate experimentally between these postulates. While the former is more widely accepted, it is not known which, if either, is correct.

During cavitation each nucleus starts to grow and this growth can take place in two ways : (1) by diffusion of dissolved air out of the water into the bubble; (2) by sudden expansion of the bubble into a large cavity.

The first process has been called "gaseous" cavitation because it results in a cavity filled primarily with air. Theory and experiments with liquid-gas systems combine to show that diffusion takes place slowly. In hydraulic machines the liquid is flowing relatively fast, so fast that there is insufficient time for any nuclei present in the moving stream to grow appreciably by this means. However, diffusion may well be important for the growth of nuclei trapped in crevices on the walls of the liquid boundary.

The second process has been called "vapourous" cavitation because the cavity grows so rapidly that the diffusion of air into it cannot be maintained, and the cavity is filled primarily with water vapour.

The two processes may take place consecutively - gradual growth of small nuclei by diffusion (especially if they are trapped on the boundary walls so that there is time for this to happen) until they reach a critical size above which they become dynamically unstable, then rapid expansion as the nuclei grow explosively by evaporation from their internal surfaces.

Gaseous cavitation may be important in some applications but in

hydraulic machinery vapourous cavitation is almost certainly the more critical. Gaseous cavitation can occur at liquid pressure greater than the vapour pressure so that its inception may be observed before that of the vapourous form, as for instance in the case of Vuskovic (6).

In the light of this discussion it is now in order to make some calculations concerning the stability of nuclei and to review the relation between mechanical stability and bubble size. For simplicity and to make the problem amenable to calculation a spherical bubble is considered and dynamic and heat transfer effects ignored. The equation for static mechanical equilibrium is

$$P_g + P_v - P = 2\frac{\delta}{r} \qquad (2.1)$$

where P_g = partial pressure of gas in bubble
P_v = liquid vapour pressure
P = surrounding local liquid pressure
δ = surface tension
r = bubble radius.

If the bubble contains a constant amount of gas (assumed perfect) at constant temperature

$$P_g = \frac{C}{r^3}$$

where C is a constant. Then

$$p - P_v = \frac{C}{r^3} - 2\frac{\delta}{r} \qquad (2.2)$$

If the L.H.S. is differentiated with respect to r and equated to zero, the minimum value of $(p - pv)$ for static equilibrium is obtained. This is designated $(p - pv)^*$ and occurs when

$$\frac{d\,(p - pv)}{dr} = -\frac{3C}{r^4} + \frac{2\delta}{r^2} = 0$$

i.e. when $r = r^* = \sqrt{\frac{3C}{2\delta}}$

$$\text{or} \quad r^* = -\frac{4\delta}{(p - pv)^*} \qquad (2.3)$$

In this equation the minus sign indicates that the critical liquid pressure is actually below the vapour pressure. If now from the condition $r = r^*$ at $(p - pv) = (p - pv)^*$, P is decreased slightly the bubble is unstable and tends to grow without bound. At pressure greater than the critical pressure, the bubble is stable and assumes an equilibrium radius satisfying equation (2.1).

At 68°F the surface tension of water is 5.00×10^{-3} lb./ft (72.8 dyne /cm) and the relation between pressure and initial diameter is then

$$(h - hv)^* \times d^* = 2.58 \times 10^{-3} \qquad (2.4)$$

where $(h - hv)^* = \frac{(p - pv)^*}{\gamma}$, ft. of water,

and d^* = bubble diameter, in.

This is shown in fig. (2.1).

It can be seen from fig. (2.1) that to initiate cavitation, tensions much higher than those encountered in most practical cases are necessary unless bubbles of microscopic size are present. This relation can be used to estimate the critical nucleus size corresponding to experimentally determined thresholds of vapourous cavitation.

More elaborate investigations have been made into the influence of time dependent factors on bubble growth, for example by Noltingk and Neppiras (7) who derived the differential equation for the growth of a spherical air bubble subject to a fluctuating pressure $p(t)$.

$$\rho\left(r\ddot{r} + \frac{3}{2}\dot{r}^2\right) - \left(p_o - p_v + \frac{2\delta}{r_o}\right)\left(\frac{r_o}{r}\right)^3 + \frac{2\delta}{r} = p_v - p(t) \qquad (2.5)$$

Here r_o is the original radius of the bubble at an external pressure p_o. This equation was solved for $p(t)$ as one cycle of a negative sine function, giving results which agreed quite well with those from the quasi-static equation, (2.3).

2.2.3 Engineering Significance of Nuclei.

It is clear that inception of cavitation is closely associated with the number, size and distribution of the nuclei in the liquid, and that carefully controlled experiments both in the laboratory and in the field should include a description of the nuclei content, i.e. a "spectrum" showing their variation in size and the number of nuclei in each size range. The wide scatter of many experimental results indicates the lack of knowledge of this spectrum. Techniques are slowly being developed for carrying out this type of measurement, in particular for distinguishing between dissolved and undissolved gas contents.

Consideration of the role of nuclei in cavitation raises questions of significance to the mechanical engineer, although many answers are not known at present. The following are a few examples :

(1) For the same relative velocities in cavitation areas, are low-head turbines more susceptible to cavitation than high-head turbines, both as regards its effect on performance and degree of damage? The penstock of a high-head turbine should be an effective means of pressurization, and thus of forcing larger nuclei into solution.

(2) For machines handling cold water at comparable velocities, are centrifugal pumps more susceptible to cavitation troubles than high-head turbines? The viewpoint here is the same as in the first question. Natural waters are exposed to a continuous rain of dust particles which serve as hosts for gas nuclei. The maximum pressurization of the water before it enters the pump impeller eye is measured by the submergence of the inlet pipe, which is very small compared to that in the penstock of a high-head turbine.

(3) Stepanoff has pointed out that a high-pressure boiler feed pump handling hot water is less susceptible to the effects of cavitation than is the same pump handling cold water under otherwise identical conditions.

He explained this by the difference in the thermodynamic properties of the liquids. However, modern boilers operate on a closed cycle with deaerated distilled water, which is highly pressurised each time it passes through the boiler. Therefore might not this improved pump performance be explained by a scarcity of nuclei?

(4) There is a general impression in the petroleum industry that there is much less trouble from cavitation in hydraulic equipment than in comparable installations using water. Is it not possible that a major reason for the difference is the higher wetting ability of most petroleum derivatives, since this would tend to decrease greatly the concentration of effective nuclei?

Effect of Gas Content.

Consider now the effect of gas content on the inception of cavitation in hydraulic machines. Only a few experiments have been reported; these dealt with cases of practical interest and studied the effect of varying air content on turbines and pumps handling cold water. Vuskovic (6) and Shmuglyakov (8) carried out tests on Kaplan turbines and Kanellopoulos (9) on a small centrifugal pump.

The results of the turbine experiments showed that increasing the air content increased the susceptibility of the machine to cavitation, that is inception took place at higher pressure at the suction or exit side of the runner. While this effect was marked at low heads (less than 15 ft.) it became less as the turbine head was raised and according to Vuskovic was negligible at heads over 30 ft. Kanellopoulos' work showed also that his pump which had a low specific speed radial impeller became more susceptible to cavitation at higher air contents, that is higher inlet pressures were required to suppress cavitation other conditions remaining the same.

The paucity and restricted nature of the results available hardly allow any general conclusions to be drawn. It is reasonable to suppose, however, that there is a correlation between the air content and the nuclei content in the water. Therefore a hydraulic machine would be expected to be more susceptible to cavitation as the gas content in the liquid passing through it is raised. This has been found to be the case in many experiments on hydrofoils and submerged streamlined bodies in water tunnels; see for example Numachi (10) Crump (11) Williams and McNulty (12) Ripken (13) and Holl (14); a few workers have found no effects from changes in air content, Kermeen et al. (15), Hammitt (16). In the field of marine propeller research Edstrand (17) determined air content to have a marked effect on cavitation inception, and he gave corrections which have to be applied to results of water tunnel experiments where air contents are low to correlate with performance in the sea where the air content is naturally high.

Hysteresis.

For his pump experiments Kanellopoulos used a closed circuit arrange-

ment in which the water was continually recirculated. He found there was a definite "hysteresis" in that the critical pressure at impeller inlet for onset of cavitation was lower when approached from the non-cavitating state ("inception") than when approached from developed cavitation ("cessation"). In America these two conditions are often distinguished as "incipient" and "desinant" cavitation respectively. Kanellopoulos found that the difference between cessation and inception pressures decreased as the gas content was increased, also that the inception conditions for low gas contents were unstable with a fairly wide scatter of results, whereas the cessation conditions were repeatable within narrow limits.

Similar results have been noted in many laboratory water tunnel experiments, Kermeen et al. (15), Holl (14). In a few cases these effects have not been found even when specifically looked for, Straub et al.(18), Hammitt (16). The occurrence of hysteresis may depend on experimental factors such as the velocity of test and the nature of the test rig, whether an open or closed circuit is used and whether a resorber is provided.

Several hypotheses have been advanced to account for hysteresis. It may be explained by considering the conditions of the gas nuclei content of the water. For low gas content the equilibrium size of gas nuclei is small and thus, when approaching cavitation from the non-cavitating state, low critical pressure should be expected. Conversely when critical conditions are approached from a developed state of cavitation, gas bubbles of comparatively large size, remaining after the collapse of the cavitation cavities and travelling with the stream may, on entering the region of minimum pressure, cause continuing cavitation of gradually decreasing intensity. Thus the cessation pressure would be expected to be higher than the corresponding inception pressure. The fact that the inception conditions are unstable may be explained by the trapping of small gas bubbles in wall crevices in the test circuit which, under some external disturbance or vibration, may part from the walls and enter the stream to start cavitation.

The Author's experience based on an extensive number of pump cavitation tests is that while hysteresis can occur it is usually only slightly greater in amount than the limits of accuracy of the test equipment. It is in fact common practice to define the onset of cavitation in a pump at the "inception" point when proceeding from non-cavitating to cavitating flow. This may mean a loss in accuracy but is justified on the ground that once cavitation has occurred, conditions within the liquid have altered : for example, one boundary of the non-cavitating flow has been displaced by an amount equal to the width of the cavitating zone. Nevertheless many research workers use the cessation point to define the beginning of cavitation in order to obtain more consistent experimental results.

Design.

The majority of turbines and pumps have to operate with cold aerated water from oceans, lakes, rivers and reservoirs, and runner design for

cavitation performance is based on the premise that cavitation begins when the minimum pressure in the runner falls to the vapour pressure. As ordinary water from these sources can be expected to contain large numbers of nuclei this procedure is correct, but for special liquids with small nuclei content it may well be conservative.

2.2.4 Boundary Layer and Turbulence Effects.

In pumps and turbines cavitation takes place in regions of low pressure and/or high velocity close to the walls of the flow boundary. This flow is almost always turbulent. It is therefore necessary to consider the effects of factors involving turbulence and boundary layer formation on the inception of cavitation. Most of the available evidence is contained in papers by Daily and Johnson (19), Kermeen et al. (15), and Holl (20).

With regard to turbulence it is clear that when attempting to predict inception account should be taken not only of the average pressure condition but also of the magnitude and duration of pressure fluctuations in regions of turbulence.

Various boundary layer effects may be important in the inception process. Firstly, the pressure gradient in the direction of flow : if this is adverse it will promote separation of the flow from the solid surface with the associated low pressures at the centres of the vortices in the separated flow. Secondly, the pressure gradient across the boundary layer : if this is large it will help to sweep away any nuclei trapped in the wall. Thirdly, the type of flow in the boundary layer : turbulence has a significant effect on the local pressure reductions.

It has been shown that in laminar boundary layers cavitation occurs first at the wall. In turbulent boundary layers it might be expected that cavitation would commence in the regions of highest turbulence intensity, at a small distance from the boundary wall where the pressure fluctuations are largest. However, in experiments with turbulent boundary layers in a rectangular nozzle Daily and Johnson (19) observed that the maximum number of cavities occurred in the central portion of the boundary layer rather than closer to the boundary as would have been expected on the basis of experimental observations of intensity of velocity fluctuation.

From this summary of the existing evidence it will be seen that there is little data available in a form useful to the designer of hydraulic machinery. The "state of the art" is such that he can only ignore the boundary layer effects discussed here on the implicit assumption that the size of any cavitation bubbles which form in his equipment are large compared to the thickness of the boundary layer. This assumption is probably true for water from oceans and rivers and should lead to safe designs for other liquids.

2.2.5 Quantitative Definition of Cavitation Inception. Critical Cavitation Number (K_i).

In the discussion of all types of cavitation problems, experimental results, and performance of equipment, some system for describing quantitatively the dynamic conditions under which cavitation is taking place is necessary.

In the ideal case of potential flow of a pure liquid around a submerged body the minimum pressure that will occur on the surface of the body can be predicted for any given configuration and will be described for all scales and velocities by a certain value of the ratio

$$\frac{p - p_{min}}{\frac{1}{2}\rho V^2} = -c_{p\,min}$$

where p = reference pressure in undisturbed liquid.
p_{min} = minimum pressure on surface of body.
V = relative velocity between the body and the liquid, normally measured where the liquid is undisturbed.
ρ = density of liquid.
$c_{p\,min}$ = minimum pressure coefficient.

As explained earlier, in most engineering applications the ability of the liquid to support a tension is ignored and it is assumed that cavitation is incipient when the minimum pressure becomes equal to the vapour pressure. The cavitation number, characteristic of the flow, is defined by

$$K = \frac{p - p_v}{\frac{1}{2}\rho V^2} \qquad (2.6)$$

and the critical conditions for onset of cavitation are

$p = p_i$, the pressure at inception.
$p_{min} = p_v$, the vapour pressure corresponding to the liquid temperature.

The critical cavitation number is then

$$K = K_i = \frac{p_i - p_v}{\frac{1}{2}\rho V^2} \qquad (2.7)$$

Thus in the design of streamlined bodies in unseparated flows, inception of cavitation is assumed to occur when

$$K_i = |c_{pmin}| \qquad (2.8)$$

For two-dimensional flow around a streamlined body the minimum pressure coefficient, $c_{p\,min}$, can be found from tests in wind or water tunnels, or in many cases can be determined from computations of the potential flow. When the system is three-dimensional results are much more difficult to obtain except in the relatively simple case of axially symmetrical bodies. It is interesting to note that water tunnel tests of aerofoil sections give results similar to those obtained in wind tunnels for lift, drag and moment coefficients, and pressure distribution, Daily (21).

The physical significance of the cavitation number K is clear. The numerator is the net pressure acting to collapse a cavity, while the denominator is the velocity pressure or velocity head of the flow. Now the variations in pressure which take place on the surface of the body or on any type of guide passage are due basically to changes in the velocity of flow. Thus the velocity head may be considered as a measure of the pressure reductions that may occur to cause a cavity to form or expand. From this point of view the cavitation number is simply the ratio of the pressure available for collapsing cavities to the pressure available for inducing their formation and growth.

When estimating value of Ki applicable to a specific design the following factors have to be kept in mind.

(1) Turbulence.

There may be corrections to the local pressures due to turbulent pressure fluctuations and similar indeterminate effects.

(2) Separation.

When predicting inception of cavitation, attached flows around streamlined bodies should be distinguished from separated flows from bluff bodies. In the latter case the minimum pressure does not occur on the surface of the body but in the cores of the vortices in its wake, and cavitation has been observed to commence in these vortex cores. The incipient cavitation number Ki cannot then be correlated with Cp min and is in fact always greater in magnitude.

Apart from special exceptions such as supercavitating pumps and propellers the design of hydraulic machinery is based on attached flows around streamlined bodies in streamlined passages of smooth profile. Separated flows are not considered although they may occur at off-design conditions or if the initial design is incorrect.

(3) Surface Roughness.

Cavitation about smooth wavy surface roughnesses is analogous to cavitation in unseparated flows, the incipient cavitation number may be determined by taking the minimum pressure coefficient and using the boundary layer velocity corresponding to the height of the roughness. Sharp-edged roughnesses produce cavitation in the separation zone just behind the roughnesses, Holl (20), Shalnev (22). As a result Ki is increased above its value for a smooth surface of the same base profile. Very few laboratory or field experiments have reported the surface roughness of the equipment tested. In most laboratory tests surface finish is smooth in order to eliminate the secondary effects discussed here and this should be clearly understood when applying the results of such tests.

(4) Air or Gas Content.

As mentioned earlier, a few research workers have found that Ki is not affected by change in the air content of the water used in their tests. This is contrary to the majority of reports which show that Ki depends on the air content and increases with it. One explan-

ation advanced for this is based on the hypothesis that inception of cavitation depends on the supply of nuclei from crevices in the flow boundaries. These nuclei may grow by a process of gaseous diffusion into bubbles of macroscopic size which are then swept off and travel along the boundary surface to the region of minimum pressure. The larger the bubbles on reaching this region the greater is the likelihood of cavitation occurring. This will in turn depend on the flow velocity the longitudinal pressure gradient and the size of the body. This process of reasoning leads to the conclusion that small submerged streamlined bodies with sharp pressure gradients tested at high velociti should show little or no variation of Ki with gas content, since these conditions would not favour the growth of nuclei into cavitation bubbles by the mechanism postulated. There is some experimental evidence to support the view that Ki can depend on gas content in cases where gaseou diffusion plays a significant part in the early stages of the inception process, but this question has not been finally resolved.

With regard to hydraulic machinery the investigation made by Vuskovic (6) is illuminating. He found that the onset of gaseous cavitation (i.e. separation of clouds of air bubbles out of the flow) was influenced to a marked degree by air content, and that this form of cavitation was more likely to occur as the air content was increased. However, changes in air content had only a very slight influence on the onset of vapourous cavitation. Vuskovic also noted that gaseous cavitation itself did not lead to any noticeable reduction in turbine efficiency nor to destruction of material. Although it is theoreticall possible for gaseous cavitation to take place at liquid pressure above the vapour pressure, he suggested that its influence could be disregarde in practice.

2.3 BUBBLE DYNAMICS

2.3.1 Description of Bubble Growth and Collapse.

So far, discussion has been centred on inception of cavitation, its mechanism and the factors affecting it. It is now proposed to consider the behaviour of bubbles formed in a liquid as a result of cavitation. In a purely cavitating flow there are myriads of tiny bubbles, which grow and collpase at very fast rates with lives of the order of milliseconds or less. Experimental observation of the growth and collapse of these bubbles makes frequent use of high-speed photography, pictures being taken at rates as high as one million frames per second in some cases.

A typical investigation will now be described, Knapp (23), and the results discussed in the light of current theories of bubble dynamics. These experiments were carried out on a streamlined smooth body of revolution in a water tunnel fitted with resorber. Conditions were such that the bubbles examined originated from comparatively large nuclei so that they were large compared to the boundary layer thickness, and their history may be regarded as typical of bubbles in an essentially irrotational flow.

The test body was a cylinder with a pointed nose, the radius of curvature of the nose being 1.5 times the diameter of the cylinder (1.5 calibre ogive). The water tunnel was operated at 40 ft./sec. and the absolute pressure in the undisturbed flow was about 4.0 p.s.i.a., equivalent to K = 0.33. Under these conditions cavitation was taking place on the nose of the body and high-speed photography was used to examine the life history of a typical cavity - its formation after first appearing as a smooth transparent bubble, its growth and subsequent collapse.

Refer now to fig. (2.2). At the top is shown the half profile of the test body. The graph below it, drawn to the same longitudinal scale, shows the pressure distribution on the surface of the body and the behaviour of the cavity from its inception to collapse. It will be noted that only the negative portion of the pressure distribution curve is shown, the ordinate for this curve being absolute pressure. The vapour pressure of the water at the temperature of the experiment is shown by the horizontal dotted line. The pressure distribution is that measured for non-cavitating conditions, i.e., for a high value of K. The dotted line having the horizontal section AB shows the changed pressure distribution for K = 0.33. Curves showing the radius and volume of the cavity were calculated from photographic records; for this the average cavity radius was assumed to be one half of the mean of its horizontal and vertical dimensions. The volume was calculated on the assumption that the cavity was a sphere of this radius.

Point A shows the position on the nose of the body at which the pressure has been reduced to the vapour pressure of the water. It will be seen that this is also very nearly the position at which the cavity was first detectable as a tiny bubble. The photographs show that the cavity moved downstream on the body into a region where the pressure tends to decrease below the vapour pressure. The cavity was observed to grow at a rapid rate, and this high rate of growth continued nearly to point B which corresponds to the position on the body at which the pressure returns to vapour pressure.

During the rapid growth of the cavity the liquid is moving outward at high speed. From A to B this outward radial flow is taking place in the direction of the pressure gradient. From B onward it is against the pressur gradient. As the curves for radius and volume show, this motion is then decelerated, and finally ceases at the point of maximum radius. The cavity radius then begins to shrink at a rate that indicates a high radially inward acceleration. Thus when viewed with respect to the pressure distribution diagram, the behaviour of the cavity is explained in a logical manner. The salient features of this behaviour are as follows:-

(1) Formation of cavity at the position on the guiding surface where the pressure is reduced to vapour pressure.

(2) Growth of cavity so long as the surface pressure is at or below vapour pressure.

(3) Deceleration of the rate of cavity growth as the pressure on the surface rises above the vapour pressure; the cavity quickly reaches its maximum size and then immediately starts to collapse.

(4) Collpase of cavity at a rate much higher than that of formation.

2.3.2 Analysis of Bubble Dynamics

By making suitable simplifying assumptions it is possible to analyse the collapse of a cavitation bubble, and to calculate the size of the cavity from the time it has reached its maximum diameter until it has completely collapsed. This was first done by Lord Rayleigh (24) who considered the collapse of an empty spherical cavity in an imcompressible frictionless fluid having a constant pressure at infinity. He equated the kinetic energy of the resulting motion of the fluid to the work done at infinity by the constant pressure acting through a change of volume equal to the change of the cavity volume. Fig. (2.3) is based on the results shown in Fig. (2.2) and gives a comparison of the observed collapse with that predicted on the basis of Lord Rayleigh's assumptions. Although these assumptions are of a comprehensive nature it will be seen that the agreement is quite good, so good in fact as to leave little doubt that the basic mechanics are as Lord Rayleigh visualised. He also calculated the pressure that would result if the cavity collapsed concentrically on to a small rigid sphere. (The reason for assuming the existence of a sphere is to obtain a finite collapse velocity, since for a perfectly incompressible fluid the collapse velocity approaches an indefinitely large value as the radius of curvature approaches zero. This assumption would not be necessary if the calculation could be made for a real compressible fluid). He abandoned the assumption of the incompressible fluid at the instant the cavity wall touched the surfac of the sphere, and proceeded to determine the pressure on the surface of the sphere on the basis that the kinetic energy present in the liquid just before the instant of contact was converted to potential energy of compression as the liquid came to rest. This is the same physical picture that underlies all calculations of water hammer pressure. If the slope of the theoretical or experimental curve in Fig. (2.3) is used to compute the radial velocity of the water as the bubble radius approaches zero it will be found that this velocity is of the order of hundreds of feet per second. Thus the maximum pressure obtained must be very high, certainly of the same order as the elastic limits of metals used in hydraulic machinery.

The prediction of these high pressures during the collapse phase sheds some light on cavitation noise. The collapse zone must be a very effective sound source, since the pressures are high and the pressure fronts are steep. Undoubtedly some of the energy involved will be dissipated in the form of pressure pulses.

In actual fact during the collapse of a cavity, the liquid is not incompressible nor infinite in extent, the pressure is not constant at its boundary, the cavity is not spherical, surface tension and viscous effects are present. Furthermore the cavity is not empty but is filled with vapour and possibly contains some permanent gas, so that processes of heat transfer and gaseous diffusion may be occurring. To derive a set of equations taking into account all these factors is well-nigh impossible. An extension of Rayleigh's theory due to (Plesset)(25) will be described here in order to give some idea of the nature of the problem.

Consider a spherical bubble in a perfect incompressible liquid of infinite extent, and let the origin of co-ordinates be at the centre of the bubble which is at rest. The radius of the bubble at any time is R and r is the radius to any point in the liquid. As is well known the velocity potential for motion of the liquid with spherical symmetry is

$$\phi = \frac{R^2 \dot{R}}{r} \qquad (2.9)$$

The Bernoulli integral of the motion is

$$-\frac{\partial \phi}{\partial t} + \frac{1}{2}(\nabla \phi)^2 + \frac{p(r)}{\rho} = \frac{p(t)}{\rho} \qquad (2.10)$$

where $p(r)$ is static pressure at r

$p(t)$ is static pressure at a distance from the bubble at time t.

From equation (2.9)

$$(\nabla \phi)^2 = \frac{R^4 \dot{R}^2}{r^4} \qquad (2.11)$$

and

$$\frac{\partial \phi}{\partial t} = \frac{1}{r}(2 R \dot{R}^2 + R^2 \ddot{R}) \qquad (2.12)$$

Equation (2.10) will be applied as r = R so that the equation of motion for the bubble radius is determined, (2.11). Then

$$\left(\frac{\partial \phi}{\partial t}\right)_{r = R} = 2\dot{R}^2 + R\ddot{R}$$

$$(\nabla \phi)^2 = \dot{R}^2$$

so that equation (2.10) became

$$\frac{3}{2}\dot{R}^2 + R\ddot{R} = \frac{p(R) - p(t)}{\rho} \qquad (2.13)$$

This is the general equation of motion of a spherical bubble in a liquid with given external pressure $p(t)$ and with the pressure at the bubble boundary $p(r)$. Rayleigh's solution is obtained as the special case with

$p(t) - p(r) = p_o$, a constant.

If the bubble is considered to be full of vapour at pressure pv and is the surface tension at the bubble surface,

$$p(r) = p_v - 2\delta/R. \qquad (2.14.)$$

Equations (2.13) and (2.14) together with a statement of the pressure relationship $p(t)$ fully define the problem. To find $p(t)$ it is usually assumed that it can be determined from the pressure distribution in non-cavitating flow.

Plesset analysed experimental observations of bubble growth and collapse in the cavitation on a submerged streamlined body in a water tunnel and found good agreement with this theory. He later carried out more detailed analysis, e.g. for the growth of a bubble in a superheated liquid (26) when heat transfer at the bubble wall retards its rate of growth appreciably. Other

detailed analyses have been carried out, notably by Gilmore (27), but a discussion of them would extend beyond the scope of this thesis.

Summing up then, it is clear that Rayleigh's idealised theory should be modified to allow for the properties of real liquids, but attempts to do this very soon bog down in laborious mathematics. The important effects of the properties of real liquids are briefly as follows. Surface tension tends to increase the rate of bubble collapse; viscous effects, compressibility effects, and the effects of entrained air (or vapour which cannot condense rapidly enough to follow the collapsing bubble walls and so acts as permanent gas) all tend to slow down the motion, and hence to reduce the maximum pressures attained.

Because of the extreme complexity of the behaviour of cavitation bubbles, and particularly because of the impossibility of describing in detail the properties of the liquid-gas system (initial size and shape of bubbles, their air content, vapour behaviour, deformations due to instability of the bubble walls) it is not possible to state unequivocally the maximum pressures developed or the pressure history during the motion and collapse of such bubbles. Recent experiments on cavitation on photoelastic specimens by Sutton (28) suggest that the impact stresses produced in the surface by bubbles collapsing on it can be as high as 200,000 p.s.i. While this figure has still to be confirmed there is no doubt that the peak pressures developed during collapse can be high enough to cause mechanical damage to materials.

2.4 DEVELOPED FORMS OF CAVITATION

Following inception, cavitating flows may continue to be composed of individual transient cavities. However, in many cases a large cavity region appears which is attached to the body on which cavitation has been induced. This is particularly likely to occur if the point of detachment is sharply defined, for example a hydrofoil with a sharp leading edge. The region is described as an attached or quasi-steady cavity; its boundaries do not alter with time although conditions inside the cavity are constantly changing in a very complicated manner.

Flows with quasi-steady, or attached cavities that are long compared with the body about which they are formed are called "supercavitating" flows. Supercavitating flows are of importance in connection with high speed marine propellers, hydrofoil boats, and low head pumps and turbines. They are discussed later in Chapter 5.

Many observations have been made of these attached cavities and it appears that the liquid flows along the boundary of the cavity and re-enters at the downstream end. Depending on a number of factors as yet incompletely understood, the re-entering fluid may fill the cavity completely and cause it to collapse, whereupon the cycle of growth, collapse, filling and collapse recurs. When the velocities are high enough, and presumably when the rate of entrainment of the re-entering liquid becomes great enough, the entrained liquid is swept out of the cavity region. The re-entrant jet has insufficient

momentum to refill the cavity, and the cavity remains essentially filled only with the vapour phase and air diffused from the neighbouring liquid. The re-entrant jet still appears but is dissipated before it can fill the cavity again. Under these conditions the trailing edge of the cavity exhibits quite an unstable motion, leading to oscillating forces that are of rather low frequency and that may be the cause of severe vibrations in hydraulic machinery.

2.5 CAVITATION DAMAGE AND PROTECTION

2.5.1 General

The onset of damage is associated with the local mechanical stressing of proximate material by the high pressures developed in the liquid surrounding cavitation bubbles. The phenomenon is a complex one involving a number of hydrodynamic and metallurgical variables and, in corrosive media, chemical and electrochemical effects as well. The nature of the damage is intimately related to the response of materials to high rates of mechanical stressing and to their chemical reactivity, so that as damage proceeds it is often difficult to separate the effects in an unambiguous way. An excellent review of the present knowledge of cavitation damage has been made by Godfrey (29).

In the necessarily brief account given here, the view of Preiser and Tytell (30) is followed : that the total damage to a surface can be divided into three distinct parts, each having a specific mechanism. These are :

(1) Cavitation Deformation and Fracture.

(2) Cavitation Fatigue.

(3) Cavitation Corrosion.

In the case of Cavitation Deformation and Fracture, all three mechanisms may be superimposed on each other to contribute to the total damage. The second case of Cavitation Fatigue may have only the corrosion mechanism operating in concert. The third case of Cavitation Corrosion implies no physical damage to the metal substrate but an electrochemical damage accelerated by cavitation collapse forces. These three mechanisms will now be described in greater detail.

2.5.2 Mechanism of Cavitation Damage

Cavitation Deformation and Fracture

Cavitation Deformation and Fracture results from the intense hydro-mechanical forces generated by collapsing cavities, and is generally experienced on specimens exposed to special accelerated laboratory tests using magnetostriction or ultrasonic apparatus. Most of the damage is due to mechanical breakdown of the material surface, and the subsequent separation and ejection of small particles from the parent body. Secondary fatigue and corrosion effects may be operating but their results are obscured. For example, in the case of cavitation on a metal in water, the collapsing bubbles first produce indentations in the surface, and it

has been suggested, Wheeler (31), that the rise in temperature at these indentation points caused by the absorption of energy can create conditions favourable to energetic chemical action between the water and the metal. The time scale for damage by cavitation deformation and fracture is so short that such secondary mechanisms probably do not contribute substantially to the total damage.

The only effective way of reducing this type of damage is by mechanically cushioning the intense implosive forces of cavitation collapse. The use of entrained air for this purpose is well-known in hydraulic structures, valves, and turbines. Cathodic protection has also been used successfully to arrest this form of cavitation damage (see for example Plesset (32). In this case the hydrogen gas is an over-voltage reaction product of the cathodic process and introduces a resilient gas cushion between the collapsing vapour cavities and the metal surface.

Cavitation Fatigue.

Cavitation fatigue occurs on metals and other materials when the implosive forces of the collapsing cavities are below the yield strength of the material. This lower intensity cavitation damage takes place over a longer time scale and therefore allows corrosion mechanisms, when existing, to influence the rate of damage substantially. This type of cavitation damage is believed to be found on most ship propellers and in hydraulic machinery.

Experimental observations indicate a damage mechanism similar to stress corrosion cracking whereby the severity of cavitation collapse dislocates grain boundaries, and causes rupture of any surface films which may have originally contributed to the corrosion resistance. The metal under these stressed conditions in a corrosive environment quickly causes anodic solution at the grain boundaries. This progresses rapidly because corrosion products are swept away from the cracks by the moving liquid, and polarization effects are removed at the adjacent cathodic grain surfaces.

This mechanism then is similar to that of corrosion fatigue and consists essentially of the transgranular cracking of the metal under a repeated cyclical stress which is within the elastic limit in a corrosive environment.

Cavitation Corrosion

When the cavitation collapse forces are of sufficiently low intensity so as not to stress the metal unduly, the damage is generally confined to the destruction of protective films on the metal surface and the removal of corrosion products. This type of damage is similar to velocity and impingement damage and forms a third mechanism called cavitation corrosion.

Velocity and turbulence effects promote corrosion by many accepted mechanisms such as : protective film breakdown, differential aeration and differential ion concentration. Other theories on the electro-chemical effects produced by cavitation collapse forces deal with thermogalvanic potentials, ion dissociation effects, etc.

The damage to a metal under these conditions is completely electro-chemical in character and can be countered by standard cathodic protection techniques.

2.5.3 Selection of Materials to Resist Cavitation Damage.

The resistance of materials to cavitation damage may be examined in relation to their mechanical properties, their metallurgical properties, and their behavioural characteristics.

With respect to mechanical properties increasing resistance is exhibited with increasing hardness, ability to work-harden, ultimate tensile strength, elasticity. However these properties alone do not define uniquely the ability of materials to withstand cavitation damage. For example it has been shown that molybdenum, which has a hardness and tensile strength of about the same magnitude as nickel and brass, exhibits damage resistance comparable with much harder materials. Molybdenum is known to exhibit large yield lag under rapidly applied stress so that, in view of the very short duration of the pressures applied by collapsing cavities, this behaviour may be expected; much more research must be carried out before this conclusion can be substantiated in detail.

Among the metallurgical properties known to be of importance in determining the resistance of materials to cavitation damage are :- crystal and grain structure - the finer the grain structure the less the damage; presence of inclusions - these tend to reduce the resistance to damage; presence of alloy constituents - these may affect the grain structure and thus the resistance to damage.
It can be seen from the discussion of the various damage mechanisms that, in general, a material with a homogeneous micro-structure should be less susceptible to cavitation damage.

Behavioural properties of importance are fatigue and corrosion fatigue. Resistance to cavitation damage appears to be correlated with fatigue properties, and, in corrosive media, with corrosion fatigue. Also materials with high strength at high temperatures exhibit good resistance.

A short, representative summary of the relative resistance of metals used in hydraulic machinery has been compiled, Rheingans (33), and is shown below. This list is in order of merit and shows the weight losses determined in laboratory experiments on cavitation damage of metal specimens in special magnetostriction oscillator device.

Alloy	Weight Loss after 2 hours - mgm.
Rolled Stellite	0.6
Welded Aluminium Bronze (83.0% cu, 10.3% Al, 5.8% Fe)	3.2
Cast Aluminium Bronze (83.1% Cu, 12.4% Al, 4.1% Fe)	5.8
Welded Stainless Steel (2 layers of 17% Cr, 7% Ni)	6.0
Hot-rolled Stainless Steel (26% Cr. 13% Ni)	8.0
Tempered, Rolled, Stainless Steel (12% Cr)	9.0
Cast Stainless Steel (18% Cr 8% Ni)	13.0
Cast Stainless Steel (12% Cr)	20.0
Cast Manganese Bronze	80.0
Welded Mild Steel	97.0
Plate Steel	98.0
Cast Steel	105.0
Aluminium	124.0
Brass	156.0
Cast Iron	224.0

2.5.4 Protection against Cavitation Damage

There are three methods of protecting against cavitation damage in hydraulic machinery, or of remedying the situation when excessive damage is occurring.

(1) Elimination of the problem at the source by hydrodynamic redesign.

(2) Use of highly resistant materials, for example, welded or sprayed overlays, in the zone of cavitation attack. This method is often used if it has been decided to operate under cavitating conditions for short lengths of time - pumps and turbines at off-design duties for instance.

(3) Use of artificial protective devices as adjuncts to the main system. In this case protection may be achieved by the injection of small amounts of air into the cavitating regions or by the use of cathodic protection.

CHAPTER 3.

MODEL LAWS AND SCALE EFFECTS IN CAVITATION

3.1 GENERAL

Models of large pumps and turbines are built and tested to check their performance and cavitation characteristics. This provides an economical method of proving the design before heavy costs are incurred in manufacture of the prototype.

The aspects of cavitation discussed so far have demonstrated its complexity, and it will readily be realized that accurate calculations of the cavitation performance of a given design are difficult. It is necessary therefore to look at the problem of predicting full-scale performance from model tests. This chapter commences with a general analysis of the subject and then examines particular features relating to pumps and turbines. Chapters 4 and 5 deal with methods of designing centrifugal and axial flow pumps for specified inlet conditions.

Certain types of high specific speed axial flow pumps have been developed to operate with cavitating or supercavitating flows. Apart from such special cases, centrifugal and axial-flow pumps are designed to operate without cavitation; this is also true for turbines although small amounts of cavitation are sometimes accepted in hydraulic turbines if the ensuing damage is small and can conveniently be repaired during annual overhauls. The discussion of the factors affecting scaling from model to prototype will therefore be confined to relationships applicable to inception of cavitation. Scaling relationships for developed forms of cavitation or for the damage process will not be included. With that point clear, similarity conditions for cavitation will now be examined.

3.2 THEORETICAL CONSIDERATIONS

3.2.1 Classical Similarity Relations for Cavitation

The classical theory of similarity applied to cavitation is based on two assumptions :-

(1) The liquid flowing through or around the model and prototype is frictionless, incompressible without the effect of gravity or other "body" forces. Thus forces other than inertia forces are not effective, and all pressure differences in the flow are proportional to ρV^2. Furthermore, the geometrical similarity between model and prototype includes surface irregularities at the flow boundaries.

(2) The pressure at which cavitation takes place is the equilibrium vapour pressure of the liquid which is known and constant for the particular flow field considered. Also cavitation takes place instantaneously whenever the vapour pressure is reached; there is no tension in the liquid and there are no time effects.

In the light of this ideal theory a simple relationship can be formulated between the velocities, pressures and fluid properties pertaining to cavitation. Thus for similar flow with cavitation the difference between any pressure in a hydrodynamic machine and the vapour pressure of the liquid is proportional to ρV^2, as is any other dynamic pressure difference in the machine. The oldest expression of this law with respect to pumps and turbines is Thoma's law of similarity :

$$\sigma = \frac{Hsv}{H} = \text{constant} \qquad (3.1)$$

where H is the total head of the machine and Hsv its total suction head above vapour pressure. Fig. (3.1) has been drawn to show clearly how this definition of Hsv is applied.

With respect to flow relative to a specified part or structure, a slightly different form of cavitation parameter is used, and the classical law of similarity for cavitation then appears in the form

$$K = \frac{p - pv}{\frac{1}{2} \rho V^2} = \text{constant} \qquad (3.2)$$

where p is usually the static pressure in a uniform flow far ahead the cavitating object, pv the vapour pressure of the liquid at an easily measured reference temperature, and V a conveniently defined reference velocity of the flow, usually at the same place where p is measured.

Thus the classical theory of cavitation is expressed by equations (3.1) and (3.2) and states that the cavitation conditions in two geometric-similar machines or structures with similar flows will be "similar" (i.e. the form and extent of the cavitation voids will be similar) if and only if the Thoma parameter or the cavitation number K have the same values for the machines or flow structures compared.

As explained earlier our interest is primarily in cavitation inception defined by

$$\sigma_i = \frac{(Hsv)_i}{H} \qquad \text{or} \qquad K_i = \frac{Pi - Pv}{\frac{1}{2} \rho V^2} \qquad (3.3)$$

While this classical theory has been widely used, some significant departures have been observed; many instances have been recorded of variations in σi and Ki in experiments on similar hydrodynamic machines and structures, for example, Kermeen et al. (15). These departures from the classical theory - the "Scale Effects" - suggest that the assumptions on which this theory is based should be re-examined.

3.2.2. General Conditions for Similarity

The discussion of scale effects falls naturally into two parts.

(1) Scale effects on the flow outside the cavitation voids which affect the minimum pressure in the liquid flowirrespective of the presence

or absence of cavitation, i.e., scale effects due to the fact that a real liquid does not behave in the ideal manner assumed.

(2) Scale effects on the cavitation process itself which may cause the pressure at the cavitation voids ("the cavitation pressure") to depart from the equilibrium vapour presence at the bulk temperature of the liquid, and may cause tension and time effects.

Scale Effects on the Minimum Pressure in the Liquid.

The actual flow and its pressures are known to depart from the ideal flow. The similarity laws governing these departures involve Reynolds number, Froude number, Mach number and surface roughness. They are as follows.

To maintain a constant ratio of inertia to viscous forces the Reynolds number must be kept constant,

$$Re = \frac{V.L}{\mu/\rho} = \text{constant.} \qquad (3.4)$$

To maintain a constant ratio of inertia forces to gravitational forces, the Froude number must be kept constant,

$$Fr = \frac{V}{\sqrt{gL}} = \text{constant.} \qquad (3.5)$$

To maintain constant effects of compressibility, the Mach number must be kept constant,

$$M = \frac{V}{a} = \text{constant.} \qquad (3.6)$$

In a given liquid the kinematic viscosity (μ/ρ) and the velocity of propagation of a pressure wave (a) are constant so that these three laws then require

$$V.L = \text{constant}$$

$$V/_L = \text{constant}$$

$$V = \text{constant.}$$

Obviously only one of these laws can be satisfied under one set of conditions. Although liquids are nearly incompressible there is no justification for neglecting changes in Mach number, since in cavitating flow a mixture of liquid and vapour (or gas) can have a low acoustic velocity.

Surface irregularities are present on all hydrodynamic bodies, and consequently, families of "similar" shapes lack exact geometric similarity since surface irregularities are usually not scaled proportionally. Surface irregularities can lower the minimum pressure significantly from that which would be predicted for a smooth surface. Thus if Cp min is the coefficient of minimum pressure for a smooth surface, then cavitation produced by surface irregularities is such that

$$K_i > Cp\ min$$

Surface irregularities thus constitute a major scale effect on the minimum pressure.

A recent investigation has been made by Holl (20) into the effects of isolated surface irregularities on the occurrence of cavitation in a turbulent boundary layer. The results showed that the most important factor appeared to be the height of the surface roughness (h) relative to the thickness of the boundary layer. If Reynolds number effects are disregarded the boundary layer thickness can be assumed proportional to the general linear dimensions of the structure (L). The resulting similarity condition is then

$$\text{Relative roughness} = \frac{h}{L} = \text{constant} \qquad (3.7)$$

This brief discussion indicates that the problems of scale effects on the minimum pressure are reasonably well understood, although it should be noted that the problem of cavitation produced by random surface roughness and the associated pattern of turbulent pressure fluctuations (Daily and Johnson (19)) are far from solution at present.

Scale Effects on Cavitation Pressure and Bubble Growth

Scale effects on the cavitation process fall into two groups which will be discussed in turn.

(1) Effects on the vapour pressure due to the change in local temperature resulting from evaporation at walls of the cavitation bubbles.

(2) Effects of molecular forces such as surface tension on the pressure at which a void will form in a liquid.

The variation of the local vapour pressure due to cooling at the bubble wall (resulting from vapourization) was investigated theoretically by Plesset and Zwick (38). They found that although the change in temperature is small, the effect on the growth of a bubble may be appreciable, particularly in superheated liquids. These findings were confirmed by Dergarabedian (39). If the vapour pressure of the liquid is low, as in cold water, the effect of vapourization on the local vapour pressure is necessarily small.

In order to estimate the local temperature drop at the bubble wall (ΔT), first assume that the entire heat transfer takes place by turbulent convection. It is reasonable to suppose that the velocity of vapour removal from the cavitation bubble (by entrainment) is proportional to the velocity of flow V so that

$$\Delta T = \text{constant} \quad \frac{a_v}{a_l} \quad \frac{v_l}{v_v} \quad \frac{\lambda}{c_l} \qquad (3.8)$$

where λ = latent heat of vapourization

c_l = specific heat of liquid

v_l = specific volume of liquid

v_v = specific volume of vapour

a_l = area of heat supply through liquid

a_v = area of vapour removal

(a_v/a_l is a form parameter of cavitation).

This is one extreme case. In the other extreme all heat transfer takes place by conduction, and for this case the previous result must be multiplied by the ratio of heat transfer by convection to that by conduction which is the Peclet number.

$$Pe = Pr.\,Re = \frac{c_l}{v_l \cdot k} \cdot (V.L)$$

where k = coefficient of heat conduction.

Thus for pure conduction

$$\Delta T = \text{constant} \cdot \frac{a_v}{a_l} \cdot \frac{v_l}{v_v} \cdot \frac{\lambda}{c_l} \cdot Pe \qquad (3.9)$$

In fact the true situation will lie somewhere between the extreme values represented by equations (3.8) and (3.9), so that

$$\Delta T = \text{constant} \cdot \frac{a_v}{a_l} \cdot \frac{v_l}{v_v} \cdot \frac{\lambda}{c_l} \cdot Pe^n \qquad (3.10)$$

where $0 < n < 1$.

A more general relation for ΔT can be derived,

$$\Delta T = \frac{c_Q}{c_H} \cdot \frac{a_v}{a_l} \cdot \frac{v_l}{v_v} \cdot \lambda \qquad (3.11)$$

where C_H = heat transfer coefficient, a function of Re, Pr, and F,

C_Q = volume entrainment coefficient, a function of at least Re and F.

The resulting reduction in vapour pressure is

$$\Delta p_v = \frac{\partial p_v}{\partial T} \Delta T \qquad (3.12)$$

where $\partial p_v / \partial T$ can be taken from vapour tables for the fluid, or calculated from Clapeyron's equation.

The cavitation number characterizing the flow is changed from K to K^1.

$$K^1 = \frac{p - (p_v - \Delta p_v)}{\frac{1}{2} \rho V^2}$$

$$\therefore \quad K^1 = K + \frac{\Delta p_v}{\frac{1}{2} \rho V^2}$$

Thus the ratio $\Delta p_v / (\frac{1}{2} \rho V^2)$ is a parameter indicating the importance of the cooling effect. Presumably then the condition for similarity is

$$\frac{\Delta p_v}{\frac{1}{2} \rho V^2} = \text{constant.} \qquad (3.13)$$

This parameter depends on the Peclet number (i.e. on V.L for a given liquid), or on some more complex combinations of Prandtl number, Reynolds number, and possibly Froude number. Clearly this imposes severe restrictions on conditions providing similarity of flow.

The effects of surface tension and other molecular forces are now considered. These influence the pressure at which a cavitation bubble will form and are principally concerned with the inception of cavitation.

Cavitation begins at weak spots or "nuclei" within the liquid and the most common postulate is that these nuclei consist of pockets of undissolved gas trapped in crevices in hydrophobic solids as illustrated in Fig. (3.2). Since the walls of the crevice are unwetted the gas pressure is less than the liquid pressure by the effect of surface tension, and therefore the liquid cannot dissolve the gas. The gas pocket is an active centre for the formation of a cavitation bubble.

When surface tension forces are considered the condition for similarity of cavitation is that the Weber number be kept constant.

$$W = \frac{\rho V^2 L}{\delta} = \text{constant.} \qquad (3.14)$$

where δ = surface tension.

With regard to the cavitation nuclei the conditions for similarity may be written

$$\frac{\Delta}{L} = \text{constant.} \qquad (3.15)$$

and $$n = N.L^3 = \text{constant}$$

or $$\sqrt[3]{n} = \sqrt[3]{N}.L = \frac{L}{\Delta l} = \text{constant} \qquad (3.16)$$

Here Δ = size of nuclei

n = number of nuclei in the flow

N = number of nuclei per unit volume.

Δl represents the average linear distance between nuclei and can be readily related to a characteristic time required for cavitation inception.

An additional relation is required to describe the nuclei spectrum which should remain unchanged in model and prototype tests. A simple form would be

$$\Delta \text{ max} / \Delta \text{ mean} = \text{constant.}$$

It should be noted that the influence of the number of nuclei per unit volume (N) may be significant only for cavitation away from the solid flow boundaries, as near to these boundaries irregularities of the solid surface may form the nuclei. Furthermore the number of nuclei is a significant variable only if every nucleus acts as a centre of cavitation.

The postulated nature of the nuclei leads to the conclusion that the scale effect of surface tension is restricted to the dimensions of the nuclei (Δ) so that conditions (3.14) and (3.15) can probably be combined into one containing the Weber number of the nucleus.

$$W_\Delta = \frac{\rho V^2 \Delta}{\delta} = \text{constant.} \qquad (3.18)$$

A further relation may be introduced to take account of the gas content α of the liquid

$$\frac{\alpha}{\alpha_s} = \text{constant.} \qquad (3.19)$$

where α_s is the gas content of the liquid when saturated. Because of experimental difficulties published work to date has either ignored this factor or recorded measurements of total gas content. It would be desirable of course to separate the effects of dissolved gases from those of undissolved

gases, and possibly to combine the latter with the description of other nuclei in the liquid.

As a full description of the mechanism of cavitation is not yet available it is impossible to state that the similarity relations derived above are complete. Nevertheless, these relations may be regarded as representing the present state of knowledge and have therefore been tabulated in Fig. (3.3). This table is similar to one in the paper by Holl and Wislicenus (40); it summarises the requirements for similarity of cavitating flow on model and prototype.

3.3 MODEL EXPERIMENTS

3.3.1 Streamlined Bodies

In the light of the above discussion it is now possible to review briefly the results of laboratory tests on hydrofoils and other streamlined bodies submerged in water. Examination of these results for cavitation inception in attached flows (Holl and Wislicenus (40)) shows that Ki varies in a bewildering fashion. In most experiments Ki has been determined visually on cessation of cavitation ("desinence") and has been found to increase with velocity in a manner which could be explained by a combination of viscous and surface tension effects. However, Ki is not a unique function of Reynolds number nor Weber number. In fact in one series of water tunnel tests by Olson a wetting agent was added to the water, and it was found that the cavitation pressure was unaffected by the change in surface tension. Comparison of tests on families of similar hydrofoil shows conflicting results for the variation of Ki with size. In the majority of cases Ki decreases with increasing size, a possible explanation for this being that the influence of surface roughness (h/L) is less on the bigger scale.

It is suspected that some of the inconsistencies in these observations of Ki may be due to failure to distinguish between gaseous and vapourous cavitation. Some may also be due to the effects of boundary layer flows and of turbulence, as well as to the unsteady flow effects associated with the pressure gradients on two different scales. Of course in all these experiments there is considerable uncertainty regarding the nature of the nuclei spectrum, and whether the nuclei are in the body of the flow or attached to its boundaries.

At present knowledge of cavitation inception and its scaling is incomplete, and there must be some uncertainty associated with the prediction of conditions for the onset of cavitation. This suggests that the best that can be done is to characterize a system by a most probable critical cavitation number based on a statistical analysis of the factors involved.

3.3.2 Pumps and Turbines

Tests on model pumps and turbines are regularly carried out by manufacturers and the operation of many large installations shows that the results of these test have been successfully applied. However, it is usually difficult if not impossible to make accurate tests on the full-scale

prototype. The model results are interpreted in an empirical manner by the manufacturer by reference to his previous experience in order to determine whether there is an adequate safety margin between the plant σ (or Hsv) and that required by the machine for operation free from the deleterious effects of cavitation. There are many points to be elucidated before this empirical approach can be discarded and the subject placed on a firm engineering foundation. In a recent study Hutton (41) has commented: "Although manufacturers may be able to predict cavitation performance empirically, it is at present impossible to stipulate any generally applicable laws for similarity of cavitation performance."

The relation has been established

$$\sigma_i = \frac{(Hsv)\ i}{H}$$

Turbines: σi is defined as the critical value of the cavitation parameter when the efficiency first begins to fall off by a measurable amount.

Pumps: σi is defined as the critical value of the cavitation parameter when the head first departs from its non-cavitating value by a measurable amount.

Thus σi is defined in terms of the performance characteristics most sensitive to it, namely turbine efficiency and pump head. Occasionally other performance variables such as pump efficiency are used to help determine σi.

Fig. (4.2) shows the results of typical cavitation tests with efficiency or head plotted against σ . Such tests are carried out for the design duty and for any other duties at which the machine has to operate.

The definition of σi considers cavitation only in the low pressure regions of the runner, although cavitation can take place at other places notably on guide vanes and in clearance spaces between runner and casing. These forms of cavitation occur less often in practice, are more easy to avoid by good design, and are therefore not considered in detail in this thesis which is devoted to a study of the influence of cavitation on runner design.

In section (3.2) it was seen that the scaling of cavitation inception could be affected by a large number of factors. With regard to pumps and turbines tested on cold water, it is likely that the most important ones are as follows.

(1) Thoma's cavitation parameter (σ).
(2) Reynolds number and surface roughness.
(3) Froude number.
(4) Air content of the water.

It is clearly impossible to keep all these quantities the same in the model and the full-scale tests, but it is nevertheless necessary to know which factors should be given the most weight.

(1) The use of the cavitation parameter σ is based on the assumption

that the critical value σi is reached when the minimum pressure in the water is equal to the vapour pressure. Then

$$\sigma_i \propto Q_1^2 \quad , \text{ say } \sigma i = B Q_1^2 \qquad (B = \text{a constant})$$

where $Q_1 = Q / (D^2 \sqrt{H})$ is the unit capacity, and it is assumed that the flow on the suction side of the runner is axial (probably correct for design point but not true away from it).

There are two difficulties here; one is that gaseous cavitation, or air-release, may occur at a pressure different from the vapour pressure, and the other that the critical onset of cavitation based on deterioration of performance may also occur at some pressure different from the vapour pressure. Even if gaseous cavitation is ignored this means that in practice σi should be written more correctly as

$$\sigma i = A + B Q_1^2 \qquad (3.20)$$

where A is an arbitrary constant. For high head machines A is negligible and σ can be used successfully to define cavitation, while at low heads A may become significant. This difficulty may be overcome by using relative not absolute values of σ such as $\sigma - \sigma i$; A is not involved but some absolute value of σi must be used as a reference datum.

(2) The model should be big enough and the Reynolds numbers high enough to ensure similar areas of laminar and turbulent flow in the hydraulic passages of the machines. From an analysis of German and Russian data on turbines and English data on cascades, Hutton suggests that the minimum Reynolds number acceptable is about 2×10^6,

$$\frac{D \sqrt{2 g H}}{\nu} \geqslant 2 \times 10^6 \qquad (3.21)$$

Surface roughness can have a marked effect on the cavitation performance of small models but its influence is secondary in models of reasonable size (runner diameter greater than 12"). When sufficient information has been accumulated it will probably be necessary to stipulate surface finishes of models in relation to full-scale machines.

(3) Some engineers believe that cavitation tests, at least on low head machines, should be carried out with the same Froude number for model and prototype, i.e.

$$\frac{H}{D} = \text{constant} \qquad (3.22)$$

Froude number is considered the essential parameter because gravity forces are the only external forces acting. The argument of Danel and Dupont (42) in favour of this is based on writing the Bernoulli equation for the local absolute pressure at a point on the runner blades of a vertical turbine

$$h = h_a - h_s - z - \sigma H$$

whence $$\sigma = \sigma_o - Z \frac{D}{H} - \frac{h}{H}$$

where $$\sigma_o = \frac{h_a - h_s}{H}$$

h_a = atmospheric pressure

h_s = suction pressure referred say to blade centreline

h = local absolute pressure at elevation z

where $Z = \frac{z}{D}$

Application of the Froude law leads to model tests at reduced heads and power outputs so that accurate measurements are made difficult and excessively low pressures are encountered on the suction side of the machine. Because of these practical difficulties and because the research work discussed in section (3.2) has not shown Froude number to have any significant effect, the great majority of model tests ignore Froude's law, and are in fact carried out with the same head on the model as on the prototype. The condition is imposed

$$H = \text{constant}$$
$$\text{which is equivalent to} \qquad (3.23)$$
$$V = \text{constant.}$$

For models tested under the actual full-scale head, Froude number effects would be insignificant for medium and high-head machines. However, they could be important in low-head machines because the gravity force differences between model and full-scale are then appreciable in comparison with the inertia forces.

Gerber (43) has presented evidence of the influence of test head on σ_i for model turbines at their design points. While not conclusive a few examples do show σ_i to increase with H. Numachi's results (44) for tests on a hydrofoil also show this tendency, Ki increasing slightly with test pressure. The question is not resolved but the well-established practice of testing models at prototype heads should be noted.

(4) The effect of air content has been referred to before in section (2.2). Generally, at low heads σ_i increases with increasing air content and Hutton quotes a semi-empirical formula developed for turbines.

$$\sigma = \sigma' + 8.48 \left(\frac{\sqrt{\alpha}}{H} - \frac{\sqrt{\alpha'}}{H'} \right) \qquad (3.24)$$

where α = ratio of total air volume to total volume of water and symbols marked with dash refer to model.

Theoretically it would be desirable to have the air content (and more generally the nuclei content) similar in model and prototype, $\alpha = \alpha'$. This is seldom possible as α may not be known and α' will depend on the design of the test rig. In tests with open circuit rigs the water is drawn from a reservoir exposed to atmosphere so that α' would be expected to be greater than or equal to the saturation content, depending on how much air is entrained. In closed circuits fitted with air absorbing apparatus α' can be controlled; usually a low value is used so that the cavitation characteristics are not masked by air release. α' should not be too low as the goal is to reduce gaseous cavitation without delaying the onset of vapourous cavitation.

A large pump or turbine is generally believed to be more susceptible to cavitation than a similar smaller machine, i.e. σ_i increases with D. For example, Gerber (43) reported that pitting on the runner blades of large turbines had been observed at points where no cavitation had been noted during model tests at the same σ. Fig. (3.4) shows the results of two

pump tests carried out by the author; these are plotted in non-dimensional form, σ_i versus Q/Q_o, the ratio of the test capacity to that at the design or best efficiency point. The larger pump was approximately twice the size of the smaller but was not an exact scale although its design was similar. While a definite conclusion cannot be drawn from these tests, the performance of the larger pump does appear significantly worse than that of the smaller.

These results and others of the same type have been recorded for cases where models and prototypes were tested at similar heads and with similar flow velocities. They are usually explained in terms of a time effect due to the fact that the nuclei in the flow take longer to traverse the region of low pressure in a large machine. Hence, if they are initially below the critical size for vapourous cavitation they have more time for growth by diffusion. They are therefore more likely to reach the critical size, vapourous cavitation is more likely to occur, and the resistance of the machine to this form of cavitation is lower. In such cases inception may be effectively prevented on the model scale but not on the prototype.

If this time scale were to be taken into account a new law of similarity would be obtained

$$\frac{\sqrt{H}}{D} = \text{constant.} \qquad (3.25)$$

To sum up, the scaling relationships for inception of cavitation in pumps and turbines have been examined. The problem is of great significance in determining turbine and pump settings in large installations where it has a major bearing on construction costs. For example, there are two pumped storage schemes under construction or being planned in Australia : Arthur's Lake, Tasmania, has one 9,500 H.P. circuit and the proposed Jindabyne pumping station in the Snowy Mountains will have two 40 MW units, probably underground. In pumps of these sizes it would obviously be desirable to predict σ_i and $(Hsv)_i$ from model tests, but only a courageous engineer would be prepared to do this on the basis of published evidence.

CHAPTER 4.

IMPELLER DESIGN FOR OPTIMUM CAVITATION PERFORMANCE

PART I - NON-CAVITATING FLOWS.

4.1 INTRODUCTION

4.1.1 Scope

This chapter is devoted to the design of centrifugal and axial-flow pump impellers for optimum cavitation performance. It begins with a classification of the types of impeller to be considered and a discussion of the definition of cavitation inception. Some general features of impeller design are dealt with, then a detailed investigation is made of the information and methods available for the design of impeller inlets for best cavitation performance. The subjects covered include the selection of impeller profiles, eye diameters, and blade angles; the results are summarised in a series of design equations and charts.

4.1.2 Classification of Impeller Types.

In this thesis impellers will be divided into four groups - radial, Francis, mixed-flow and axial-flow; fig. (4.1) illustrates the main features of each type.

The radial impeller, as its name implies, has a meridional or through-flow velocity wholly in the radial direction. The layout of the impeller blades is essentially two-dimensional, and at any radius the blade angle is constant across the blade section at that radius. In the Francis impeller the meridional velocity at the periphery is still radial and the blades have a double curvature so that at any radial section the blade angle can be varied to suit the velocities in the relative flow. The mixed-flow impeller also has doubly curved blades but the meridional velocity at any point within the impeller has an axial as well as a radial component. In an axial-flow impeller the through-flow is purely axial with no radial component. The approximate range of specific speeds covered by each of these impeller types is shown in fig. (4.1). It may be noted that this classification is based primarily on blade design, not on impeller performance.

In all types of impeller except the purely radial, the blade angle β at inlet varies with the radius in such a way that there is correct matching of the blading to the oncoming flow. If the variation of β is compatible with the velocity distribution in the flow the overall efficiency is improved as is the cavitation resistance. For this reason Francis impellers are often used at low specific speeds in preference to radial; and the greater part of the discussion on centrifugal impellers will therefore be devoted to the Francis and mixed-flow types.

4.1.3. Definition of Cavitation Inception.

The conditions for inception of cavitation in pumps and turbines have already been defined in section 3.3.2 as

$$\sigma_i = \frac{(Hsv)i}{H}$$

Refer now to fig. (4.2) which shows the results of a typical pump cavitation test and illustrates the progressive fall-off in head with decreasing σ as cavitation develops. Initially, this fall-off is gradual so that it is difficult to decide the exact value of σ at which it begins. Nevertheless the author believes that it is possible to make this decision with reasonable accuracy, particularly if the efficiency curve is used as a cross-check to make sure that it begins to droop at the same value of σ as the head curve, as indicated in fig. (4.2). This definition of cavitation inception was used by Wood et al. (46) and will be used by the author in presenting the results of his own tests. However, Gongwer in his pioneering work (47) defined the effective onset of cavitation by the value of σ when the total head had been reduced by an amount ΔH where

$$\frac{\Delta H}{\left(\frac{u^2}{2g}\right)} = 0.02$$

Stepanoff (104) used $\frac{\Delta H}{H} = 0.03$ in commercial testing but recommended that the inception point be defined more accurately in laboratory tests. The general procedure for conducting cavitation tests is described in the A S M E Pump Test Code (48). In this code the datum plane for measuring the pressure at entry to a horizontal pump is taken as the horizontal plane through the top of the impeller eye, shown as A - A in fig. (4.1.), because this is the region of lowest static pressure. Despite the provision of the code most writers have reported their results referred to the pump horizontal centreline, and the author has followed this example in a series of tests on horizontal pumps which are described later. As the average impeller eye diameter for these tests was less than 6" any error introduced was negligible.

The variations in the definitions of σi are unfortunate but are a consequence of this empirical approach to the subject. In practice their effect is small, small enough for the results of different writers to be compared without introducing serious error. In this thesis the inception of cavitation in a centrifugal or axial flow pump is defined as that condition at which the pump head first departs from its constant non-cavitating value. This definition is justified on practical grounds because the user of the pump is only interested in cavitation in so far as it affects the performance (or, if cavitation develops beyond the incipient stage, whether it gives rise to vibration or damage). The problem for the designer then is to design an impeller for a given flow and speed of rotation which will operate free from cavitation at as low suction pressure as possible, i.e. σi to be a minimum.

While the discussion has so far considered cavitation in terms of

pump performance, it is in fact highly probable that small pockets of vapour bubbles form in the liquid in the regions of maximum pressure reduction in the impeller at a stage before the performance is affected to any significant extent. Relatively few photographic studies of cavitation in pumps and turbines have been published, but reference can be made to Hartmann and Soltis (49), Minami et al. (50), Tenot (51), Vuskovic (6), Wood (52). These visual observations confirm this statement but experience has shown that the practical significance of the first small vapourous cavities is negligible : performance is not affected and the impeller suffers no material damage.

Wood's experiments on a series of mixed-flow impellers are particularly interesting. In his work Wood took great care to de-gas and de-mineralise the water used in the tests in order to ensure that as far as possible any cavities observed consisted of vapour and were not formed from non-condensable gases. He made an extensive photographic record and found that in all impellers cavities consisting of clouds of bubbles were formed at much higher values of N P. S H than those associated with a drop in performance, and that this was the case at the design flow as well as at flows greater than and less than design. While cavitation was observed to start at the tips of the blade inlets several different patterns of flow of the vapour bubbles were observed during its subsequent development.

The study by Minami et al. (50) on four Francis impellers is noteworthy. These workers also observed pockets of cavitation bubbles to form some time before the pump performance was adversely affected, this effect being more pronounced at off-design conditions.

It is clear that there is scope for further work to be done to correlate visual observations of the onset of cavitation in an impeller with observations of its fall-off in performance. Better methods are needed for determining cavitation inception; acoustic methods at present under development show the most promise. These operate by detecting the change in noise level when the bubbles formed during cavitation first start to collapse, and they therefore offer a means of distinguishing between vapourous cavitation and the less important gaseous form.

It is pertinent to note that in certain types of pump it is accepted practice to tolerate small amounts of cavitation. This applies in installations where operation at the lowest possible value of N P S H may result in an appreciable saving in capital cost, for example in petroleum refining where many volatile liquids are handled. In certain cases no objectionable effects have been observed under conditions of controlled cavitation apart from a slight reduction in efficiency, for example when operating at $\sigma = \sigma_i - 0.25 (\sigma_{b.d} - \sigma_i)$. No doubt other circumstances then contribute to pump safety against cavitation damage, in particular the use of higher quality materials such as stainless steel in oil refinery pumps.

In the great majority of applications pumps must operate with performance unaffected by cavitation and, accordingly, this chapter will be

primarily concerned with the design of impellers for conditions where the adverse effects of cavitation are to be absent.

4.2. IMPELLER DESIGN

4.2.1 General

Some general features of impeller design will now be discussed, in preparation for an attack on the problem of optimum cavitation performance.

Hydrodynamic machines such as pumps and turbines depend for their action on the change of momentum of the liquid passing through them. To prevent cavitation in these machines it is necessary to determine how much the velocity of the liquid can be changed without reducing the local pressure to or below the vapour pressure. However, the local pressure on critical surfaces is determined not only by the local momentum change but also by the local radius of curvature and, in the case of flow past stationary or rotating guide vanes, by the blade profile. If possible, all these factors should be taken into account in the final design.

4.2.2 Characteristics of the Flow at Impeller Entry.

First the influence on design of the flow at impeller inlet will be examined. Consider the general case of the flow of a liquid approaching a rotating impeller, as illustrated in fig. (4.3) which also defines the symbols used. Fig. (4.3) has been drawn for a Francis impeller but similar arguments apply to mixed-flow and axial-flow designs.

The blade inlet angles are found from the inlet velocity triangles, and in order to construct these triangles it is necessary to make some assumptions concerning the nature of the flow entering the impeller, in particular how the meridional velocity v_m varies with radius and whether there is any pre-rotation present. (Note that v_m is slightly higher than v_a, the axial velocity of approach at the impeller eye, because at v_m the cross-section area for the flow is reduced by the blade thickness and because the impeller inlet is usually placed slightly behind the eye).

With regard to v_a and v_m the simplest assumption is that they are constant across any surface normal to the meridional flow. However, at the impeller inlet this flow follows a curved path, and it can be argued that for angular momentum to be conserved the velocities must be highest in the region where the radius of curvature of the flow-lines is highest, i.e., near the front shroud of the impeller. Pfleiderer (53) has given a semi-graphical method for deriving this asymmetric velocity distribution; this is shown in fig. (4.4) for a typical case. If this method of design is used the peak value of v_m occurs at the blade tip, the region most susceptible to cavitation, and is approximately 50% higher than the mean value. This suggests that design for best cavitation performance should instead be based on constant v_m. In practice for Francis impellers the assumption of constant v_m leads to values of β at the blade tip $2^\circ - 5^\circ$ lower than those obtained using the "Pfleiderer" distribution. The difference between the two methods can be larger for mixed flow impellers.

Wislicenus (54)(55) has pointed out that while the assumption of a potential flow distribution at the impeller inlet leads to the conclusion that v_m should increase towards the outer shroud, there is likely to be a compensating action from the impeller vanes. This results from the fact that the bound vortex lines of the vanes are inclined towards radial planes in such a way as to give the meridional inflow a vorticity of significant magnitude. With standard impeller vane designs the direction of this vorticity may be expected to produce a circulation Γ in the meridional inflow such as to change the velocity distribution in the potential flow in the direction of more uniform velocity. Qualitatively this influence can be estimated as being of considerable practical importance, but no adequate rational analysis of this important flow phenomenon has been published.

Pre-rotation in the liquid approaching the impeller always exists at off-design conditions; but may or may not be present at the design duty. The simplest basis for design is to assume pre-rotation absent; this is common practice especially in cases where there are straightening vanes placed in the flow ahead of the impeller. If pre-rotation does occur its effect can be represented on the inlet velocity diagram by a circumferential velocity u_p as shown in fig. (4.5c). The inlet angle has then to be increased from its original value β' to a new value β where

$$\frac{\tan\beta}{\tan\beta'} = \frac{u}{u - up} = \frac{1}{1 - \frac{up}{u}} \qquad (4.1)$$

As will be seen later it is possible to design for pre-rotation in order to obtain better cavitation performance.

Fig. (4.5) shows typical inlet velocity triangles for the cases discussed. These have been drawn for zero angle of incidence ($\alpha = o$) which is the standard design criterion for Francis and mixed-flow impellers. Sometimes small positive values of α are used if the impeller has to operate at over-capacities for any length of time, say $\alpha = 1^o$ to 3^o. Axial-flow impellers are designed on the basis of aerofoil theory and may also operate at small angles of incidence.

The designer has considerable latitude in his choice of v_m distribution, $\frac{up}{u}$ and α. Even if the flow initially departs from the design assumptions it will tend to adapt itself to the conditions imposed on it by the designer. Thus if the approach axial velocity profile differs from the profile built into the impeller, relatively small radial pressure gradients in the space immediately upstream of the blades will suffice to bring it into conformity so long as the axial velocity heads are not too high. Some mechanism such as this presumably accounts for the fact that impellers based on uniform velocity of approach perform very satisfactorily at their design flow.

4.2.3 Practical Aspects of Impeller Design.

In centrifugal pumps the design of the impeller inlet depends on the conditions at pump entry and is essentially independent of the total head developed or the impeller outside diameter. For this reason the main

geometrical proportions of the impeller inlet profile r_s/D and A/D in fig. (4.3), would be expected to be common to several specific speeds. For a wide range of Francis designs Stepanoff and Stahl (56) found

$$\frac{r_s}{D} = 0.25$$

$$\frac{A}{D} = 0.45$$

Similar proportions were arrived at independently by the author and found to be satisfactory. To determine the inlet profile of this class of impeller it remained then to select the eye diameter D, and this is dealt with in sections (4.4) and (4.5). The discussion is extended to axial flow pumps in section (4.6).

Once the impeller profile has been chosen the blade design can proceed. First the centreline is laid out to give the desired angles, then the thickness is superimposed. Each blade has a rounded leading edge with a radius usually about 1/16" to 1/8". Apart from some special cases pump impellers are metal castings and their surfaces have a rough finish. The rougher the surface the more prone it is to cavitation at the surface irregularities; it is therefore often standard practice to clean up the blade surfaces of impeller castings (this of course also improves efficiency). When experimental results are presented and discussed it will be generally assumed that the impeller inlets have been cleaned by hand to give a reasonable surface finish with rounded leading edges that have not been specially filed to sharp points.

Gongwer (47) has drawn attention to a detail of the blade design that is often over-looked, namely the importance of providing smooth fillets where the blades meet the front shroud. He pointed out that in the analogous case of the junction between the wing and fuselage of a subsonic aircraft, carefully designed fairing is necessary in the region of the re-entrant angle to prevent separation of the flow due to interference effects between the suction side of the wing and the fuselage. Similarly in an impeller it can be expected that interference between the inner surface of the front shroud and the under-pressure side of the blade would lead to undesirable flow separation and poor cavitation performance unless care is taken to provide proper fillets.

4.2.4 Theoretical Aspects of Impeller Design

A rational basis of impeller design for optimum cavitation performance would be based on a complete knowledge of the pressure distribution within the liquid passages of a rotating impeller. Because of the complex three-dimensional nature of the flow within an impeller this raises problems of considerable difficulty. It is the purpose of this section to examine some of these problems to see to what extent the theory available can be used in achieving the objective of best cavitation performance.

There is an extensive literature on impeller design and only references or particular importance or relevance to the argument of this thesis will be

quoted here. Broadly speaking the subjects may be divided into two inter-related parts : firstly the nature of the flow through the impeller, and the calculation of the blade centreline to suit this flow; secondly the selection of the blade profile to be superimposed on this centreline. Whereas many investigations have been carried out into the flow conditions in all types of impeller, close study of the selection of blade profiles has been confined to axial-flow pumps, the design of axial impellers being based on the application of aerofoil data. On radial and mixed-flow impellers blade profiles are obtained by adding the blade thickness to the centreline already chosen; with few exceptions this thickness is determined more or less arbitrarily from successful past experience. A brief discussion of the main impeller types will help to clarify the position.

Radial Impellers.

Experiments on the pressure distributions around the blades of a radial pump impeller have been made by Uchimaru (57), Acosta and Bowerman (58), and Acosta (59). The first two investigations were purely experimental. The third developed a theoretical solution to the problem of calculating the flow of a perfect, incompressible fluid through a radial, two-dimensional impeller fitted with logarithmic spiral blades; a series of tests were undertaken to check the results of this theory. The agreement observed between calculated and measured pressure distributions was encouraging but not sufficiently close to be useful for design purposes. Moreover, the results were of limited applicability because Acosta took special steps to ensure that the liquid entered the impeller blade system as nearly as possible in the radial direction. He did this by using an impeller profile with very large shroud entry radius r_s, much larger than would be used in practice. Even so it was found that there was rapid growth of the boundary layer on the front shroud, and at present there is no way of incorporating this and other real fluid effects into a unified theoretical picture of the flow.

Francis and Mixed-Flow Impellers.

The great majority of Francis and mixed-flow pumps operating today have been designed on a semi-empirical basis, with impeller blade centre-lines laid out to conform to the chosen radial profile and to give the required inlet and outlet angles. Frequent recourse is had to past successful experience to help determine this profile and the outlet angles, also the manner in which the blade angles are to be changed along the length from the values at inlet to those at outlet.

The application of fluid mechanics theory to the design of mixed-flow pump impellers has been retarded by the complexity of the problem and by the fact that good designs have been developed by these semi-empirical methods. However, Hamrick et al. (60) have established a theory for mixed-flow compressor impellers and this has recently been used in pump design. Unfortunately, the computations required are even more laborious than those of Acosta for radial impellers, and are only suitable for design if a computer is available to assist the work. Hamrick's method is based on perfect fluid theory, and if blade pressure distributions are calculated

in this manner the question has still to be settled as to how they should be modified to allow for viscous effects.

Axial-Flow Impellers

Axial-flow impellers offer the best prospects for a useful theoretical approach because extensive work has been carried out on aerofoils for the design of aircraft wings and propellers. If the simplified case of two-dimensional flow is first considered then wind-tunnel test data are available for a large number of aerofoil profiles, for example in Abbott et al. (61), these tests being carried out in flows of constant total pressure. A number of profiles have also been tested in water tunnels, and good agreement obtained in measurements of force and moment coefficients. Daily (21) reported tests on an NACA 4412 hydrofoil and some results on an NACA 16012 hydrofoil are included in Holl's paper (14). Reference can also be made to a series of papers by Numachi and others although space precludes more than a passing mention here.

While the NACA 4412 profile is not suitable for use in hydraulic machines because of its peaked pressure distribution, Dailey's tests are of interest because he measured the cavitation inception coefficient Ki and compared it with values predicted from wind tunnel measurements of the minimum pressure coefficient $(Cp)_{min}$. The results of this comparison are shown in fig. (4.6) where Ki is plotted against angle of incidence α, and the observed values of Ki are seen to agree quite well with the predicted values for $-2^\circ < \alpha < 7^\circ$. For angles of incidence outside this range, prediction from wind-tunnel tests gave conservative values of Ki. (In his paper Daily suggested that this discrepancy between the observed and predicted cavitation inception coefficients might have been due to small inaccuracies in the manufacture of the hydrofoil so that its profile departed from the correct form.) It will be noticed that there are two curves in fig. (4.6), one for incipient cavitation on the upper surface of the hydrofoil, the other for incipient cavitation on the lower. These two curves cross at $\alpha = 1.4^\circ$ when cavitation appears simultaneously on top and bottom surfaces. For any other value of α cavitation appears on one surface before the other.

The results of these tests confirm that wind-tunnel data can be used in hydrodynamics problems involving cavitation. The moving guide vanes in hydrodynaic machinery can broadly be divided into two classes : those operating at constant stream pressure, and those in a variable pressure field. The free-stream propeller is typical of the first class, and aerodynamic data can be applied more readily than in the case of pump impellers where the technique of extrapolating results obtained for constant pressure flows to variable pressure flows is not clear. Also interference effects due to adjacent blades and walls or shrouds have to be taken into account as well as three-dimensional effects such as radial flows within the impeller and, in the case of open impellers, secondary flows across the blade tips.

Returning to consideration of the aerofoil in two-dimensional-flow,

it should be noted that the problem of constructing the profile of an isolated aerofoil to give a specified pressure distribution has been solved, Peebles (62). The next step is to consider a two-dimensional cascade of aerofoils, noting that the properties of an aerofoil in a cascade can be appreciably modified by the presence of its neighbours if the space-chord ratio is less than about 1.5. A method of calculating the pressure distribution for inviscid incompressible flow through a given cascade has been proposed by Schlichting (63), see also Weinig (64). The inverse problem, i.e. the calculation of the blade profiles to be used to give a specified distribution in a cascade has been treated by a number of writers including Lighthill (65), Johnson (66) and Scholz (67).

The problem of transferring results for two-dimensional flows to three dimensional rotating impellers is discussed at length by Vavra (68). In general one can say that further information is required on the influence of blade aspect ratio, the existence of radial flows, the influence of blade rotation on the boundary layer, and on other matters concerning the nature of the flow through an axial impeller. However, Kovats and Desmur (69) and Wislicenus (70) have analysed the results of tests on axial-flow pumps and derived curves showing (c_L' / c_L) as a function of space-chord ratio and mean blade angle, c_L' being the lift coefficient of the isolated aerofoil in two-dimensional flow, and c_L its effective value when the aerofoil is used in the blades of an axial-flow impeller.

While the flow through an axial impeller is fully three-dimensional, in fact many successful designs have been evolved by making simplifying assumptions which reduce the problem to one in two-dimensions. It is worthwhile therefore examining two-dimensional blade profiles even if empirical corrections have to be applied later to enable the results of this examination to be used in design. The blade profile of an axial-flow impeller may be defined by

(1) The camber line.
(2) The position of the blade maximum camber.
(3) The blade maximum thickness.
(4) The position of the blade maximum thickness.
(5) The leading edge radius.
(6) The trailing edge radius.

Some of these variables may be determined by factors quite separate from hydrodynamics. Thus maximum thickness may be controlled by the allowable stress, and trailing edge radius dictated by manufacturing methods.

Blade profiles used in axial-flow impellers to give optimum cavitation performance should satisfy the following requirements.

(1) They should have smooth velocity and pressure distributions.
(2) Their pressure distributions should be insensitive to changes in angle of incidence.
(3) They should be easy to manufacture.

These requirements may conflict. The first suggests the use of one

of the low-drag series of aerofoils which have been specially designed to have flat pressure distributions, e.g. the NACA 6-series. Fig. (4.7) compares the velocity distributions on the upper and lower surfaces of a conventional aerofoil, NACA 4412, and a low-drag aerofoil, NACA 16-209. The second requirement applies if the impeller is to operate over a range of capacities in which case the blade incidence will vary. The performance of some profiles deteriorates markedly at high incidence. Fig. (4.8) compares the performance of two aerofoils and it is seen that the low-drag profile NACA 66-212 is superior to NACA 4412 only in the range of lift coefficients between 0 and 0.4. It may be noted that the 4412 aerofoil itself is quite sensitive to incidences: fig. (4.6) shows that at $\alpha = 10^{\circ}$ the value of Ki (for two-dimensional flow) is three and a half times its minimum value, while at $\alpha = -10^{\circ}$, $Ki/(Ki)_{min} = 3.1/0.7 = 4.4$. If the profile is to be insensitive to angle of incidence, the selection of the shape of its leading edge and tip radius become very important, although as pointed out by Carter (71) little work has been done on this aspect of blade design.

To obtain a profile with flat pressure distribution it is necessary to place the positions of maximum thickness and maximum camber well back, possibly near the mid-chord position or behind it. In practice blade profiles have often been selected on the basis of ease of manufacture, and one of the simplest from this point of view is that in the form of a segment of a circle. Wind-tunnel tests show that such profiles with suitable leading and trailing edge radii give reasonable lift-drag ratios, and since their maximum thickness is at mid-chord their cavitation performance can be expected to be satisfactory. Axial-flow pumps with "segmental" blade profiles have been built for many years and similar profiles are often used on ships' propellers.

The selection of blade profiles for axial-flow machines has been discussed by Carter (71) for pumps, fans, and compressors, and by Hutton (72) for Kaplan turbines. Implicit in the argument of both authors is acceptance of the fact that good designs of axial-flow pumps and turbines have been evolved, largely on an empirical basis. For example the firm of Escher-Wyss have reported (73) experiments with various blade profiles in Kaplan turbine runners, the liquid pressures on the blade surfaces being measured to ascertain which design gave the smoothest pressure distribution. But Carter and Hutton hope that a more fundamental approach can be made to the subject leading eventually to better designs by systematic analysis of the flow regimes in impellers and the logical selection of blade profiles for these regimes.

This discussion of axial-flow impellers would not be complete without reference to another form of cavitation which may appear in the vortices shed from the blade tips near the impeller periphery. This cavitation is associated with the high-velocity, low pressure cores of the trailing vortex system of the blade lifting surface. In its incipient state it does not give rise to damage of the impeller blades, but it may seriously affect the upstream entry to the diffuser. A recent paper by McCormick(74)

has studied this phenomenon which is, however, more often encountered in ships' propellers than in pumps. A complete analysis of it would consider overall impeller design, development of total head, blade circulation and the strength of the trailing vortices, subjects of intrinsic interest but extending beyond the scope of this thesis.

To sum up, the complex nature of the flow through a pump impeller gives rise to problems for which the mathematical answers are as yet unknown. While a number of partial solutions have been derived on the basis of perfect fluid theory, the simplifying assumptions made restrict the applicability of the results, since the mathematical model of the flow corresponds only approximately with the real state of affairs.

In practice, therefore, design for optimum cavitation performance rests on a semi-empirical basis : theory is used to derive the important parameters or coefficients describing the flow, the results of pump tests are analysed to determine values of these coefficients which are then used in the preparation of new designs.

4.3 SIMILARITY CONSIDERATIONS

4.3.1 Introduction

It is desired to predict the cavitation behaviour of a new impeller to meet given cavitation requirements. Such a prediction should be derived from the hydrodynamic theory of the flow through the impeller. However, as explained, the present knowledge of the actual flow conditions permits only an approximate theoretical description of them; the results of this theory are fragmentary and it is necessary to rely largely on experimental evidence.

As a first step conditions for similarity are established, that is, comparisons are made between machines with geometrically similar inlet passages and hydraulically similar flow conditions in these passages. To make use of similarity considerations tests must be carried out to determine the cavitation characteristics of existing impeller designs, these characteristics being expressed in a general non-dimensional form. The objective then is to derive suitable non-dimensional parameters to describe the flow at impeller entry, so that new designs may be compared with those already tested within the range of existing values of these parameters. In order to go beyong the range of existing data, it is necessary to formulate a semi-empirical theory which describes the mechanism of flow sufficiently well to allow extrapolation into untried fields. The development of such a theory forms the subject of the next section, (4.4).

4.3.2 Non-Dimensional Parameters.

The flow conditions in geometrically similar pumps are similar if the impeller and fluid velocities at similarly located points change from one

pump to another by a factor which is constant throughout the two pumps compared. The velocity diagrams computed from the rates of flow and the cross-sectional areas of the waterways and from the peripheral velocities of the rotating parts are therefore similar at similarly located points. This is the Kinematic condition for similarity and at the impeller inlet it requires that the velocity diagrams formed by the axial fluid velocity and the peripheral velocity of the impeller remains constant, i.e.,

$$\frac{v_a}{u} \left(\text{or } \frac{v_m}{u} \right) = \text{constant} \qquad (4.2)$$

No account will be taken of changes arising from the influence of viscosity and turbulence, that is of changes in Reynolds number. As the flow in pump impellers is always fully turbulent, the effects of changes in Reynolds number on flow patterns in the fluid stream are small, except perhaps in the immediate vicinity of the flow boundaries. Also in this discussion the surface roughness of the waterways is ignored as the effects of changes in relative roughness are usually of the second order of magnitude and in any case cannot be easily incorporated in the theory.

The net positive suction head Hsv is the difference between the total head at the point near the impeller eye where the suction head is measured and the static head in the region of cavitation (assumed to be equal to the vapour pressure). It follows that similarity of flow will be maintained if this head difference Hsv follows the same dynamic relation as the pump total head H, or for that matter any other head difference in the machine. The oldest method of meeting this requirement consisted of making Hsv proportional to H. This led to the Thoma law of similarity for cavitation in pumps (and turbines)

$$\sigma = \frac{Hsv}{H} = \text{constant} \qquad (4.3)$$

σ is the Thoma cavitation parameter, and according to this definition it should not be affected by changes in rotative speed; for this reason the results of cavitation tests are often presented in the form of performance characteristics placed against σ. It may be noted in passing that while σ has been found to be independent of speed in many tests, "speed effects" have been observed in some cases. For example, Wood et al. (46) recorded that σ increased at low speeds, less than half the design speed, and the author has occasionally noted similar effects. There appears to be a critical speed, usually about half the design speed, above which σ is not affected by speed changes. This observation may be explained by time effects in the cavitation process, as at the lower speed there is more time for potential cavitation bubbles to form in the liquid passing through the impeller.

The Thoma law of similarity is not the only method of applying similarity relations to hydrodynamic machines under cavitating conditions; it is equally permissible to introduce the net positive suction head Hsv into the dynamic relations. In accordance with the definition of similarity of flow conditions, all pressure or head differences inside geometrically

similar impellers will change proportionally as the square of the velocities so long as the flows remain similar. Hence the dynamic relations for similarity require that the ratio of the net positive suction head to the velocity head of entry fluid velocity in the impeller eye and to the velocity head of the peripheral velocity at the eye should remain constant, i.e.

$$\frac{Hsv}{\left(\frac{v_a^2}{2g}\right)} \quad \text{or} \quad \frac{Hsv}{\left(\frac{v_m^2}{2g}\right)} = \text{constant} \qquad (4.4)$$

$$\text{and} \quad \frac{Hsv}{\left(\frac{u^2}{2g}\right)} = \text{constant} \qquad (4.5)$$

The velocities in equations (4.4) and (4.5) can be expressed in terms of flow Q, rotational speed N, and eye diameter D, thus:

$$v_a = \frac{Q}{\frac{\pi}{4} D^2 (1 - \xi^2)}$$

$$u = \frac{\pi}{60} ND$$

so that

$$\frac{2g\, Hsv\, D^4 (1 - \xi^2)^2}{Q^2} = \text{constant}$$

and

$$\frac{2g\, Hsv}{N^2 D^2} = \text{constant}$$

when D is eliminated the condition is obtained

$$\frac{1}{\sqrt{1 - \xi^2}} \frac{NQ^{\frac{1}{2}}}{(Hsv)^{\frac{3}{4}}} = \text{constant} \qquad (4.6)$$

The non-dimensional group $\left\{ \frac{NQ^{\frac{1}{2}}}{(Hsv)^{\frac{3}{4}}} \right\}$ is the well-known suction specific speed and will be denoted by S. For impellers having shafts through their eyes or with hubs projecting forward into the eye, and an adjusted specific speed S^1 is introduced where from equation (4.6)

$$S^1 = \frac{S}{\sqrt{1 - \xi^2}} \qquad (4.7)$$

The suction specific speed prescribes combinations of operating conditions that permit similarity of flow in geometrically similar hydrodynamic machines. Its importance lies in the fact that it defines the conditions for similarity in terms of the operating variables only. Furthermore the objective of achieving optimum cavitation performance can now be expressed quantitatively by saying that the suction specific speed is required to be a maximum.

The non-dimensional parameters which can be used to describe the inlet flow to an impeller are listed below. Different writers have used different parameters and all are listed here for completeness. Also, various units have been used in the calculations of suction specific speed; the most common practice has been to express N in r.p.m., Q in cusecs, dimensions in feet, velocities in ft./sec., and heads in feet. These units will be used in this thesis.

Inlet flow coefficient (ϕ) :

$$\phi_a = \frac{v_a}{u} \qquad \phi_m = \frac{v_m}{u}$$

Cavitation coefficient (K) :

$$K_a = \frac{H_{sv}}{\left(\frac{v_a^2}{2g}\right)} \qquad K_m = \frac{H_{sv}}{\left(\frac{v_m^2}{2g}\right)} \qquad K_u = \frac{H_{sv}}{\left(\frac{u^2}{2g}\right)} \qquad (4.8)$$

Suction specific speed (S) :

$$S = \frac{NQ^{1/2}}{H_{sv}^{3/4}} \qquad S' = \frac{S}{\sqrt{1-\xi^2}}$$

The following important relations have already been established or follow immediately from these definitions.

$$Q = v_a \frac{\pi}{4}(D^2 - D_h^2) = \frac{\pi}{4} v_a D^2 (1-\xi^2)$$

$$Q = v_m b \left(\pi d - \frac{zt}{\sin \beta_{ave}}\right) \qquad (4.9)$$

$$u = \frac{\pi N D}{60}$$

$$\phi_a = 24.3 \left(\frac{1}{1-\xi^2}\right)\left(\frac{Q}{N}\right)\left(\frac{1}{D^3}\right)$$

$$\phi_m = f_1 \phi_a \quad \text{where } f_1 = v_m / v_a \qquad (4.10)$$

$$K_u = \phi_a^2 K_a = \phi_m^2 K_m$$

$$S' = 384.5 \frac{\phi_a^{1/2}}{K_u^{3/4}} = 384.5 \frac{1}{\phi_a K_a^{3/4}}$$

$$S' = \frac{384.5}{f_1^{1/2}} \cdot \frac{\phi_m^{1/2}}{K_u^{3/4}} = \frac{384.5}{f_1^{1/2}} \cdot \frac{1}{\phi_m K_m^{3/4}} \qquad (4.11)$$

The Thoma cavitation parameter can be expressed in terms of the suction specific speed S and the performance specific speed N_s, thus

$$\sigma = \left(\frac{N_s}{S}\right)^{\frac{4}{3}} \qquad (4.12)$$

For impeller design it is necessary to establish the relationship between either the cavitation coefficient or the suction specific speed and the flow coefficient for conditions of incipient cavitation : once this has been done the designer can determine ϕ_a and fix the inlet diameter using equation (4.10). He assumes f_1 to obtain ϕ_m and constructs the inlet velocity triangles from which he derives values of β ; a check is then made that the value assumed for f_1 is correct.

4.4 CENTRIFUGAL IMPELLERS - PART I.

4.4.1 Theory

A theory of the entry flow in an impeller under cavitating conditions should consist of a quantitative explanation of the pressure drop from the pump inlet to the region of cavitation. First consider an impeller operating at its designed inlet condition; the absolute velocity of the liquid approaching it is assumed to be wholly axial with no rotational component, there is no "pre-rotation".

The theory to be developed here is based on the following simple equation for the net positive suction head.

$$H_{sv} = K_o \frac{v_a^2}{2g} + \Delta h \qquad (4.13)$$

The first term on the right hand side describes the pressure drop due to the axial fluid velocity in the eye of the impeller, i.e. the pressure drop that occurs independent of the influence of the impeller blades. The coefficient K_o is larger than unity and is introduced to account for local increases in the absolute through-flow velocity over the mean velocity v_a, and to allow for any losses between the pump inlet and the impeller eye.

The second term expresses the pressure drop that is due to the presence of the blades. It may be expected to vary in proportion to the square of the maximum velocity of the fluid relative to the blade inlets. This velocity is determined by the relation $w^2 = v_a^2 + u^2$ so that

$$\Delta h = K \frac{w^2}{2g} = K \frac{v_a^2 + u^2}{2g}$$

The coefficient K corresponds to the blade minimum pressure coefficient. Its value depends on the control of the liquid flow into the impeller, and is higher for vane systems giving comparatively large flow deflections and having small radii of curvature, factors which give rise to large local underpressures on the blade surfaces.

From equation (4.13),

$$H_{sv} = (K_o + K)\frac{v_a^2}{2g} + K\frac{u^2}{2g}$$

$$\therefore \quad H_{sv} = K_{1a}\frac{v_a^2}{2g} + K\frac{u^2}{2g} \qquad (4.14)$$

$$\text{where} \quad K_{1a} = K_o + K$$

If the velocity v_m is considered instead of v_a

$$H_{sv} = K_{1m}\frac{v_m^2}{2g} + K\frac{u^2}{2g} \qquad (4.14)$$

Division by $\frac{u^2}{2g}$ yields

$$K_u = K_{1a}\phi_a^2 + K$$

$$\text{or} \quad K_u = K_{1m}\phi_m^2 + K \qquad (4.15)$$

$$\text{where} \quad K_{1a} = f_1^2 K_{1m}$$

It can be readily established also that

$$K_a = K_{1a} + \frac{K}{\phi_a^2}$$

and $$K_m = K_{1m} + \frac{K}{\phi_m^2} \qquad (4.16)$$

The derivation of these equations is discussed in greater detail in Appendix I.

Equations (4.11) and (4.15) can now be used to express the suction specific speed as

$$S^1 = \frac{384.5}{\phi_a\left(K_{1a} + \frac{K}{\phi_a^2}\right)^{3/4}}$$

and $$S^1 = \frac{384.5}{f_1^{1/2}\phi_m\left(K_{1m} + \frac{K}{\phi_m^2}\right)^{3/4}} \qquad (4.17)$$

If the K_1's and K are assumed to be constants independent of ϕ, the suction specific speed has now been expressed as a function of the flow coefficient. From analysis of existing pump test data it is possible to determine K_{1a}, K_{1m} and K for a wide range of impeller designs. Fig. (4.9) shows S^1 plotted against ϕ_a for typical values of K_{1a} and K. It is clear that for given K_1 and K there is an optimum value of the flow coefficient which leads to maximum suction specific speed and thus to best cavitation performance.

For the time being the flow coefficient ϕ_a is preferred to ϕ_m as it is of more direct use to the designer. It is clear from equation (4.17) that ϕ_a will have its optimum value when the expression $\phi_a\left(K_{1a} + K\phi_a^{-2}\right)^{3/4}$ is a minimum. If this expression is differentiated with respect to ϕ_a holding K_{1a} and K constant and the result equated to zero, it is found that

$$(\phi_a)_{opt} = \sqrt{\frac{K}{2K_{1a}}} \qquad (4.18)$$

Then $$S^1_{max} = \frac{239}{\sqrt[4]{K^2 K_{1a}}} \qquad (4.19)$$

Fig.(4.10) has been drawn to show how S^1_{max} and $(\phi_a)_{opt}$ depend on the coefficients K_{1a} and K.

When $(\phi_a)_{opt}$ has been determined the optimum eye diameter can then be calculated from equation (4.10).

$$D_{opt} = 2.90\left\{\sqrt{\frac{2K_{1a}}{K}}\left(\frac{Q}{N}\right)\left(\frac{1}{1-\xi^2}\right)\right\}^{1/3} \qquad (4.20)$$

The same result is obtained by using equation (4.14) to express Hsv in terms of D and putting $\frac{d\,Hsv}{d\,D} = 0$.

The simplest way of handling equation (4.20) is to calculate D opt for $\xi = 0$ (overhung impeller) and then to apply the following correction.

For	ξ =	0	0.1	0.2	0.25	0.3	0.4	0.5
increase	D by	0	0.3%	1.4%	2.2%	3.0%	6.0%	10.0%

Consider now the case where pre-rotation is present in the flow approaching the impeller so that the absolute velocity v of the liquid has a rotational component u_p in the direction of rotation of the impeller. Assuming that the axial velocity of approach is constant across the inlet, the inlet velocity diagram for the blade tip takes the form shown in fig.(4.5) and it follows in a manner similar to equation (4.14) that

$$Hsv = K_o \frac{v^2}{2g} + K \frac{w^2}{2g}$$

$$\therefore Hsv = K_o \frac{1}{2g}(v_a^2 + u_p^2) + K \frac{1}{2g}\{v_a^2 + (u - u_p)^2\}$$

$$= (K_o + K)\frac{1}{2g}(v_a^2 + u_p^2) + K \frac{u^2}{2g}\left(1 - \frac{2u_p}{u}\right)$$

$$\therefore Hsv = K_{1a} \frac{1}{2g}(v_a^2 + u_p^2) + K \frac{u^2}{2g}\left(1 - \frac{2u_p}{u}\right)$$

$$\therefore Ku = K_{1a}(\phi_a^2 + \epsilon^2) + K(1 - 2\epsilon) \qquad (4.21)$$

where $\epsilon = \dfrac{u_p}{u}$

$$\therefore S^1 = \frac{384.5\ \phi_a^{1/2}}{\{K_{1a}(\phi_a^2 + \epsilon^2) + K(1 - 2\epsilon)\}^{3/4}} \qquad (4.22)$$

When this result is compared with equation (4.17) it is seen that the denominator has been reduced by an amount

$$(2K\epsilon - \epsilon^2 K_{1a})^{\frac{3}{4}}$$

Clearly ϵ must be less than $2K/K_{1a}$. In fact for the greatest increase in S^1, the expression $(2K\epsilon - \epsilon^2 K_{1a})$ must be a maximum. Hence, according to this analysis the optimum value of ϵ is K/K_{1a}; when ϵ has this value

$$S^1 = \frac{384.5\ \phi_a^{\frac{1}{2}}}{\left(K_{1a}\phi_a^2 + K - \frac{K^2}{K_{1a}}\right)^{3/4}}$$

By differentiating again the new values of $(\phi_a)_{opt}$ and S^1_{max} are found.

$$(\phi_a)_{opt} = \sqrt{1 - \frac{K}{K_{1a}}}\ \sqrt{\frac{K}{2K_{1a}}} \qquad (4.23)$$

$$S^1_{max} = \frac{1}{\sqrt{1 - \frac{K}{K_{1a}}}}\ \frac{239}{\sqrt[4]{K^2 K_{1a}}} \qquad (4.24)$$

Thus the values previously obtained are modified by the factor $\sqrt{1 - \frac{K}{K_{1a}}}$. For the values of K and K_{1a} found in practice this factor lies between 0.89 and 0.93, so that the maximum increase in S1 predicted by this analysis is about 10%. In fact designing impellers for pre-rotation is found to give considerably higher increase in suction specific speed, indicating that this simple theory is inadequate.

It is necessary therefore to modify this simple theory by recognising

that a flow with pre-rotation can be expected to have a non-uniform velocity distribution in which v_a (or v_m) varies with radius. To carry this investigation further in a form amenable to theoretical attack, assume that the pre-rotation is produced by a stationary axial vane system with irrotational inflow. For the flow of a perfect incompressible fluid leaving this vane system Smith et al. (75) have established that

$$u_p\left(\frac{\partial u_p}{\partial r} + \frac{u_p}{r}\right) + v_a \frac{\partial v_a}{\partial r} = 0 \qquad (4.25)$$

Here v_a and u_p are the axial and circumferential components of the absolute fluid velocity approaching the impeller at radius r. Following Wislicenus (10) it is further assumed that the rotation of the liquid has the form of solid body rotation in which u_p is proportional to radius, i.e.,

$$\frac{u_p}{u_{p_o}} = \frac{r}{r_o}$$

where the subscript "0" denotes conditions at the outermost radius. A coefficient λ is introduced which assists the development of the mathematics at a later stage.

$$\lambda = \frac{u_{p_o}}{v_{a_o}}$$

Substitution for u_p and $\frac{\partial u_p}{\partial r}$ in equation (4.25) gives

$$2r\left(\frac{u_{p_o}}{r_o}\right)^2 + \frac{\partial\left(\frac{1}{2}v_a^2\right)}{\partial r} = 0$$

$$\therefore\ v_a^2 = -2\left(\frac{u_{p_o}}{r_o}\right)^2 r^2 + \text{constant}$$

$$\therefore\ v_a^2 = v_{a_o}^2 + 2u_{p_o}^2\left(1 - \frac{r^2}{r_o^2}\right)$$

$$\therefore\ v_a^2 = v_{a_o}^2\left\{1 + 2\lambda^2\left(1 - \frac{r^2}{r_o^2}\right)\right\} \qquad (4.26)$$

Now ϕ_a is defined as $(v_a)_{ave} / u$ and

$$(v_a)_{ave} = \frac{1}{r_o^2}\int_o^{r_o} v_a\, dr^2$$

$$= \frac{v_{a_o}}{r_o^2}\int_o^{r_o}\left(1 + 2\lambda^2 - \frac{2\lambda^2}{r_o^2}r^2\right)^{1/2} dr^2$$

$$\therefore\ \frac{(v_a)_{ave}}{v_{a_o}} = -\frac{1}{3\lambda^2}\left[\left(1 + 2\lambda^2 - \frac{2\lambda^2}{r_o^2}r^2\right)^{3/2}\right]_o^{r_o}$$

$$\therefore\ \frac{v_{a_o}}{(v_a)_{ave}} = \frac{3\lambda^2}{(1+2\lambda^2)^{3/2} - 1} = f(\lambda) \qquad (4.27)$$

The energy equation applied to conditions at the tips of the blade inlets in a manner similar to that for equation (4.21) yields

$$\text{Hsv} = K_{1a}\frac{1}{2g}\left(v_{a_o}^2 + u_{p_o}^2\right) + K\frac{u^2}{2g}\left(1 - \frac{2u_{p_o}}{u}\right)$$

$$\therefore\ \text{Ku} = K_{1a}\frac{v_{a_o}^2}{u^2}\left(1 + \frac{u_{p_o}^2}{v_{a_o}^2}\right) + K\left(1 - 2\frac{u_{p_o}}{v_{a_o}}\cdot\frac{v_{a_o}}{u}\right)$$

$$\therefore\ \text{Ku} = K_{1a}(1+\lambda^2)\left\{f(\lambda)\right\}^2\phi_a^2 + K\left\{1 - 2g(\lambda)\phi_a\right\} \qquad (4.28)$$

where $g(\lambda) = \lambda f(\lambda)$.

The suction specific speed is thus given by

$$S^1 = \frac{384.5}{\phi_a \left[K_{1a} (1+\lambda^2) \{f(\lambda)\}^2 + \frac{K}{\phi_a^2} \{ 1 - 2\, g(\lambda)\, \phi_a \} \right]^{3/4}} \qquad (4.29)$$

The functions $f(\lambda)$, $g(\lambda)$ and $(1+\lambda^2)\{f(\lambda)\}^2$ are plotted in fig. (4.11).

Although equation (4.29) looks unwieldy it is possible to make some simple deductions from it by observing from fig. (4.11) that

$$(1+\lambda^2)\{f(\lambda)\}^2 \simeq 1$$

When this approximation is made,

$$S^1 = \frac{384.5}{\phi_a \left\{ K_{1a} - \frac{2K\, g(\lambda)}{\phi_a} + \frac{K}{\phi_a^2} \right\}^{3/4}} \qquad (4.30)$$

The value of ϕ_a which makes S^1 a maximum can then be shown to be

$$(\phi_a)_{opt} = \frac{K}{4K_{1a}} g(\lambda) + \sqrt{\frac{K}{2K_{1a}} + \left\{ \frac{K}{4K_{1a}} g(\lambda) \right\}^2} \qquad (4.31)$$

As will be seen later values obtained in practice for K and K_{1a} are such that

$$\frac{K}{4K_{1a}} g(\lambda) \simeq 0.025.$$

The value of $(\phi_a)_{opt}$ given by equation (4.31) is somewhat higher than $\sqrt{K/2K_{1a}}$, the value previously obtained for conditions without pre-rotation.

One can use equations (4.17) and (4.30) to show that for a given ϕ_a the ratio by which the suction specific speed can be increased by using pre-rotation is approximately

$$P = \left\{ \frac{K_{1a} + \frac{K}{\phi_a^2}}{(K_{1a} + \frac{K}{\phi_a^2}) - \frac{2K\, g(\lambda)}{\phi_a}} \right\}^{3/4}$$

$$\therefore \quad P = \frac{1}{\left\{ 1 - \frac{2K\, g(\lambda)}{K_{1a}\phi_a^2 + K}\, \phi_a \right\}^{3/4}}$$

Now if $\phi_a = \sqrt{K/2K_{1a}}$ which is close to the optimum value predicted by this theory,

$$P = \frac{1}{\left\{ 1 - \frac{4}{3} g(\lambda) \sqrt{\frac{K}{2K_{1a}}} \right\}^{3/4}}$$

For the case $\phi_a = \sqrt{\frac{K}{2K_{1a}}} = 0.25$ this further reduces to

$$P = \frac{1}{\left\{ 1 - \frac{1}{3} g(\lambda) \right\}^{3/4}} \qquad (4.32)$$

The graph of P versus λ has been drawn in Fig. (4.12). This shows that for $\lambda = 1.0$ the predicted increase in suction specific speed is 23% and for $\lambda = 2.0$ it is 32%. For $\lambda > 2$ the rate at which P increases becomes progressively less and little advantage is to be gained by having λ greater than 2 .

Fig. (4.13) shows the variation of suction specific speed with flow coefficient, calculated from equation (4.29). Curves have been drawn for

the cases λ = 0, & 2 ; K = 0.1, 0.2, 0.3 ; K_{1a} = 1.2 + K. The influence of the pre-rotation coefficient λ is clearly demonstrated.

4.4.2 Experimental Evidence

Several writers have recommended values of the coefficients K and K_1 for use in design. These are tabulated below, and except as noted for Gongwer's results they apply for conditions at inception of cavitation.

AUTHOR	K	K_{1a}	K_{1m}	REMARKS
Gongwer (47)	0.23	1.80		inception
	0.085	(1.40 + K)		breakdown
Pfleiderer (53)	0.25 - 0.35		(1.1 - 1.3+K)	
Kovats (69)	0.16 - 0.30		(1.1 + K)	
Balje (76)	0.20 - 0.35	(1.2 + K)		
Wislicenus (55)		(1.1 + K)		thought optimistic.

Gongwer's results were obtained as a result of extensive cavitation tests on sixteen Francis impellers at the California Institute of Technology. Where other writers have recommended a range of values for K , the lower values apply to impellers of lower specific speed.

The author has conducted and analysed cavitation tests on a number of centrifugal pumps and the results of this work are presented in the table below, together with the results of analysis of the published data of Wood et al. (46) and Bowerman (77).

IMPELLER			GENERAL					CAVITATION PERFORMANCE						COMMENTS	
ITEM	TYPE	POSITION OF INLET	N_s	$\frac{r_s}{D}$	$\frac{A}{D}$	ξ	Z	ϕ_a	S	S'	K_u	SUGGESTED K_{1a}	SUGGESTED K	DESIGNED FOR PRE-ROTATION	VELOCITY - vm DISTRIBUTION
F_1	Francis	Side	46	0.21	0.46	0.523	5	0.370	335	390	0.507	1.80	0.26	No	Pfleiderer
F_2	"	"	57	0.17	0.30	0.463	5	0.156	580	655	0.143			Yes	constant
F_3	"	End	62	0.22	0.51	0	4	0.259	400	400	0.384	1.80	0.26	No	Pfleiderer
F_4	"	Side	71	0.23	0.43	0.488	5	0.243	430	493	0.281	1.60	0.19	No	Pfleiderer
F_5	"	"	74	0.23	0.41	0.451	5	0.274	393	440	0.354	1.80	0.23	No	Pfleiderer
F_6	"	"	74	0.24	0.42	0.415	4	0.252	405	445	0.331	1.80	0.22	No	constant
F_7	"	End	130	0.22	0.55	0	6	0.293	430	430	0.381	1.80	0.23	No	constant
F_8	"	"	136	0.28	0.53	0	6	0.298	415	415	0.407	1.80	0.25	No	Pfleiderer
M_1	Mixed Flow	"	214	0.71	-	0.153	3	0.343	470	480	0.365	1.60	0.18	No	Pfleiderer
M_2	"	"	393		-	0.355	6	0.413	383	410	0.512	1.70	0.22	No	constant
M_3-A	"	"	-	0.67	-	0.208	6	0.294	635	650	0.218			No	constant
-B	"	"	-	0.67	-	0.208	5	0.272	665	680	0.197			No	constant
-C	"	"	-	0.67	-	0.208	4	0.273	645	660	0.205			No	constant
A_1	Axial Flow	"	427		-	0.600	2	0.284	300	375	0.448	1.80	0.30	No	constant

In all the author's tests care was taken to maintain a reasonable standard of accuracy. Flow was measured by orifice plate strictly in accordance with B.S. 1042, inlet pressure by mercury manometers from tappings in the straight length of horizontal pipe adjoining the pump suction flange, rotative speed by calibrated tachometer checked by "Strobotac". A typical test rig is shown diagrammatically in fig. (4.14); the pump in which the impeller is installed is driven either by Heenan and Froude swinging frame dynamometer or by calibrated electric motor. Fig. (4.2) illustrates a typical set of results, plotted non-dimensionally. Bearing in mind that difficulty is sometimes experienced in defining precisely the point of cavitation inception, it is considered that the values of suction specific speed given in the above table are accurate to within $\pm$ 3%. It is interesting to note that in the case of impeller "F4" two series of cavitation tests were carried out at an interval of three and a half years, and the results agreed to within 1%, showing a high degree of repeatability.

After examination of this evidence the following comments can be made.

(1) Of the group of eight Francis impellers seven were designed for no pre-rotation in the approach flow. Although the specific speed of these seven impellers varies from 46 to 136 (cosec units), the suction specific speed remains fairly constant at a value near 400; the inlet geometry represented by the ratios $\frac{r_s}{D}$ and $\frac{A}{D}$ does not vary greatly. There is little difference in cavitation performance between impellers designed for uniform approach velocity and those designed to conform to a potential flow distribution.

(2) For these seven Francis impellers, values of K and K_{1a} for inception of cavitation can be assumed which agree closely with those formed by Gongwer, namely,

$$K = 0.23 \quad ; \quad K_{1a} = 1.80.$$

(3) The performance of impeller "F_2" shows the marked improvement which can be obtained by designing for pre-rotation in the entry flow. This impeller was designed in accordance with a method to be discussed in section (4.5), but it may be noted at this stage that the observed increase in suction specific speed is 10% higher than that predicted by equation (4.29) if K_{1a} and K are taken as 1.80 and 0.23 respectively.

(4) The mixed-flow impellers "M_1" and "M_2" follow the same trends as the Francis impellers although the values of K and K_{1a} are slightly lower. However the impellers "M_3" - A, B and C described by Wood et al. (46) have significantly better performance. These impellers were designed on the assumption of no pre-rotation in the approach flow; velocity traverses made during the cavitation tests showed that in fact the pre-swirl was small, always less than 2° and usually less than 1°. In his paper Wood compares the performance of his impellers at cavitation breakdown and shows that the results are in reasonable agreement with those of Gongwer, with $K = 0.085$ and $K_{1a} = 1.485$. However, at their design points the Wood impellers have a narrower cavitation region.

Thus

$$(S\ b.d.)\ \text{Wood} \simeq (S\ b.d.)\ \text{Gongwer}$$

$$\text{but}\quad (S\ i\ )\ \text{Wood} > (S\ i\ )\ \text{Gongwer}$$

Unfortunately, Wood does not give explicit values of the suction specific speed corresponding to incipient cavitation. The values quoted here have been calculated from graphical data in his paper and their accuracy is limited to $\pm$ 5% because of the small scales on these graphs. While not conclusive this evidence does indicate that impellers designed by the methods of Hamrick et al. (60) give superior suction performance, higher suction specific speeds being possible before pump head and efficiency begin to deteriorate.

4.4.3 Applications to Design.

From this examination of the experimental evidence it can be concluded that for many Francis and mixed-flow impellers, inlet design for specified cavitation performance without pre-rotation can be based on the use of the coefficients K and K_{1a}, where

$$K = 0.23 \quad , \quad K_{1a} = 1.80.$$

This method is not precise because of the observed variations in these coefficients. For example, K varies from 0.19 to 0.26 which is sufficient to give an overall change in suction specific speed of 10%. However if these values are adopted, the optimum value of the inlet flow coefficient without pre-rotation is then

$$(\phi_a)_{opt} = \sqrt{\frac{0.23}{3.60}} = 0.252$$

whence

$$D_{opt} = 4.58\left\{\left(\frac{Q}{N}\right)\left(\frac{1}{1-\xi^2}\right)\right\}^{1/3} \qquad (4.33)$$

and

$$S^1_{max} = 430$$

From the observation that suction specific speed remains constant for a wide range of specific speeds it follows from equation (4.12) that

$$\sigma \propto N_s^{4/3}$$

This result has been plotted graphically in fig. (4.15).

Return now to fig. (4.13) showing suction specific speed versus flow coefficient. On this diagram are marked values of suction specific speed which have been observed in practice. In certain special types of condensate and process pumps very high values of S^1 are obtained by allowing the impellers to operate with cavitating flows. If these exceptional cases are ignored it is clear that the values of S^1 that can be achieved without cavitation are sufficiently high for some pre-rotation to be present in the impeller entry. In an attempt to develop a theory which would describe the effects of pre-rotation quantitatively equations (4.21) to (4.32) were derived. However, study of the Francis "F_2" impeller shows that this theory underestimates by 10% the increase that can be obtained in the suction specific speed. Also it predicts too high a value for $(\phi_a)_{opt}$, leading to velocity triangles which differ in shape from those which have

been found in practice to give successful designs.

This gap between theory and practice has led to the development of alternative, more empirical, methods of design such as that to be presented in the next section. Nevertheless this discussion has been useful in examining the subject of impeller inlet design and defining possible limits of performance.

4.5 CENTRIFUGAL IMPELLERS - PART II.

4.5.1 Introduction.

The suction specific speed can be written

$$S^1 = \left(\frac{384.5}{f_1^{\frac{1}{2}}}\right)\left(\frac{1}{\phi_m \, K_m^{\frac{3}{4}}}\right) \qquad (4.11)$$

As a basis for design it is necessary to obtain a relation between S^1 and ϕ_m. In what follows an empirical relation is established expressing the coefficient K_m as a function of S^1 and ϕ_m

$$K_m = f(\phi_m, S')$$

A design can then be prepared using this relation in conjunction with equation (4.11).

4.5.2 Design Procedure

The method of impeller inlet design to be discussed here is based on a recent paper by Stepanoff and Stahl (78). It is first necessary to define certain additional factors introduced by these writers. The cavitation coefficient is

$$K'_m = \frac{Hsv}{\left(\frac{v_m'^2}{2g}\right)} \qquad (4.34)$$

where v_m' is the meridional velocity at the impeller inlet when the blade thickness is ignored, i.e.

$$v_m' = \frac{Q}{\pi d b}$$

and

$$\phi_m' = \frac{v_m'}{u}$$

The inlet velocity diagram has been drawn in fig. (4.16) which also shows the geometry of the impeller inlet. As before attention is confined to the blade tips, the region most susceptible to cavitation. Unfortunately, Stepanoff and Stahl define their cavitation and flow coefficients in terms of v_m' and do not use v_m so it is not easy to make a direct comparison between their data and those of other writers. They use an experimental factor R by which v_m' is multiplied to allow for the effects of vane interference and any leakage flow being recirculated by the impeller. Thus

$$\tan\beta = R\,\frac{v_m'}{u} = R\,\phi_m'$$

$$\text{or} \quad R = \frac{\tan\beta}{\phi_m'} \qquad (4.35)$$

In normal impeller design for best efficiency, zero incidence angle and no pre-rotation, R can vary from 1.15 for end inlet to 1.25 for pumps with "side elbow" inlet.

As Stepanoff and Stahl point out, it is a well-established fact that low N P S H values are obtained with impellers having small inlet angles and hence also large eye diameters. However, the minimum practical value of β is about 15° as it is usually found that at angles smaller than 15° N P S H is not further reduced and the efficiency is impaired. For small pumps the minimum value of β may be slightly higher, say 18°.

With β set at its minimum value further reduction in N P S H is possible by decreasing the meridional velocity v_m and increasing the eye diameter. This means that a higher value of R is used : R = 1.80 is quite common and R = 2.0 is occasionally found in low N P S H pumps. In effect the impeller inlet is then designed to suit a larger pump and is operated at partial capacities. Thus high values of R are selected to give low N P S H but this is done by making some sacrifice in efficiency.

To relate the eye diameter to the impeller blade inlet a coefficient f_2 is defined (analogous to f_1 in section (4.4)).

$$f_2 = \frac{v_m'}{v_a} = \frac{D^2 (1 - \xi^2)}{4\, db} \qquad (4.36)$$

In practice f_2 can vary widely from 0.8 to 1.20, common values being 0.9 for single stage pumps and 0.8 for multi-stage pumps. Then,

$$\frac{S}{\sqrt{1-\xi^2}} = \frac{384.5}{f_2^{\frac{1}{2}}} \frac{1}{\phi_m' (K_m')^{3/4}} = \frac{384.5}{f_2^{\frac{1}{2}}} \frac{R}{\tan\beta} \frac{1}{(K_m')^{3/4}} \qquad (4.37)$$

Equation (4.37) connects the impeller inlet design elements (β, R, ξ , f_2) with the cavitation characteristics of the impeller (S, K_m').

K_m' is now related to ϕ_m' and S' by a multiplier M where

$$K_m' = \frac{M}{\phi_m'}$$

Equation (4.37) can then be written

$$S' = \frac{384.5\, (K_m')^{\frac{1}{4}}}{f_2^{\frac{1}{2}}\, M}$$

$$\text{or } S' = \frac{384.5\, (\phi_m')^{\frac{1}{4}}}{f_2^{\frac{1}{2}}\, M^{\frac{3}{4}}} \qquad (4.38)$$

As a result of an extensive analysis of experimental data for single and multi-stage pumps Stepanoff and Stahl derived their criterion for the inception of cavitation in centrifugal impellers,

$$S' M = 615 \qquad (4.39)$$

which applies for $S' > 300$.

The use of this criterion in conjunction with equation (4.38) yields the following design equations.

$$\frac{K'_m}{f_2^2} = 6.50$$

$$S' \phi'_m f_2^2 = 94.5 \quad (S' > 300) \qquad (4.40)$$

A short calculation will indicate the suction specific speeds predicted by this method. For example, some designers recommend that f_2 be unity, and if β and R are given typical values, say 16° and 1.80 respectively, then

$$\phi'_m = 0.159$$

and

$$S' = 595 .$$

The procedure to be adopted in designing an impeller for best cavitation performance when handling a given quantity Q of liquid is as follows.

(1) Select β and R .
Usually $\beta_{min} = 15^\circ$ and R = 1.80 approximately; ϕ'_m is calculated from equation (4.35).

(2) Assume ξ and f_2 from previous experience of the geometry of centrifugal impellers.

(3) Use the criterion $S'M = 615$.
K'_m and S' can then be determined from equation (4.40).

(4) Calculate S from equation (4.8).
If the impeller speed is given the minimum N P S H can then be determined. Alternatively, if N P S H is given, the maximum speed is found, also from equation (4.8).

(5) Calculate v'_m and u , using equations (4.34) and (4.35).

(6) Calculate D and v_a from equation (4.9).

(7) Check that the final values of ξ and f_2 agree with the original assumptions, if not repeat these calculations until satisfactory agreement is obtained.

It will be seen that the crucial stage in this design procedure is the use of the cavitation criterion, equation (4.39). While there are a large number of existing designs to support its use, there is nevertheless sufficient scatter in the experimental results to limit the accuracy obtainable. Besides, a number of design elements have not been included in this discussion, e.g. the form of the impeller approach passage, the number of impeller blades, and the surface finish of the blades. Stepanoff and Stahl therefore suggest that a tolerance of 10% should be allowed when estimating N P S H by this procedure.

4.6 AXIAL-FLOW IMPELLERS

In the present state of development of the axial-flow pump, the impeller consists of a few vanes disposed radially outward from a cylindrical hub and rotating in a cylindrical duct. The number of vanes seldom exceeds five and the vane width is comparable with the hub diameter. In most cases the vanes do not overlap, the solidity is low, and it has been customary to use simple aerofoil theory for the design of the vane camber and attitude, see for example O'Brien and Folsom (79), Pfleiderer (53). It is assumed that each circumferential strip of the vane behaves as if it were part of an infinitely long straight wing of uniform section in a linear flow which is defined in magnitude and direction by the relative velocity at the strip. For the infinite wing it is possible to calculate the pressure distribution over the aerofoil, and the results of such calculations are in satisfactory agreement with experimental data. The question arises as to whether it is possible to calculate the pressure distribution around an element of the blade of an axial-flow impeller, bearing in mind that the attitude of the aerofoil, its chord length, and the relative velocity vary continuously along the radius from the hub to the duct wall.

Morelli and Bowerman (80) carried out tests on axial-flow impellers designed by conventional aerofoil methods, and measured the blade pressure distributions. Unfortunately, their paper gives only a brief comparison between measured and calculated values; fig. (4.17) taken from the paper shows that the agreement obtained was reasonable but not close. Similar experiments have been carried out by Kamimoto et al. (81) on axial-flow turbine runners.

In the discussion in section (4.2) reference was made to attempts to refine the theory in order to give a mathematical model which corresponds more closely to the actual state of affairs. Improved theories have been developed which give closer predictions of real performance but this has only been done at the expense of considerable mathematical complication. Bowerman (77), for example, uses perfect fluid theory to determine the corrections that should be applied to the characteristics of two-dimensional aerofoil sections when they are subjected to the influence of the cylindrical boundaries of an axial-flow pump and when there are mutual interference effects between the blades. While other attempts have been made to account for interference based on calculations of simple cascades of aerofoils in two dimensions, Bowerman uses corrections based on a three-dimensional model, the blades being treated as spokes of a wheel. This work is of particular interest here because he designs for optimum cavitation performance on the assumption that the blade pressure distribution can be closely predicted by the correction process developed. In order to produce a pump with best overall cavitation performance he proposes that all blade sections should be made equally susceptible to to cavitation.

The optimizing analysis then affords the first step in the design procedure by permitting proper choice of the blade section coefficients, the number of blades and their approximate geometry, and the speed of operation. The interference corrections are applied to determine the finished shapes of the blade sections.

There is no space to enter into details of Bowerman's theory, but his tests on an impeller designed by this method can be discussed briefly. This impeller had two blades, each with symmetrical parabolic camber lines (N A C A series 65) and series 16 thickness function, this combination being chosen to give a smooth pressure distribution. The measured head and quantity at the maximum efficiency point were close to their design values, and the measured cavitation parameter σ_i was 1.6, slightly better than the calculated value of 1.7 . σ_i was found to be very nearly constant with radius. These results are encouraging but tests on one impeller are hardly adequate to confirm the value of Bowerman's design.

The methods of the preceding sections (4.4) and (4.5) can be extended to include axial-flow impellers. Thus in section (4.4) the impeller designated M_2 is a high specific speed mixed-flow design, very close to a fully axial impeller. In this case the values calculated for the coefficients K and K_1 are fairly close to those for Francis impellers. They may be compared with Kovats' recommendation (69) for axial-flow impellers :

$$K_1 = 1.25 \; ; \quad K = 0.25$$

$$\text{whence} \quad D_{opt} = 4.25 \left(\frac{Q}{N} \cdot \frac{1}{1 - \xi^2} \right)^{\frac{1}{3}} \text{ ft.}$$

This value of D_{opt} might have to be modified if it is found to give too high a peripheral speed with excessive blade stresses.

Stepanoff and Stahl (78) have examined evidence published from several sources for high specific-speed axial flow pumps and inducers. They found that their cavitation criterion still held fairly well, although impellers with uniform straight inlets performed better than those with bellmouth entries, the latter leading to higher local velocities.

The data given by Bowerman for his impeller have been analyzed by the author and the results entered into the table in section (4.4) in the row marked impeller "A_1". It is seen that the coefficients K and K_1 are somewhat higher than for the other impellers but not unduly so. If the S'M criterion is applied to the Bowerman impeller it is found that S'M = 595 ; this is within $3\frac{1}{2}\%$ of the stated figure of 615. The cavitation tests reported by Horie and Kawaguchi (82) for an axial-flow pump also show good agreement with this criterion which can therefore be used as a suitable basis for design.

4.7 PERFORMANCE AT OFF-DESIGN CONDITIONS.

So far discussion has been concentrated on the subject of impeller design to meet given inlet conditions. However, for a pump operating over a range of duties the question arises as to how the impeller will perform at conditions away from the original design point. The departure of the flow through the impeller from its design value Q_o introduces additional complications into the theory and makes quantitative predictions difficult, but a qualitative picture can be given.

The results of pump cavitation tests carried out at various capacities can be expressed non-dimensionaly by plotting cavitation coefficient or suction specific speed against inlet flow coefficient. Some typical tests are shown in fig. (4.18), K_u is plotted against ϕ_a for impeller "F4" for flows in the range 50% to 130% of design. It will be seen that for incipient cavitation $(Ku)_i$ increases rapidly on over-discharge, $Q > Q_o$, as larger values of N P S H are required to suppress cavitation. The rate at which this increase occurs varies with different impeller designs : $(K_u)_i$ at $1.25\,Q_o$ can be from 1.25 to 2.0 times its value at Q_o. The average increase for good designs is about 1.4 to 1.5 , i.e.

$$(K_u)_i \text{ at } 1.25Q_o \simeq 1.45\ (K_u)_i \text{ at } Q_o$$

On under-discharge, $Q < Q_o$, $(K_u)_i$ usually decreases slowly to a minimum around $0.75\,Q_o$ after which it begins to rise again gradually as the flow is further reduced. In some cases this "gradual" rise becomes most pronounced, as for example for the Francis impeller whose performance is shown in fig. (4.19). Great care was taken by the author in testing the pump containing this impeller in order to establish the head-capacity characteristic as accurately as possible. This characteristic was found to have a small zone of instability or "kink" at flows close to the region of rapid increase in $(K_u)_i$. The Francis impellers tested by Gongwer also exhibited this behaviour, and a similar observation was made by Minami et al. (50) although it is interesting to note that they found the steep increase in $(K_u)_i$ to occur only when incipient cavitation was defined by visual means, $(K_u)_i$ measured by deterioration in performance did not show any increase at partial capacities. Gongwer advanced a very plausible explanation to account for the steep increase in $(K_u)_i$ and the dip in the H - Q curve, suggesting that both were due to separation of the flow from the leading edges of the impeller blades at the high angles of incidence occurring at partial capacities. Under these conditions there is insufficient energy in the boundary layer to maintain the flow along the blade surface against the abrupt pressure increases which follow high local underpressures.

When cavitation breakdown is considered $(K_u)_{b.d}$ is found to increase continuously with flow, as shown in figs. (4.18) and (4.19) which are typical in this respect. There is a general trend for the range of cavitation to increase at capacities other than design; the difference between $(K_u)_i$ and $(K_u)_{b.d}$ is a minimum near the design flow and increases

as one moves away from this flow.

In section (4.4) equation (4.15) was derived, viz.,

$$K_u = K_{1a} \phi_a^2 + K$$

It is reasonable to suppose that for incipient cavitation the variations of K_u with ϕ_a is due to variation of the factor K, as this represents the local underpressures on the surfaces of the impeller blades and will increase with increasing angle of incidence. The factor K_{1a} is primarily dependent on the profile of the liquid passages at impeller inlet and could be expected to remain constant. If the variation of K_u with ϕ_a is determined experimentally and K_{1a} is taken as constant it is then possible to plot K versus ϕ_a, and this has been done in fig. (4.20) for the impellers "F4" and "F5". "F4" and "F5" were chosen for this analysis as they have nearly the same specific speed and their hydraulic design is closely allied but not identical. It will be seen that the two curves obtained of K versus ϕ_a are similar. Thus if the relation between K and ϕ_a has been established for an impeller of existing design, it can be used to predict the variation of K_u with ϕ_a for a new impeller of similar design, and hence to calculate its cavitation performance at off-design conditions. As impellers of differing designs have been found to give widely varying $K - \phi$ curves this approach is of restricted application, but it can be extremely useful in estimating the performance of new impellers.

Another qualitative check can be made by applying the "S'M" criterion, as Stepanoff and Stahl suggest that it can be used at partial capacities, perhaps down to $0.5Q_o$. However, the author's attempts to use this criterion at partial capacities have not met with the success these writers claim for it, and the method can only be used as a rough guide. This is, of course, better than having no guide at all.

4.8 CONCLUSION

An investigation has been undertaken into the design of centrifugal and axial-flow pump impellers for optimum cavitation performance. After a general discussion of impeller design similarity relations were introduced in order to determine the important parameters that must be used to describe cavitation performance. This led to the definition of suction specific speed, and the problem was then to achieve a design which would make this a maximum. For this purpose it was necessary to establish the relationship between suction specific speed and flow coefficient. In the present knowledge of fluid mechanics it was not possible to do this on purely theoretical grounds and recourse was had to semi-empirical methods. The suction specific speed was expressed in the forms

$$S' = 384.5 \frac{\phi_a^{\frac{1}{2}}}{(K_u)^{\frac{3}{4}}}$$

and

$$S' = \frac{384.5}{(f_2)^{\frac{1}{2}}} \frac{1}{\phi_m (K_m)^{\frac{3}{4}}}$$

In section (4.4) K_u was derived as a quadratic in ϕ_a, $K_u = K_{1a}\,\phi_a^2 + K$, it being assumed that K_{1a} and K were constant coefficients independent of ϕ_a. This procedure gave rise to higher optimum flow coefficients than were used in practice and failed to predict closely the increase in suction specific speed to be gained by designing for pre-rotation.

A second design procedure was then considered. This was based on analysis of a large number of test results leading to the empirical relation

$$K'_m = \frac{615}{S'\,\phi'_m} \qquad (S' > 300)$$

This in turn yielded

$$S'\,\phi'_m\,f_2^{\,2} = \text{constant} \qquad (S' > 300)$$

which expresses in mathematical terms the well-known observation that small flow coefficients can be used to give high suction specific speeds. Of course small values of ϕ adversely affect impeller efficiency and the minimum practical value is therefore around 0.15.

It was pointed out that a number of design elements had not been included explicitly in either of these design procedures, the most important ones being the form of the impeller approach passages and the number of impeller blades. The approach passages should be designed to give as nearly uniform entry velocity as possible although this may be difficult where pump layouts are restricted by space limitations. With respect to the number of blades the evidence of the table in section (4.4) does not show this to have any significant effect on cavitation performance. It could be argued that there must be an optimum number, because too many blades would lead to excessively narrow impeller passages so that a small pocket of cavitation on each blade surface would have a large effect on the total flow. On the other hand if there are too few blades the pressure difference across each blade is higher in order to transmit the energy to the liquid and the maximum blade underpressure is increased.

It has been suggested that considerable improvements in cavitation performance can be obtained by designing impellers to have oversize passages in which local cavitation can take place (and perhaps cause local damage) without affecting the bulk of the flow or the overall hydraulic performance. Thus the Wood "M_3" impellers had high suction specific speed based on performance measurements, but observation of the impeller passages showed that in fact pockets of vapour bubbles formed at considerably lower suction specific speeds. The "F_2" Francis impeller also gave a high suction specific speed; it was designed with wide suction passages and it may well have been that pockets of cavitation bubbles formed before any deterioration in performance was noted. However, observations to check this hypothesis have not been made. It should be recorded that for both the "F_2" and "M_3" impellers the suction specific speed at cavitation breakdown $S'_{b.d}$ was approximately 750 although details of impeller design and blade profile were very different in the two cases. Thus the fact that they can operate at high suction specific speeds depends on their ability to postpone the

adverse effects of incipient cavitation; the ultimate suction specific speed at which there is complete breakdown has not been advanced : Gongwer reported $S'_{b.d} = 740$ in his original work .

CHAPTER 5.

IMPELLER DESIGN FOR OPTIMUM CAVITATION PERFORMANCE. PART II - CAVITATING FLOWS.

5.1 INTRODUCTION.

In order to attain the highest possible suction specific speeds, pump impellers must operate in cavitating flows. Chapter 4 dealt with the design of impellers in which cavitation was to be suppressed, and this chapter goes on to consider the design of axial-flow impellers for operation in cavitating and super-cavitating flows. The theory of hydrofoils in cavitating flows is outlined and its application to pump design examined.

Cavitating and super-cavitating flows are of increasing importance in engineering, particularly with respect to high-speed marine propellers, hydrofoil ships, and low head pumps and turbines. There is a constant spur to operate a hydrodynamic machine at the highest possible speed because of the advantages to be gained in reduced size, weight and cost. In some cases these factors are of critical importance, a good example being the turbo-pumps used in liquid fuel rockets where it has been demonstrated that the dry weight of the complete power plant depends very largely on the suction specific speed of its fuel pumps.

For such applications high-speed pumps have been developed having a so-called "inducer" stage as the first rotative element in the high-speed pumping system; extensive experimental programmes are being conducted to investigate the cavitating flows associated with inducers. The primary function of an inducer is to act as a specially designed axial stage which will operate with cavitation and gradually add momentum to the fluid until, as it enters advanced sections, the vapour is recompressed and rapid momentum addition can then be made as in a conventional impeller. These conditions imply that an inducer should have long passages, blading of moderately high solidity, with certain sections of the blades operating under cavitating conditions. In turn long passages would give rise to added frictional losses and consequently reduced overall efficiency. Also the presence of cavitation is conducive to damage. Experiments and practical use of inducers have shown that these shortcomings can be minimised and that lower efficiency and the possibility of damage are more than compensated by the improvement in suction performance.

The inducer stage may be followed by a conventional centrifugal stage as illustrated in fig. (5.1), or by further axial stages. In the special field of liquid fuel rockets, the fuels may be exotic liquids such as hydrogen and the pumps may consist of three axial stages - inducer, intermediate and high pressure stages. The intermediate stage then operates near incipient cavitation and develops an appreciable pressure rise to set up the liquid flow distribution for the following high pressure stage.

Super-cavitating marine propellers have been designed and tested, Tachmindji et al. (88) and (89); these have special blade sections designed to give good lift - drag ratios in super-cavitating flows when the cavity springs from the leading edge of the blade and extends a distance downstream equal to several times the length of the blade. Nearly all the performance data for super-cavitating hydrofoils are in the form of analytical or experimental results on isolated hydrofoil sections in two-dimensional flow. For the design of propellers and pumps this information can be used in an "aerofoil" method of analysis in which blade sections at representative radii are considered, say hub, tip, and mean; the lift and drag coefficients for two-dimensional flow are then applied to these sections for the flow relative to them, the relative velocity at each section being taken as the vectorial mean of the velocities upstream and downstream of it, see for example Van Niekirk (90) and previous references to axial-flow pump theory. Data on hydrofoils will be presented first, and then applications to inducers and super-cavitating axial-flow pumps will be discussed.

5.2 THEORETICAL CONSIDERATIONS.

5.2.1 Isolated Hydrofoils.

In cavitating flows hydrofoils of conventional aerofoil shapes suffer serious changes in their force characteristics. Furthermore, when operated at cavitation numbers sufficiently high so that the cavity is shorter than or only slightly longer than the foil (partial cavitation), the forces on the foil may be subject to severe fluctuations and the foil itself to harmful cavitation damage. In general, as the cavitation number is lowered the lift and lift - drag ratio fall off to a marked degree, so much so that the conventional aerofoil shapes are not satisfactory for operation under cavitating conditions. Recently much attention has been given in the United States and elsewhere to the problem of developing new hydrofoils giving better characteristics in cavitating flows, and special sharp-nosed and blunt-based foils have been successfully tested.

First consider the simplest shape, a thin flat plate in a flow of uniform approach velocity. The lift of such a plate at zero cavitation number was calculated by Rayleigh. Fig.(5.2) shows this together with the lift for larger values of K as obtained by Wu (91) for the two-dimensional case using the Roshko finite-cavity model. For these calculations and in fact, for all theoretical calculations in this discussion the fluid is considered inviscid and incompressible, and the problem solved by analytical techniques which are based on conformal mapping and which are widely used in free streamline theory, Plesset (92), Tulin (93) (94), Wu (91). The results shown in fig. (5.2) are in good agreement with experiment particularly for $K < 1.0$.

For $K = 0$ and at small angles of incidence it can be shown that the lift - drag ratio of a flat plate is theoretically

$$\frac{C_L}{C_D} = \frac{\pi}{C_L}$$

if only the drag due to the cavity is taken into account. In practice there will of course be additional frictional drag on the lower wetted surface, so that in super-cavitating flow the lifting efficiency of the flat plate is small.

In order to obtain higher lift - drag ratios (that is, high enough to be useful in hydraulic machinery), the effect of the shape of the bottom surface of the hydrofoil has been studied, and it has been found that certain positively cambered hydrofoil shapes lead to cavitation drags much lower than for the flat plate, the lift in both cases being the same. These low-drag hydrofoils are designed to have rearward placed centres of pressure. A family of such super-cavitating hydrofoils has been tested and used in the blades of super-cavitating propellers, Tachmindji et al. (89). The bottom shape of these hydrofoils is shown in fig. (5.3) and the theoretical lift - drag ratios at $K = 0$ in fig. (5.4). These foils are intended to operate with a cavity springing from the leading edge and with an entirely unwetted upper surface. They have been designed to produce high lifting efficiencies and not to cavitate on their bottom surfaces. The shape of their upper surfaces must be such that they are completely enveloped within the cavities which extend from the leading edges. The allowable shapes have been calculated, and it has been found that the thickness of the hydrofoil should increase approximately linearly from the leading edge to the trailing edge. The maximum allowable thickness t_{max} of the section at the trailing edge is given by

$$\frac{t_{max}}{c} = 0.17\, C_L + 0.02\, \alpha'$$

where c = chord length

α' = angle of attack of low-drag hydrofoils relative to angle of attack when foil is being operated at design lift.

α' is expressed in degrees; recommended design practice is $\alpha' \simeq 1.5^\circ$.

Theory is available to calculate the performance of arbitrary, thin, cambered lifting hydrofoils in super-cavitating flows, Plesset (92), Tulin (93) (94). The results for the simplest case, that of circular arc profiles, will be quoted here. The lift and drag coefficients are expressed as functions of cavitation number K and angle of attack α in an approximate form which is sufficiently accurate for flows with cavities at least 4 chord lengths long.

$$C_L = \frac{\pi}{2}(1+K)\left(\alpha + \frac{7\theta}{8}\right) + K^2(1+K)\frac{3\pi}{32}\cdot\frac{1}{\alpha + \frac{\theta}{4}}$$

$$C_D = \frac{\pi}{2}(1+K)\left(\alpha + \frac{\theta}{4}\right)^2 + K^2(1+K)\frac{3\pi}{32}\cdot\frac{\alpha + \frac{7\theta}{4}}{\alpha + \frac{\theta}{4}}$$

$$\frac{L}{C} = 1 + \frac{4\left(\alpha + \frac{\theta}{4}\right)^2}{K^2}$$

The symbols are defined in fig. (5.5).

It should be made clear that this theory for super-cavitating hydrofoils rests on the assumption of cavity detachment at the leading edge. To achieve this the hydrofoil has to be kept thin, because if the thickness is too great

the cavity detaches some distance downstream of the leading edge, giving considerably increased drag and loss in lifting efficiency. Thus the allowable thickness of the supercavitating hydrofoil is restricted and this is a major source of difficulty in structural design.

In this discussion the possible effects of gravity on the flow around a super-cavitating hydrofoil have been ignored. Work has been carried out on this aspect of the subject, particularly with respect to ships' underwater structures, and it has been shown that the results are usually not of importance in hydrodynamic machines where gravity effects are relatively small.

5.2.2 Super-cavitating Cascades.

Lifting foils in cascade operating under supercavitating conditions have been studied particularly in connection with the stalled operation of aerodynamic compressors and turbines, the assumption being made that the flow past a completely stalled cascade is very similar to that in a "choked" supercavitating cascade, i.e. a cascade where the cavities extend for an infinite length downstream. Calculations have shown that lifting cascades will shed infinite-length cavities or choke at cavitation numbers greater than zero; thus the operation of cascades at low cavitation numbers is limited. The cascade effect is to decrease the lift developed by the foil, just as in fully wetted flow, and this effect may be severe. Even for a space-chord ratio as large as 5, it has been calculated that the lift on super-cavitating flat plates in cascade may be reduced by over 10% for a 0° stagger configuration and by over 60% for 30° stagger.

In this thesis on the influence of cavitation on impeller design consideration is primarily being given to the performance characteristics of the impeller inlet rather than to the overall performance of the impeller, that is the head it develops. An attempt is now made therefore to develop a theory which predicts the inlet conditions of a super-cavitating cascade. Later this is compared with the results of experiments on special axial-flow impellers and semi-empirical coefficients are introduced to try and correlate theory with experiment and thus provide a rational basis for design.

Consider then a series of thin flat plate hydrofoils arranged in an infinite cascade in a cavitating flow with a free streamline originating from the leading edge of each hydrofoil. The flow is assumed to be two-dimensional, irrotational, inviscid, incompressible, and non-oscillatory. Two cases will be examined, first when the length of each cavity is less than the chord of the hydrofoil, second when each cavity is infinitely long and the cascade is choked. The first case corresponds to partial cavitation and the analysis of this condition will be simplified by taking the chord length to be infinitely long, and studying the development of the cavity in the inlet region of each hydrofoil. The pressure in the cavities is assumed to be constant and equal to the vapour pressure at the bulk temperature of the liquid.

There are several models which can be adopted to describe mathematically the termination of a constant pressure cavity of finite length. Following

Stripling and Acosta (95) the one used here is the wake (or Roshko dissipation) model. The free streamline springs from the leading edge of the hydrofoil and closes upon a flat surface parallel to it, where there is a gradual recovery of pressure from the value determined by the cavitation number to the free stream value. Of course, as the wake thickness and structure of the real flow cannot be found from a perfect fluid theory there is considerable arbitrariness in any mathematical model chosen to represent the flow.

Fig. (5.6) illustrates a partially cavitating cascade and fig. (5.7) a super-cavitating cascade. Some simple results follow from application of momentum theory. Thus for partial cavitation and with the symbols defined in fig. (5.6), the following relations can be derived.

Continuity : $$Q = w_1 s \cdot \sin(\beta - \alpha) = w_2 (s-h) \sin\beta \qquad (5.1)$$

Energy : $$\frac{p_1}{\gamma} + \frac{w_1^2}{2g} = \frac{p_v}{\gamma} + \frac{w_c^2}{2g} = \frac{p_2}{\gamma} + \frac{w_2^2}{2g} \qquad (5.2)$$

Momentum : $$p_1 s \cdot \sin\beta - p_2 (s-h)\sin\beta - p_v h \sin\beta = Q \frac{\gamma}{g} (w_2 - w_1 \cos\alpha) \qquad (5.3)$$

From equation (5.1) $$\frac{h}{s} = 1 - \frac{w_1 \sin(\beta-\alpha)}{w_2 \sin\beta}$$

From equation (5.3)

$$(p_1 - p_2) s \cdot \sin\beta + (p_2 - p_v) h \sin\beta = \frac{\gamma}{g} w_1 s \cdot \sin(\beta-\alpha)(w_2 - w_1\cos\alpha)$$

Hence from equation (5.2)

$$(w_2^2 - w_1^2) + (w_c^2 - w_2^2)\frac{h}{s} = 2 w_1 \frac{\sin(\beta-\alpha)}{\sin\beta}(w_2 - w_1\cos\alpha)$$

Substituting for $\frac{h}{s}$ in this expression and re-arranging gives

$$\frac{w_c}{w_2} + \frac{w_2}{w_c} = \left(\frac{w_c}{w_1} + \frac{w_1}{w_c}\right)\cos\alpha + \left(\frac{w_c}{w_1} - \frac{w_1}{w_c}\right)\sin\alpha \cot(\beta-\alpha) \qquad (5.4)$$

If the cavitation number for the flow is defined as

$$K = \frac{p_1 - p_v}{\frac{1}{2}\rho w_1^2} \qquad (5.5a)$$

then the Bernoulli relation, equation (5.2), gives

$$w_c = w_1 \sqrt{1+K} \qquad (5.5b)$$

w_c can be eliminated from equations (5.4) and (5.5b) to give K in terms of the angle of incidence α, the blade angle β, and the velocity ratio R (the ratio of the relative approach velocity w_1 to the relative downstream jet velocity w_2)

$$K = \frac{W_c^2}{W_1^2} - 1 = \frac{\left(\frac{1}{R} + R\right) - 2\cos\alpha}{\cos\alpha - R + \sin\alpha\cot(\beta-\alpha)} \qquad (5.6)$$

Next consider the super-cavitating cascade in which the jet issues with velocity W_2 at an angle θ to the direction of the hydrofoil. The symbols for this case are defined in fig. (5.7).

Continuity : $Q = W_1 s \cdot \sin(\beta - \alpha)$

Energy : $\frac{p_1}{\gamma} + \frac{W_1^2}{2g} = \frac{p_2}{\gamma} + \frac{W_2^2}{2g}$

Momentum : $(p_1 - p_2) s \cdot \sin\beta = Q\frac{\gamma}{g}(W_2\cos\theta - W_1\cos\alpha)$

The result is obtained,

$$2\cos\theta = \left(\frac{W_2}{W_1} + \frac{W_1}{W_2}\right)\cos\alpha + \left(\frac{W_2}{W_1} - \frac{W_1}{W_2}\right)\sin\alpha\cot(\beta-\alpha)$$

or $$2\cos\theta = \left(\frac{1}{R} + R\right)\cos\alpha + \left(\frac{1}{R} - R\right)\sin\alpha\cot(\beta-\alpha) \qquad (5.7)$$

When $\theta = 0$, equation (5.7) becomes

$$2R = (1 + R^2)\cos\alpha + (1 - R^2)\sin\alpha\cot(\beta-\alpha)$$

This can be solved for R to give

$$R^* = \frac{W_1}{W_2} = \frac{\sin(\beta-\alpha) - \sin\alpha}{\sin(\beta - 2\alpha)} \qquad (5.8)$$

This result corresponds to the limiting case for equation (5.4) when the cavitation number in the partially cavitating cascade is reduced to its minimum value. The cascade then becomes fully super-cavitating and the cavities extend an infinite distance downstream. Conditions in this limiting case of "choked" flow will be denoted by an asterisk. Since W_2 is then equal to Wc,

$$W_2 = W_c = W_1\sqrt{1 + K}$$

it follows that

$$K^* = \frac{1}{R^{*2}} - 1 \qquad (5.9)$$

The minimum value of the cavitation number K is

$$K^* = \left\{\frac{\sin(\beta - 2\alpha)}{\sin(\beta-\alpha) - \sin\alpha}\right\}^2 - 1$$

whence $$K^* = \frac{2\sin\alpha\sin(\beta-\alpha)}{1 + \cos\beta} \qquad (5.10)$$

Equation (5.10) brings out clearly that to obtain small cavitation numbers, β should be small.

To derive results suitable in axial-flow pump design, suppose that the cascade is rotating about a central axis with a peripheral speed u, and that

the results obtained for flow relative to the stationary cascade can still be applied. It has been assumed that there are no friction losses and that gravity forces are negligible so that the energy equation in conjunction with the definition of net positive suction head yields

$$Hsv = \left(h_1 + \frac{v_a^2}{2g}\right) - h_v$$

$$\therefore \quad Hsv = (h_1 - h_v) + \frac{v_a^2}{2g}$$

$$\therefore \quad Hsv = K \frac{W_1^2}{2g} + \frac{v_a^2}{2g} \qquad (5.11)$$

This is equivalent to equation (4.14) with the simplification that K_o has been taken as unity in this case.

The inlet velocity triangle fig. (5.7) shows that

$$W_1 = u \sec(\beta - \alpha)$$
$$v_a = u \tan(\beta - \alpha)$$
$$W_1^2 = v_a^2 + u^2$$

The flow coefficient is

$$\phi = \frac{v_a}{u} = \tan(\beta - \alpha)$$

Equation (5.11) is expressed non-dimensionally by putting $Ku = Hsv / (u^2/2g)$, whence

$$Ku = K(1 + \phi^2) + \phi^2 \qquad (5.12)$$

Under the extreme super-cavitating condition, $Ku = Ku^*$ can be related to K^*, R^*, α and β in the following manner.

$$Ku^* = K^*(1 + \phi^2) + \phi^2$$

$$\therefore \quad Ku^* = \left(\frac{1}{R^{*2}} - 1\right)(1 + \phi^2) + \phi^2$$

$$= \frac{1 + \phi^2}{R^{*2}} - 1$$

$$\therefore \quad Ku^* = \frac{\sec^2(\beta - \alpha)}{R^{*2}} - 1 \qquad (5.13)$$

Ku^* can also be expressed as a function of β and ϕ

$$Ku^* = K^*(1 + \phi^2) + \phi^2$$

$$= \frac{2 \sin\alpha \sin(\beta - \alpha)}{1 + \cos\beta} \cdot \frac{1}{\cos^2(\beta - \alpha)} + \phi^2$$

$$= 2\phi \frac{\sin\alpha}{(1 + \cos\beta)\cos(\beta - \alpha)} + \phi^2$$

$$= 2\phi \frac{\sin\beta\cos(\beta - \alpha) - \cos\beta\sin(\beta - \alpha)}{(1 + \cos\beta)\cos(\beta - \alpha)} + \phi^2$$

$$= 2\phi \frac{\sin\beta}{1 + \cos\beta} + \phi^2 \frac{1 - \cos\beta}{1 + \cos\beta}$$

$$\therefore \quad Ku^* = 2\left(\frac{\sin\beta}{1 + \cos\beta}\right)\phi + \left(\frac{\sin\beta}{1 + \cos\beta}\right)^2 \phi^2 \qquad (5.14)$$

Equations (5.11) to (5.14) are usually applied to the blade tips where velocities are highest. It is instructive to investigate radial effects, in particular how the net positive suction head at breakdown Hsv^* varies with radius. For any radius r, equation (5.13) may be written

$$(Ku^*)_r = \left(\frac{Hsv^*}{\frac{u^2}{2g}}\right)_r = \frac{1 + \cos(\beta - 2\alpha)}{(1 + \cos\beta)\cos^2(\beta - \alpha)} - 1$$

If α is small compared to β, the expression on the R. H. S. reduces to $\tan^2\beta$, so that for cases of practical interest it is approximately true to say

$$(Hsv^*)_r \propto (r \tan \beta)^2$$

Thus for a constant pitch inducer ($r \tan \beta$ = constant) operating with uniform axial velocity at inlet, Hsv^* is only slightly dependent on the radial station. It appears quite possible to design an inducer with the blade angle and incidence angle varying radially in such a way that the *theoretical* value of Hsv^* remains essentially constant across the inlet.

Before leaving this topic it should be noted that for optimum cavitation performance, the suction specific speed S' is a maximum. S' is related to K_u and ϕ by equation (4.11)

$$S' = \frac{S}{\sqrt{1 - \xi^2}} = 384.5 \frac{\phi^{\frac{1}{2}}}{(K_u)^{\frac{3}{4}}}$$

The present analysis follows Stripling and Acosta and puts

$$S' = 384.5 \frac{\phi^{\frac{1}{2}}}{\{K(1+\phi^2) + \phi^2\}^{3/4}}$$

Differentiation with respect to ϕ (holding K constant) and equating to zero gives the theoretical relation between the optimum value of ϕ and K.

$$K = \frac{2\phi_{opt}^2}{1 - 2\phi_{opt}^2} \quad \text{or} \quad \phi_{opt} = \sqrt{\frac{K}{2(1+K)}} \qquad (5.15)$$

Then $$K_u = \frac{3\phi_{opt}^2}{1 - 2\phi_{opt}^2} \quad \text{or} \quad K_u = \frac{3K}{2} \qquad (5.16)$$

and $$S'_{max} = \frac{239}{\sqrt[4]{K^2(1+K)}}$$

These equations are similar to equations (4.18) and (4.19) previously derived.

Returning now to the partially cavitating cascade fig. (5.6) it will be remembered that in the postulated model of the flow a free streamline originates at the leading edge of each plate and closes upon a flat surface parallel to the original surface. The problem is now to determine the length l of the cavitating region and its height h as functions of the blade angle β (or stagger angle δ), angle of attack α, and the cavitation number K which relates the upstream velocity W_1 to the

velocity along the constant pressure surface W_c. The slant height of the cascade is taken as 2π to facilitate the mathematical analysis; it can be changed to any other value by introducing a suitable scale factor. As is customary in problems involving free streamlines, it is convenient to discuss the flow with reference to the hodograph plane, in which the streamlines that describe the wetted surfaces and constant pressure surfaces are sketched as functions of the hodograph variable $\zeta = u - i v$. If $F = \bar{\varphi} + i \bar{\psi}$ is the complex potential of the flow, with $\bar{\varphi}$ the velocity potential and $\bar{\psi}$ the stream function, then

$$\zeta = \frac{dF}{dZ} = u - i v$$

where u, v are the x- and y- velocity components in the physical plane, and $Z = x + i y$ is the complex variable in the physical plane. The solution rests upon the fact that the imaginary part of F is known around the boundary of the flow as seen in the hodograph plane. This is shown in fig. (5.8) and corresponding points in the physical and hodograph plane are identified. If F can be determined as a function of ζ, then physical co-ordinates for corresponding points in the ζ - plane can be determined by integration, i.e.

$$Z = \int \frac{dF}{\zeta} + \text{const.}$$

In this case the hodograph is sufficiently simple for the solution $F(\zeta)$ to be determined by inspection.

The solution is greatly assisted by recognizing that the uniform flows at infinity correspond to source-vortexes located at their corresponding points in the hodograph plane. For example,

$$F = W_1 e^{-i(\delta+\alpha)} \ln(\zeta - W_1 e^{-i\alpha})$$

represents a source-vortex in the ζ - plane located at the point corresponding to $Z = -\infty$. Then, from integration, the corresponding physical co-ordinates are

$$Z = W_1 e^{-i(\delta+\alpha)} \int \frac{d\zeta/\zeta}{\zeta - W_1 e^{-i\alpha}}$$

$$= e^{-i\delta} \ln\left(\frac{\zeta - W_1 e^{-i\alpha}}{\zeta}\right) + \text{constant}$$

When $W_1 e^{-i\alpha}$ is encircled once in the counter-clockwise direction, Z moves a distance 2π to a corresponding point on the next step of the cascade. Also it is readily shown that the streamlines in the ζ - plane near the origin of the vortex are uniform and inclined at the angle α to the x - axis in the physical plane.

The complex potential must have the appropriate singular behaviour indicated above at each of the points $-\infty$, $+\infty$ of fig. (5.8). In addition the real axis and the circle $|\zeta| = W_c$ must be streamlines in the hodograph. Finally it is necessary that the point $\zeta = 0$ be a stagnation point of this flow which requires that

$$\left(\frac{dF}{d\zeta}\right)_{\zeta = 0} = 0$$

The potential satisfying these conditions, determined by the method of images is

$$\frac{1}{W_1} F(\zeta) = e^{-i(\delta+\alpha)} \ln(\zeta - w_1 e^{-i\alpha}) + e^{i(\delta+\alpha)} \ln(\zeta - w_1 e^{i\alpha}) + e^{i(\delta+\alpha)} \ln(\zeta - \frac{w_c^2}{w_1} e^{-i\alpha}) + e^{-i(\delta+\alpha)} \ln(\zeta - \frac{w_c^2}{w_1} e^{i\alpha}) - 2\cos(\delta+\alpha)\{\ln(\zeta - w_2) + \ln(\zeta - \frac{w_c^2}{w_2})\} + \text{constant}.$$

In order that $\frac{dF}{d\zeta} = 0$ at $\zeta = 0$ the following relationship between the velocity ratios must hold :

$$\frac{w_c}{w_2} + \frac{w_2}{w_c} = \left(\frac{w_c}{w_1} + \frac{w_1}{w_c}\right)\cos\alpha + \left(\frac{w_c}{w_1} - \frac{w_1}{w_c}\right)\sin\alpha \tan(\delta+\alpha)$$

This has already been derived from momentum considerations above and is another statement of the fact that the force on the hydrofoils is normal to the chord.

The physical co-ordinates of the flow, obtained by integration are

$$z = e^{-i\delta}\ln(\zeta - w_1 e^{-i\alpha}) + e^{i\delta}\ln(\zeta - w_1 e^{i\alpha}) + \frac{w_1^2}{w_c^2} e^{i(\delta+2\alpha)} \ln(\zeta - \frac{w_c^2}{w_1} e^{-i\alpha}) + \frac{w_1^2}{w_c^2} e^{-i(\delta+2\alpha)} \ln(\zeta - \frac{w_c^2}{w_1} e^{i\alpha}) - 2\frac{w_1}{w_2}\cos(\delta+\alpha)\{\ln(\zeta - w_2) + \frac{w_2^2}{w_c}\ln(\zeta - \frac{w_c^2}{w_2})\} + \text{constant}. \quad (5.17)$$

The length l of the cavity from the leading edge and the height h of the wake normal to the hydrofoil can then be derived. After some manipulation they are found to be

$$h = 2\pi\cos\delta\left\{1 - \frac{w_1}{w_2}\cdot\frac{\cos(\delta+\alpha)}{\cos\delta}\right\} \quad (5.18)$$

$$l = \left\{\cos\delta + \frac{w_1^2}{w_c^2}\cos(\delta+2\alpha)\right\}\ln\frac{w_c^2 - 2w_1\cos\alpha + w_1^2}{w_c^2 + 2w_1\cos\alpha + w_1^2} - 2\cos(\delta+\alpha)\left(\frac{w_1}{w_2} + \frac{w_1 w_2}{w_c^2}\right)\ln\frac{w_c - w_2}{w_c + w_2} + 2\left\{\sin\delta + \frac{w_1^2}{w_c^2}\sin(\delta+2\alpha)\right\}\tan^{-1}\frac{2w_1 w_c \sin\alpha}{w_c^2 - w_1^2} \quad (5.19)$$

The solution to the problem is then represented by equations (5.4), (5.18) and (5.19).

Using this ideal theory Stripling and Acosta (95) carried out extensive computations of the characteristics of this cascade flow to determine K, Ku, and cavity shape. Their paper contains graphs of cavitation number K versus cavity length - spacing ratio l/s for a wide range of values of the inlet angle α and the blade angle β. The results will not be presented in detail here but it should be noted that the minimum cavitation number is found to occur when the length - spacing

ratio is about unity for all except the smallest blade angles. Now in practice most inducer pumps have been built with blade chord to spacing ratios of about 1.5 to 2 so it appears that the assumption of infinite blade chord should not invalidate the results of the present calculations for practical configurations. In fact it suggests that inducers of considerably lower solidity could be used to good effect.

The cavitation number is not particularly convenient for use in design, and Stripling and Acosta have also given graphs of Ku versus $^1/_s$ for various α and β, that for $\beta = 15^\circ$ being reproduced in fig. (5.9). The low values of Ku that can be obtained are immediately evident.

To realise the cavitation performance of this ideal theory, it is necessary that the suction side of the blade not interfere with the free streamline. This is particularly important near the leading edge where the cavity may be quite thin. Representative free streamlines have been calculated for a typical case with $\beta = 15^\circ$, $\alpha = 6^\circ$, using equation (5.17), and these are shown in fig. (5.10). It will be seen that a rather pointed leading edge contour is required, and if the blade shape is blunter than the free streamline shape for the desired operating cavitation number, a drag force parallel to the blade chord will be experienced. This will adversely affect the performance of the cascade and its minimum cavitation number will be increased. This conclusion is borne out in practice as it has often been noted that blunt leading edge shapes have inferior cavitation performance to slender shapes, and those that have the pressure side of the blade filed are inferior to those with the suction side filed in conformance to the above ideas.

5.3 APPLICATIONS

5.3.1 Introduction.

A recent paper, Stripling (96), has considered the application of this theory of super-cavitating cascades to the design of cavitation inducers. The discussion on inducers which follows is based on this work, and its approach to the subject may be compared to that in a Russian article, Dumov (97), which gives rules for inducer design apparetly derived by empirical "cut-and-try" methods. Dumov's results are followed by an examination of the advantages and disadvantages of designing axial-flow impellers for super-cavitating flows in which the cavities are longer than the blade chord.

5.3.2 Cavitation Inducers.

In his study of cavitation inducers Stripling used the theory developed for two-dimensional cascades in cavitating flows and introduced correction factors to correlate it with the results of tests on seven experimental inducers. In the ideal theory the flow is assumed to be two-dimensional, irrotational and inviscid, conditions which are never achieved with real fluids. These tests showed that in fact much higher values of the net positive suction head Hsv^* are required to produce complete head breakdown than the theory predicts.

It is assumed, therefore, that the "real" fluid effects may be allowed for by introducing into the theory a correction coefficient X defined as the ratio of the reduced or actual through flow area to the ideal area at the point corresponding to the wake closure. The downstream velocity W_2 being constant, continuity shows that the ideal through-flow area divided by the blade-to-blade normal spacing is

$$Ai = 1 - \frac{h}{s.\sin\beta}$$

$$\therefore \quad X = \frac{Aa}{Ai} = \frac{(W2)i}{(W_2)a} = \frac{Ra}{Ri} \qquad (5.20)$$

The suffix "a" refers to the actual conditions, and the suffix "i" to the ideal conditions described by equations (5.1) to (5.19). As before an asterisk will be used to denote the limiting case of super-cavitation when the cavity length approaches infinity, and there is complete breakdown of the head developed by the inducer.

This coefficient X can be used to relate actual and ideal values of Ku, since from equation (5.13)

$$(Ku^*)i = \frac{\sec^2(\beta - \alpha)}{(Ri^*)^2} - 1$$

$$(Ku^*)a = \frac{\sec^2(\beta - \alpha)}{(Ra^*)^2} - 1$$

and elimination of $\sec^2(\beta - \alpha)$ gives

$$(Ku^*)a = \frac{1}{(X^*)^2}\left\{(Ku^*)i + 1\right\} - 1 \qquad (5.21)$$

This relation enables the correction factor at breakdown X^* to be calculated from a comparison of the measured and theoretical values of the cavitation parameter Ku^*.

Combining equations (5.21) and (5.14) gives

$$(Ku^*)a = \frac{1}{(X^*)^2}\left\{1 + \frac{2\sin\beta}{1+\cos\beta}\phi + \left(\frac{\sin\beta}{1+\cos\beta}\right)^2\phi^2\right\} - 1 \qquad (5.22)$$

The suction specific speed can be expressed in terms of X, β, and ϕ, thus

$$S' = \frac{S}{\sqrt{1-\xi^2}} = 384.5\,\frac{\phi^{\frac{1}{2}}}{(Ku)a^{\frac{3}{4}}}$$

and at breakdown

$$(S')^* = 384.5\,\phi^{\frac{1}{2}}\left\{\frac{1}{(X^*)^2}\left(1 + \frac{\sin\beta}{1+\cos\beta}\phi\right)^2 - 1\right\}^{-3/4} \qquad (5.23)$$

Fig. (5.11) has been drawn to show the influence of the factor X^* on suction specific speed. This has been done for a typical blade tip angle β of 14.0° and for values of X^* ranging from 0.985 to 1.000. (These values of X^* are consistent with experimental data, see fig. (5.14).

It is interesting to note that for a given value of X^* less than unity the suction specific speed increases as the flow coefficient ϕ decreases until it reaches a peak at some optimum value, ϕ opt, after which it decreases as ϕ is further reduced. The same general characteristics were observed by Gongwer (47) and Wood et al. (46) during tests on Francis and mixed-flow impellers.

Differentiation of equation (5.23) yields the optimum flow coefficients corresponding to the peak suction specific speed for a given blade angle and constant X^*, i.e.

$$\frac{\partial S'}{\partial \phi} = 0$$

$$\therefore \phi_{opt} = \frac{1}{4} \frac{1+\cos\beta}{\sin\beta} \left\{ \sqrt{9 - 8(X^*_{opt})^2} - 1 \right\} \qquad (5.24)$$

This may be re-arranged to give the breakdown correction factor for these optimum conditions.

$$(X^*_{opt})^2 = 1 - \frac{\sin\beta}{1+\cos\beta} \phi_{opt} - 2\left(\frac{\sin\beta}{1+\cos\beta}\right)^2 \phi^2_{opt} \qquad (5.25)$$

From equations (5.22), (5.23) and (5.25) the peak suction specific speed is expressed as

$$(S')^*_{opt} = \left(\frac{S}{\sqrt{1-\xi^2}} \right)^*_{opt}$$

$$\therefore (S')^*_{opt} = 168.5 (\phi_{opt})^{\frac{1}{2}} \left\{ \frac{1+\cos\beta}{\sin\beta} \frac{1}{\phi_{opt}} - 2 \right\}^{\frac{3}{4}} \qquad (5.26)$$

Equation (5.26) is the equation to the curve passing through peak values of S^* for constant X^*. This equation is shown plotted in fig. (5.12) for blade angles ranging from 5° to 25°; lines of constant X^* are also shown.

The actual value of the net positive suction head at breakdown corresponding to the peak suction specific speed may be computed from the following relation.

$$\frac{(H_{sv}{}^*)_a}{\left(\frac{v_a^2}{2g}\right)} = \frac{(K_u{}^*)_a}{(\phi_{opt})^2}$$

$$\therefore \frac{(H_{sv}{}^*)_a}{\left(\frac{v_a^2}{2g}\right)} = \frac{3}{(\phi_{opt})^2} \left\{ \frac{1+\cos\beta}{\sin\beta} \cdot \frac{1}{\phi_{opt}} - 2 \right\}^{-1} \qquad (5.27)$$

The inlet axial velocity of the fluid v_a is assumed to have a uniform distribution across the inducer inlet. Equation (5.27) is plotted in fig. (5.13) for blade angles from 5° to 25° and corresponding constant X^* lines are shown.

Thus the cavitation performance of the inducer has been investigated with particular reference to the maximum suction specific speeds and minimum net positive suction heads attainable. These have been derived in equation (5.26) and (5.27) in terms of blade angle and optimum flow coefficient, and the latter depends in turn on a correction factor which has to be determined from experimental results.

At this stage it should be noted that the term $\left(\frac{\sin\beta}{1+\cos\beta} \cdot \phi\right)$ occurs in many of the expressions. This suggests that a new parameter Θ be introduced to correlate the data, where

$$\Theta = \left(\frac{\sin\beta}{1+\cos\beta}\right) \phi$$

Then from equation (5.14) the value of the cavitation parameter Ku at breakdown according to the ideal theory is

$$(Ku^*)_i = 2\Theta + \Theta^2 \qquad (5.28)$$

and from equations (5.22) and (5.25) the actual value of Ku under breakdown conditions is

$$(Ku^*)a = \frac{3\theta}{1 - 2\theta} \qquad (5.29)$$

The correction coefficient becomes (equation (5.25))

$$X^*_{opt} = \sqrt{1 - \theta - 2\theta^2} \qquad (5.30)$$

It will be seen that for small values of θ i.e. for small blade angles and low flow coefficients,

$$\frac{(Ku^*)a}{(Ku^*)i} = \frac{3}{2 - 3\theta - 2\theta}^2 \simeq 1.5$$

so that the actual value of the cavitation parameter at breakdown is approximately one and half times its ideal value.

The last three equations (5.28) (5.29) and (5.30) indicate that the cavitation performance data may be plotted as a single function of θ irrespective of the inducer geometry and flow conditions. They can be applied to any chosen radius, and if this is done it is found that while $(Ku^*)i$ varies only slightly with radius in a constant pitch inducer, $(Ku^*)a$ calculated from equation (5.29) does depend on radius, particularly in the case of inducers with large blade angles and large flow coefficients.

Equation (5.30) is plotted in fig. (5.14) which also shows the range of test results for the ratio A^*a / Ai^* computed by Stripling from experimental data obtained by his colleagues. It will be seen that use of the new parameter θ gives quite a good correlation, and that the data tend to follow equation (5.30) which may therefore be used in design, at least for preliminary calculations.

Further experimental data from Stripling are shown in fig. (5.15) where suction specific speed at complete head breakdown $(S')^*$ is plotted against flow coefficient ϕ . There is close agreement between the modified theory and the results for one inducer (inducer "A" for which $\beta = 18.0^\circ$), but for inducers with lower blade angles the experimental values are considerably less than predicted by the theory.

To sum up this investigation, the following conclusions may be drawn regarding the design and application of inducer pumps.

(1) Cavitation performance data at complete head breakdown conditions can be expressed as a function of the correlation parameter θ irrespective of the inducer's geometry and flow conditions.

(2) The influence of the "real fluid effects" on the cavitation performance of an inducer may be estimated by assuming a correction coefficient X^* defined as the ratio of the actual through-flow area to the ideal area. Small changes in X^* impose severe limitations on the maximum suction specific speed obtainable from an inducer.

(3) For a constant value of the correction coefficient X^* there exists an optimum flow coefficient at which the suction specific speed is a maximum. This unique solution permits the suction performance of an inducer to be estimated by a modified free-streamline method without a knowledge of the X^*opt value. However, values other than X^*opt must be determined experimentally.

(4) Blade leading edge profiles can seriously affect the suction performance of an inducer. Thinner blade sections are required for lower incidence angles, and the suction surface should be carefully filed so that the blade profile lies wholly within the shape of the free streamline.

While the above discussion has made extensive use of fluid mechanics theory it is interesting to note that some Russian results have been published, Dumov (97), giving design rules for the construction of cavitation inducers. These rules have apparently been developed by successive trial and error and no indication is given of what theoretical justification they have, if any.

In his paper Dumov refers to the difficulties in arriving at a rational method for designing pumps for good cavitation performance. These arise from the fact that in most cases of practical interest an exact solution does not exist for the problem of determining the maximum pressure drop on the surface of a blade in a rotating cascade. While such difficulties arise when dealing with perfect fluids, in practice the problem is even more complex because of the way in which the properties of real liquids depart from the ideal.

The arrangement Dumov recommends is shown in fig. (5.16) for the case where an axial inducer is placed before a centrifugal impeller. The inducer consists of two blades each laid out on a helical spiral with the axial pitch approximately two-thirds of the outside diameter, or

$$p \simeq \frac{1}{3} r_o$$

More precise values of p are given in a nomogram in Dumov's paper. The pitch is to be constant with radius so that

$$r \tan\beta = \frac{p}{2\pi}$$

The hub-tip ratio should be within the limits

$$r_i/r_o = 0.30 - 0.33$$

The chord - spacing ratio is approximately unity,

$$\frac{z\,c}{2\pi r} \simeq 1$$

As shown in fig. (5.16) the leading edge of each blade is inclined to the flow in such a way that its radius of curvature is

$$r_{L.E.} = 0.64\ r_o$$

The blade profile is given in the table below, x being the distance measured along the chord and t the blade thickness, see fig. (5.16).

x / c %	0	5	10	20	30	40	43	50	60	70	80	90	100
t / tmax %	20	45	60	79	92	99	100	97	87	73	57	37	16

The maximum thickness is equal to 3% of the chord and occurs at a distance 43% of the chord from the leading edge. The tip radii at the leading edge and trailing edge are 10% and 8% of the maximum thickness t_{max} respectively.

Dumov recommends that the inducer have a circular rim in order to eliminate the possibility of cavitation in the gap between an open impeller and the casing and also to eliminate the hydraulic losses associated with

secondary flows in this gap. This advice is contrary to that of Ross and Banerian (98) who say that the secondary flows across the blade tips of an open impeller help to alleviate the effects of tip cavitation, and that inducers therefore should not have outer shrouds or rims. Unpublished evidence available to the author tends to support this view.

The Russian paper states that the maximum suction specific speed obtainable from a conventional impeller can be increased by a factor of four by the use of an inducer of the above design. This is apparently accomplished without any loss in efficiency but whether the inducer operates under partially cavitating conditions is not made clear, although one would assume this to be the case. The limited results published by Dumov show that the collapse of head under extreme cavitation takes place very suddenly for the pump-inducer combinations he designed.

5.3.3 Super-cavitating Axial Flow Pumps.

The use of super-cavitating hydrofoils in axial-flow pumps is a recent idea and it is too early to pronounce definitely on the prospects for its successful development. In the super-cavitating axial flow pump the impelle operates with cavities extending downstream from the leading edge of each blade; the length of the cavities is greater than the blade chord and they finally collapse some distance behind the blades. The operation of pumps in super-cavitating regimes enables the highest suction specific speeds to be attained, but at the cost of reduced efficiency, increased blade stresses and increased susceptibility to vibration. Furthermore there will be many problems to be overcome in designing a suitable diffuser to obtain reasonabl pressure recovery in the flow from the impeller.

In the ensuing discussion it is assumed that the aerofoil method of analysis can be applied to any radial station in an axial-flow super-cavitating impeller. While this assumption is necessary to provide a rational basis for discussion, it may represent a drastic simplification of the real state of affairs because the possibility of large radial flows is ignored.

In the design of a super-cavitating hydrofoil the pressure surface is specified and the upper surface is then chosen so as not to interfere with the free streamline springing from the leading edge. As has been seen in fig. (5.10) the forward part of a hydrofoil tends to be very thin, giving rise to problems of blade stress and vibration which are absent in conventional impellers.

Fig. (5.17) shows a typical blade section together with the appropriate velocity triangles, and defines the symbols used. The flow relative to the blade is considered, the velocity at the blade W being taken as the vectorial mean of the velocities upstream and downstream. If K is the cavitation number for this blade section, the net positive suction head is

$$Hsv = \left(h_1 + \frac{v_a^2}{2g}\right) - h_v$$

$$\therefore Hsv = K\frac{w^2}{2g} + \frac{v_a^2}{2g}$$

$$H_{sv} = \frac{v_a^2}{2g}\left(1 + K \operatorname{cosec}^2\beta\right)$$

$$= \frac{v_a^2}{2g}\left[1 + K\left\{1 + \frac{1}{\phi^2}\left(1 - \frac{v_w}{2u}\right)^2\right\}\right]$$

In this way the theoretical result is obtained

$$S' = \frac{S}{\sqrt{1-\xi^2}} = \frac{384.5}{\phi\left[1 + K\left\{1 + \frac{1}{\phi^2}\left(1 - \frac{v_w}{2u}\right)^2\right\}\right]^{3/4}} \qquad (5.31\ a)$$

A more general expression is obtained by multiplying the entry velocity head $v_a^2/2g$ by a coefficient $K_o (K_o > 1)$ so that

$$S' = \frac{S}{\sqrt{1-\xi^2}} = \frac{384.5}{\phi\left[K_o + K\left\{1 + \frac{1}{\phi^2}\left(1 - \frac{v_w}{2u}\right)^2\right\}\right]^{3/4}} \qquad (5.31\ b)$$

This equation is similar to equation (4.17) previously derived; it has been plotted in fig. (5.18) for several important cases.

(a) $K = 0$, $K_o = 1$. This is theoretically possible for a super-cavitating hydrofoil and S' is then proportional to $\frac{1}{\phi}$ and increases without limit as ϕ is reduced. However in this case cavitation would be expected to occur in the pump entry so that in practice $K_o > 1$.

(b) $K = 0$; $K_o = 1.2$, $K_o = 1.5$. These curves show the upper limits of S' which are within the bounds of possibility.

(c) $K = 0.01$ and $K = 0.05$. These curves show values of S' which may be set as possible design objectives for super-cavitating pumps.

(d) $K = 0.1$. A curve has been drawn which represents the upper limit of S' at which cavitation occurs in conventional axial-flow pumps. It corresponds closely to $K = 0.1$.

Fig. (5.18) demonstrates that much higher suction specific speeds may be obtained in super-cavitating pumps than in pumps of conventional design. The attainment of very high S values would involve the use of low values of ϕ, and hence reduced efficiencies.

At the present time lift - drag ratios of super-cavitating hydrofoils are lower than those designed for non-cavitating flows, and the efficiencies which might be obtained are therefore lower. In his preliminary study, Norbury (99) discussed a series of super-cavitating designs based on a lift - drag ratio of 10, quite a realistic value. Using an "aerofoil" analysis he calculated possible pump efficiencies for these designs at high suction specific speeds, and found that they lay closely on one curve which is plotted in fig. (5.19). It will be seen that the efficiency falls from about 62% at S' = 1000 to 40% at S' = 5000. If the lift-drag ratio could be increased to 25, the calculated efficiency is around 73% for these suction specific speeds. However, while a lift-drag ratio as high as this for a super-cavitating hydrofoil is not impossible it is definitely an optimistic estimate at present.

The super-cavitating pump is attractive in theory for applications where its lightness and compactness outweigh its lower efficiency, but its successful development depends on the solution of a number of problems. These include :-

(1) The nature of the flow through super-cavitating impellers, in particular whether the flow behaves approximately in the manner assumed here and whether the aerofoil method of design is valid.

(2) The development of more efficient super-cavitating sections.

(3) The avoidance of cavitation in the pump entry.

(4) The development of axial or radial diffusers to handle the unsteady and non-uniform flow leaving the impeller.

(5) Problems of stress and vibration associated with the thin leading edges of super-cavitating blades. Furthermore at medium or high heads blade tip speeds become very high, possibly beyond the strength and erosion resistance of existing materials.

(6) Problems of erosion associated with the collapse of the vapour cavities.

Operation with fully developed cavitation offers prospects of major advances in the suction specific speed of axial-flow pumps; This may provide the spur for the necessary time and money to be devoted to the project. A simple example quoted by Wislicenus (55) illustrates the advantages to be gained. Suppose that a high pressure pump is required to deliver 3 cusecs when the NPSH available is 20 ft. A single stage super-cavitating pump could operate at 15,000 - 20,000 r.p.m. corresponding to suction specific speeds of 2,700 - 3,600 cusec units. An impeller of only $4\frac{1}{2}$" dia. would give a head of at least 5,000 ft. so that if 70% efficiency could be obtained the power required would be 2,400 h.p. The performance specification for this pump would then be :

$Q = 3$ cusecs
$Hsv = 20$ ft.
$H = 5000$ ft.
$N = 15{,}000 - 20{,}000$ r.p.m.
$S = 2{,}700 - 3{,}600$.
$\eta = 70\%$
$P = 2{,}400$ h.p.

also Impeller O.D. $\simeq 4\frac{1}{2}$"
and Casing O.D. $\simeq 10$".

Such a machine would be ideally suited to steam or gas turbine drive and would, of course, be extremely compact.

However, upon reflection one cannot help but feel that the super-cavitating pump will remain an engineering curiosity and that its commercial development will be slow; the difficulties to be surmounted require the expenditure of large amounts of time and money. The example of the supersonic axial-flow compressor supports this view. The supersonic compressor has similar advantages and disadvantages to the super-cavitating pump : low weight but lower efficiency and thinner blades. Despite large research programmes in government and private laboratories the use of supersonic compressors remains very restricted. Perhaps the same fate awaits the super-cavitating pump unless some engineering breakthrough changes the picture radically.

CHAPTER 6.

REVIEW OF CAVITATION IN CENTRIFUGAL AND AXIAL-FLOW PUMPS.

6.1 CAVITATION IN LIQUIDS OTHER THAN WATER.

In chapters 4 and 5 reference was made to experimental results obtained by the author and to data published by other writers. This experimental evidence was obtained from pump cavitation tests on cold water; it can be safely applied to other liquids, since all the available evidence tends to show that centrifugal and axial-flow pumps are more susceptible to cavitation when handling cold water, possibly because more cavitation nuclei are present. Other liquids handled by centrifugal and axial-flow pumps include

(1) hot water at elevated temperatures and pressures

(2) hydrocarbon liquids and associated organic compounds

(3) cryogenic liquids

(4) liquid metals

(5) molten salts.

In most applications these liquids are used under conditions of temperature and pressure which are closer to their boiling points than is the case for cold water. Thermo-dynamic considerations can therefore be expected to play a larger part in the development of cavitation, since heat transfer to and from a cavitation bubble may appreciably affect its growth and collapse.

The sensitivity of pump performance to cavitation depends on the properties of the fluid, including latent heat of vapourization, specific heat, ratio of liquid to vapour density, and the rate of change of vapour pressure with temperature. Of these the most important is the liquid to vapour density ratio. Thus when water cavitates the volume of vapour created is 1,600 times the volume of vapourized liquid, and this vapour may change completely the flow in the impeller passages so that performance falls off drastically. In oxygen the density ratio is 257 : 1 and the effect of cavitation is less than for water. In hydrogen at its normal boiling point of 37° R the ratio is only 52 : 1 , and when liquid 37°R hydrogen flashes to vapour a relatively small increase in flow volume occurs, thus minimising the change in flow characteristics in the impeller. Pumps designed to operate with liquid hydrogen can be made much less sensitive to cavitation than is the case for water, as is illustrated in fig. (6.1) for a typical example.

The effect of cavitation on the performance of pumps handling less exotic liquids has been discussed by Salemann (103) and Stepanoff (104)

for hot water (up to 420°F), hydrocarbon liquids and freon. Empirical corrections have been proposed to predict the cavitation performance of pumps handling these liquids once their performance on cold water is known. These corrections have been derived in terms of a thermodynamic criterion, the ratio of the volume of vapour produced in cavitation to the volume of liquid passing through the cavitation zone. This ratio is a major factor in determining the extent of the cavitation zone in the impeller. While the data presented by these writers is useful it is too restricted for any positive conclusions to be made regarding the range of applicability of the proposed criterion.

Cavitation in pumps handling liquid metals has been studied by Grindell (105) and Smith et al. (106). Their work was hampered by uncertainty concerning the vapour pressures of liquid metals, but the general conclusion was that pump cavitation performance on liquid metals was similar to that on water.

To sum up, the inference to be drawn from this discussion is that impellers designed for certain suction conditions with cold water will operate satisfactorily at the same suction conditions with another liquid. The performance of impellers handling fluids with low liquid to vapour density ratios is less sensitive to cavitation, and this fact has assisted the development of inducer-type pumps for special liquids such as hydrogen.

6.2 CONCLUSION

This thesis began with a discussion of the phenomenon of cavitation in hydro-dynamics and then moved on to consider its influence on the design of impellers for centrifugal and axial-flow impellers. In general there are two performance criteria for impeller design :

(1) Maximum efficiency at specified duty (or duties)

(2) Optimum cavitation performance at specified duty (or duties).

The primary objective of the thesis has been to develop methods for meeting the second criterion, which may not necessarily be compatible with the first It was pointed out in Chapter 4 that a centrifugal impeller for high suction specific speed would not give the maximum efficiency possible, because in effect its entry would be designed for a flow greater than that specified, whereas its outlet and the delivery passages in the pump casing would be designed for the flow specified.

In order to provide a rational basis for the design of centrifugal and axial-flow impellers for optimum cavitation performance, it is necessary to have

(1) quantitative knowledge of the mechanics of cavitation

(2) quantitative knowledge of the flow in a rotating impeller.

Chapters 2 and 3 surveyed current ideas of the mechanics of cavitation, and some of the theoretical aspects of the flow in impellers were discussed in Chapter 4. These are both complex subjects, so much so that at the present time it is not possible to calculate from first principles the

cavitation performance of a new impeller. By analyzing experimental data from tests on existing designs, it is possible to build up a semi-empirical theory which can be extended to make predictions of the performance of new designs.

Centrifugal and axial-flow pumps have been built for many years and in many respects the art of their design is well developed. There are, however, exceptions to this generalization, particularly in the field of performance under cavitating conditions and at off-design conditions generally. With regard to cavitation, this thesis has examined current design practice; it is noteworthy that progress to date has been achieved without a solution of several problems of a fundamental nature, namely, the definition of cavitation inception, the problem of scale effects, and the determination of blade pressure distribution.

(1) Definition of Cavitation Inception.

A number of questions arise here. Should the inception of cavitation be defined by visual or sonic means or by observations of performance? Does inception of cavitation occur at the vapour pressure or will the liquid support a tension? What is the importance in practice of the difference between "desinent" and "incipient" cavitation? Can the onset of "gaseous" cavitation be distinguished from that of "vapourous" cavitation?

(2) Scale Effects.

Under what conditions is it possible to predict the cavitation performance of large hydraulic machinery from tests on models? While individual manufacturers may have been able to obtain partial answers to this question in the light of their own operating experience, a general answer is not known.

(3) Blade Pressure Distribution.

The question here is - What is the pressure distribution around an impeller blade? Detailed calculations of the flow in a rotating impeller can be carried out based on perfect fluid theory but this involves laborious mathematics. The advent of the electronic computer has now made the results of such calculations available to the designer. Commercial factors then enter the picture : is it economically worthwhile for the designer to hire or buy a computer in order to obtain a more complete mathematical description of the flow through the impeller, bearing in mind that this description is limited by the assumptions of perfect fluid theory and that he can achieve a design almost as good himself at lower cost. The position may well be reached where a large amount of money and effort is expended in attempts to obtain marginal improvement in performance.

Fig. (4.13) summarised the limits of performance of conventional pumps, but it was later shown that these limits could be greatly extended by designing for cavitating and super-cavitating flows. A strong impetus has been given to this subject by the requirements of light, high-speed pumps for liquid fuel rockets, also by the prospect of increasing ships' speeds with super-cavitating propellers. In these fields more prosaic

engineering considerations tend to be superseded by the requirements of military technology, national defence, and national prestige. One can expect therefore that developments in the use of cavitating impellers will be rapid, and that these developments will be firmly based on the theory of cavitating and super-cavitating flows. Some of the important aspects of this theory have been studied in Chapter 5, and an estimate has been made of the ultimate limits that may be placed on the cavitation performance of centrifugal and axial-flow pumps.

In conclusion, the subject of cavitation has been considered from the viewpoint of the pump designer, who is concerned not so much with making a deep theoretical study but with developing methods which will enable him to achieve good design, even if this means taking short cuts on the way. The thesis has been written with the intention of combining an account of the theory of cavitation with an examination of the practical details of its influence on impeller design. Where the inevitable gaps between theory and practice have appeared, the way has been pointed to further studies which would help to eliminate them.

APPENDIX I.

The impeller cavitation coefficient may be expressed either by using the mean axial velocity of approach at the impeller eye v_a, or the mean velocity at the blade inlet v_m. Thus,

$$Ka = \frac{Hsv}{\left(\frac{v_a^2}{2g}\right)}$$

$$Km = \frac{Hsv}{\left(\frac{v_m^2}{2g}\right)}$$

In what follows suffixes "a" and "m" will be used with the coefficients k, Ko and K_1 to denote whether they are based on v_a or v_m. Equation (4.13) can be written

$$Hsv = K_{oa}\frac{v_a^2}{2g} + k_a\frac{w_a^2}{2g} \qquad (a)$$

$$\text{or } Hsv = K_{om}\frac{v_m^2}{2g} + k_m\frac{w_m^2}{2g} \qquad (b)$$

$$\therefore Hsv = (K_{oa} + k_a)\frac{v_a^2}{2g} + k_a\frac{u^2}{2g} \qquad (c)$$

$$\text{and } Hsv = (K_{om} + k_m)\frac{v_m^2}{2g} + k_m\frac{u^2}{2g} \qquad (d)$$

$$\therefore Hsv = (K_{1a})\frac{v_a^2}{2g} + k_a\frac{u^2}{2g} \qquad (e)$$

$$\text{and } Hsv = (K_{1m})\frac{v_m^2}{2g} + k_m\frac{u^2}{2g} \qquad (f)$$

In the text the two expressions for Hsv, (e) and (f), were made equivalent by putting

$$k_a = k_m = K$$

$$\text{and } K_{1a}v_a^2 = K_{1m}v_m^2$$

$$\text{i.e. } K_{1a} = f_1^2 K_{1m} \qquad (g)$$

APPENDIX II.

BIBLIOGRAPHY

This bibliography is arranged so that the references are grouped under the chapters in which they occur. They are numbered in the order in which they appear in the text, with the proviso that where additional references are given which are not mentioned in the text, these additions are placed at the end of the list for the particular chapter to which they apply.

CHAPTER 2

1. Briggs, L. J. "Limiting Negative Pressure of Water," J. Appl. Physics, Vol. 21, 1950, p. 721.

2. Harvey, E. N., McElroy, W. D. and Whiteley, A. H. "On Cavity Formation in Water". J. Appl. Physics, Vol. 18, 1947, p.162.

3. Knapp, R. T. "Cavitation and Nuclei." Trans. ASME, Vol. 80, 1958, p.1315.

4. Strasberg, M. "Undissolved Air Cavities as Cavitation Nuclei." Proc. N.P.L. Symposium on Cavitation in Hydrodynamics, H.M.S.O., London, 1956.

5. Richardson, E. G. "The Mechanism of Cavitation," Wear, Vol. 2, 1958, p. 97.

6. Vuskovic, I. "Investigations on the Influence of Air Content on Cavitation and Corrosion in the case of Water Flow." Escher-Wyss News, Vol. 13, 1940, p.83.

7. Noltingk, B. E. and Neppiras, E. A. "Cavitation Produced by Ultrasonics." Proc. Phys. Soc. B, Vol. 63, 1950, p. 674, and Vol. 64, 1951, p.1032.

8. Shmuglyakov, L. S. "The Relation Between the Cavitation Coefficient and Content of Air Dissolved in Water." Energomachinostroenie, 1956, No. 5, p.11; D.S.I.R. translation No. 441.

9. Kanellopoulos, E. V. "Cavitation Tests on a Small Centrifugal Pump." N.E.L. Fluids Report No. 95, 1960.

10. Numachi, F. "The Effect of Air Content on the Appearance of Cavitation in Distilled, Salt, and Sea Water." Ordnance Research Laboratory, Pennsylvania State College, 1946.

11. Crump, S. F. "Determination of Critical Pressures for the Inception of Cavitation in Fresh and Sea Water as Influenced by Air Content." David Taylor Model Basin Report No. 575, 1949.

12. Williams, E. E. and McNulty, P. "Some Factors Affecting the Inception of Cavitation." Proc. N.P.L. Symposium on Cavitation in Hydrodynamics, H.M.S.O., London, 1956.

13. Ripken, J. F. "A Study of the Influence of Gas Nuclei on Cavitation Scale Effects in Water Tunnel Tests." St. Anthony Falls Hydraulic Laboratory Report No. 58, 1958.

14. Holl, J. W. "An effect of Air Content on the Occurrence of Cavitation." Trans. ASME, Series D, Journal of Basic Engineering, Vol. 82, 1960, p. 941.

15. Kermeen, R. W., McGraw, J. T. and Parkin B. R. "Mechanism of Cavitation Inception and the Related Scale Effects Problem." Trans. ASME, Vol. 77, 1955, p.533.

16. Hammitt, F. G. "Observations of Cavitation Scale and Thermodynamic Effects in Stationary and Rotating Components." ASME Paper No. 62-HYD-1.

17. Edstrand, H. "The Effect of Air Content of Water on the Cavitation Point and upon the Characteristics of Ship's Propellers." State Shipbuilding Experimental Tank Report No. 6, Goteberg, Sweden, 1946.

18. Straub, L. G., Ripken, J. F. and Olson, R. "The 6-inch Water Tunnel at the St. Anthony Falls Hydraulic Laboratory and its Experimental Use in Cavitation Design Studies." Proc. N.P.L. Symposium on Cavitation in Hydrodynamics, H.M.S.O., London, 1956.

19. Daily, J. W. and Johnson, V. E. "Turbulence and Boundary Layer Effects on Cavitation Inception from Gas Nuclei." Trans. ASME, Vol. 78, 1956, p. 1695.

20. Holl, J. W. "The Inception of Cavitation on Isolated Surface Irregularities." Trans. ASME, Series D, J. Basic Eng., Vol. 82, 1960, p. 169.

21. Daily, J. W. "Cavitation Characteristics and Infinite Aspect Ratio Characteristics of a Hydrofoil Section." Trans. ASME, Vol. 71, 1949, p. 269.

22. Shalnev, K. K. "Experimental Study of the Intensity of Erosion due to Cavitation." Proc. N.P.L. Symposium on Cavitation in Hydrodynamics, H.M.S.O., London, 1956.

23. Knapp, R. T. "Cavitation Mechanics and its Relation to the Design of Hydraulic Equipment." Proc. I. Mech. E., Vol. 166, 1952, p. 150.

24. Rayleigh, Lord. "On the Pressure developed in a Liquid During the Collapse of a Spherical Cavity." Phil. Mag., Vol. 34, 1917, p. 94.

25. Plesset, M. S. "The Dynamics of Cavitation Bubbles." Trans. ASME, J. Appl. Mech., Vol. 16, 1949, p. 271.

26. Plesset, M. S. and Zwick, S. A. "On the Dynamics of Small Vapour Bubbles in Liquids." J. Maths. Phys., Vol. 33, 1955.

27. Gilmore, F. R. "The Growth or Collapse of a Spherical Bubble in a Viscous Compressible Liquid." Cal. Inst. of Tech. Hyd. Lab. Report 21-19, 1954.

28. Sutton, G. W. "A Photoelastic Study of Strain Waves caused by Cavitation." Trans. ASME, J. Appl. Mech., Vol. 24, 1957, p. 340.

29. Godfrey, D. J. "Cavitation Damage - A Review of Present Knowledge." Chem. and Ind., Vol. 23, 1959, p. 686.

30. Preiser, H. S. and Tykell, B. H. "The Electrochemical Approach to Cavitation Damage and its Prevention." Corrosion, Vol. 17, No. 11, Nov. 1961, p. 107.

31. Wheeler, W. H. "Indentation of Metals by Cavitation." Trans. ASME, Series D, J. Basic Eng., Vol. 82, 1960, p. 184.

32. Plesset, M. S. "On Cathodic Protection in Cavitation Damage." Trans. ASME, Series D, J. Basic Eng., Vol. 82, 1960, p. 808.

33. Rheingans, W. J. (Editor). Symposium on Resistance of Various Materials to Cavitation Damage. ASME, 1957.

34. Blake, F. G. "The Onset of Cavitation in Liquids." Acoustics Research Laboratory, Harvard University, Tech. Report No. 12, Sept., 1949.

35. Frenkel, J. "Kinetic Theory of Liquids." Dover Publications, New York, 1955.

36. Streeter, V. L. (Editor). Handbook of Fluid Dynamics, McGraw-Hill, New York, 1961.

37. Wheeler, W. H. "Mechanism of Cavitation Erosion." Proc. N.P.L. Symposium on Cavitation in Hydrodynamics, H.M.S.O., London, 1956.

CHAPTER 3.

38. Plesset, M. S. and Zwick, S. A. "A Nonsteady Heat Diffusion Problem with Spherical Symmetry." J. Appl. Phys., Vol. 23, 1952, p. 95.

39. Dergarabedian, P. "The Rate of Growth of Vapour Bubbles in Superheated Water." Trans. ASME, J. Appl. Mech., Vol. 20, 1953, p. 537.

40. Holl, J. W. and Wislicenus, G. F. "Scale Effects on Cavitation." Trans. ASME, Series D, J. Basic Eng., Vol. 83, 1961, p. 385.

41. Hutton, S. P. "Basic Problems in Predicting Water-Turbine Performance from Model Tests." N.E.L. Fluids Report No. 84, 1959.

42. Danel, P. and Dupont, J. "The Selection of Length and Head Scales for Cavitation Tests." Trans. ASME, Series D, J. Basic Eng., Vol. 82, 1960, p. 784.

43. Gerber, H. "Some Reflections on Model Scale Formulae for Cavitation Phenomena." Proc. N.P.L. Symposium on Cavitation in Hydrodynamics, H.M.S.O., London, 1956.

44. Numachi, F. "Effect of Static Pressure Differences on the Cavitation Characteristics of Hydrofoil Profiles." Proc. N.P.L. Symposium on Cavitation in Hydrodynamics, H.M.S.O., London, 1956.

45. Thoma, D. "Experimental Research in the Field of Water Power." Proc. First World Power Conference, Vol. 2, London, 1924, p. 536.

CHAPTER 4.

46. Wood, G. M., Murphy, J. S. and Farquhar, J. "An Experimental Study of Cavitation in a Mixed-Flow Pump Impeller." Trans. ASME, Series D, J. Basic Eng., Vol. 82, 1960, p. 929.

47. Gongwer, C. A. "A Theory of Cavitation Flow in Centrifugal Pump Impellers." Trans. ASME, Vol. 63, 1941, p. 29.

48. ASME Power Test Code for Centrifugal Pumps, No. PTC 8.1 - 1954.

49. Hartmann, M. J. and Solfis, R. F. "Observation of Cavitation in a Low Hub-Tip Ratio Axial - Flow Pump." ASME Paper No. 60-HYD-14.

50. Minami, S., Kawaguchi, K. and Homma, T. "Experimental Study on Cavitation in Centrifugal Pump Impellers." Bulletin JSME, Vol. 3, No. 9, 1960, p. 19.

51. Tenot, M. A. "Phenomenes de la Cavitation." Mem. Soc. Ing. Civils France Bull., May and June 1934, p. 377.

52. Wood, G. M. "Visual Cavitation Studies of Mixed-Flow Pump Impellers." ASME Paper No. 62-HYD-12.

53. Pfleiderer, C. "Die Kreiselpumpen." Julius Springer, Berlin, 1955.

54. Wislicenus, G. F. "Fluid Mechanics of Turbomachinery." McGraw-Hill, New York, 1947.

55. Wislicenus, G. F. "Critical Considerations on Cavitation Limits of Centrifugal and Axial-Flow Pumps." Trans. ASME, Vol. 78, 1956, p. 1707.

56. Stepanoff, A. J. and Stahl, H. A. "Dissimilarity Laws in Centrifugal Pumps and Blowers." Trans. ASME, Series A, J. Eng. Power, Vol. 83, 1961, p. 381.

57. Uchimaru, S. "Experimental Research on the Distribution of Water Pressure in a Centrifugal Pump Impeller." Journal, Faculty Eng., Tokyo Imp. Uni., Vol. 16, 1925.

58. Acosta, A. J. and Bowerman, R. D. "An Experimental Study of Centrifugal Pump Impellers." Trans. ASME, Vol. 79, 1957, p. 1821.

59. Acosta, A. J. "An Experimental and Theoretical Investigation of Two-Dimensional Pump Impellers." Trans. ASME, Vol. 76, 1954, p. 749.

60. Hamrick, J. T., Ginsburg, A. and Osborn, W. M. "Method of Analysis for Compressible Flow Through Mixed-Flow Centrifugal Impellers of Arbitrary Design." NACA report No. 1082.

61. Abbott, I. H., van Doenhoff, A. E. and Stivers, L. S. "Summary of Airfoil Data." NACA Report No. 824, 1945.

62. Peebles, G. H. "A Method for Calculating Airfoil Sections from Specifications on the Pressure Distribution." J. Aero Sciences, Vol. 14, 1947, p. 451.

63. Schlichting, H. "Berechnung der Reibungslosen In Kompressiblen Stromung fur ein Vorgegebenes ebenes Schaufelgitter." 1955, VDI - Forsch. - Heft 447, Dusseldorf.

64. Weinig, K. "Die Stromung und die Schaufeln von Turbomaschinen." Barth, Leipzig, 1935.

65. Lighthill, M. J. "A Mathematical Theory of Cascade Design." Aero. Research Committee, R. & M. No. 2104, 1946.

66. Johnson, C. H. J. and Howard, W. "Simplification in the Lighthill Method of Design of Aerofoils in Cascade." Aust. Dept. of Supply, Note ARL/ME 216.

67. Scholz, N. "Stromungsuntersuchungen an Schaufelgittern. Teil II : Ein Berechnungsverfahren zum Entwurf von Schaufelgitterprofilen." 1954, VDI - Forsch.- Heft 442, Dusseldorf.

68. Vavra, M. H. "Aero-Thermodynamics and the Flow in Turbomachines." John Wiley and Son, New York, 1960.

69. Kovats, A. de, and Desmur, G. "Pumps, Fans, and Compressors." Blackie and Son, London, 1958.

70. Wislicenus, G. F. "A Study of the Theory of Axial-Flow Pumps." Trans. ASME, Vol. 67, 1945, p. 451.

71. Carter, A.D.S. "Blade Profiles for Axial-Flow Pumps, Fans, Compressors." Proc. I. Mech. E., Vol. 175, 1961, p. 775.

72. Hutton, S. P. "Thin Aerofoil Theory and the Application of Analogous Methods to the Design of Kaplan Turbine Blades." Proc. I. Mech. E., Vol. 163, 1950, p. 81.

73. Escher - Wyss News, Vol. 12, 1939, Nos. 1 and 2.

74. McCormick, B. W. "On Cavitation Produced by a Vortex Trailing From a Lifting Surface." Trans. ASME, Series D, J. Basic Eng., Vol. 84, 1962, p. 369.

75. Smith, L. H., Traugott, S. C. and Wislicenus, G. F. "A Practical Solution of a Three-Dimensional Flow Problem of Axial-Flow Turbomachinery." Trans. ASME, Vol. 75, 1953, p. 789.

76. Balje, O. E. "A Study on Design Criteria and Matching of Turbomachines : Part B." Trans. ASME, Series A, J. Eng. Power, Vol. 84, 1962, p. 103.

77. Bowerman, R. D. "The Design of Axial-Flow Pumps." Trans. ASME, Vol. 78, 1956, p. 1723.

78. Stepanoff, A. J. and Stahl, H. A. "Cavitation Criterion for Dissimilar Centrifugal Pumps." Trans. ASME, Series A, J. Eng. Power, Vol. 84, 1962, p. 329.

79. O'Brien, M. P. and Folsom, R. G. "The Design of Propeller Pumps and Fans." Uni. of Cal. Publications, Vol. 4, No. 1, p.1, 1939.

80. Morelli, D. A. and Bowerman, R. D. "Pressure Distributions on the Blade of an Axial-Flow Propeller Pump." Trans. ASME, Vol. 75, 1953, p. 1007.

81. Kamimoto, G., Ando, H. and Akamatsu, T. "On the Flow in a Water-Turbine of an Axial-Flow Type." Bulletin, JSME, Vol. 2, No. 8, 1959, p. 616.

82. Horie, A. and Kawaguchi, K. "Cavitation Tests on an Axial-Flow Pump." Bulletin, JSME, Vol. 2, No. 5, 1958, p. 187.

83. Rutchi, K. "Pfleiderer's Suction Number as a Criterion of the Suction Performance of Centrifugal Pumps." Schweizerische Bauzeitung, 24th March, 1960, p. 199.

84. Spannhake, W. "Centrifugal Pumps, Turbines and Propellers." M.I.T., 1934.

85. Stepanoff, A. J. "Centrifugal and Axial-Flow Pumps." John Wiley and Sons, New York, 1957.

86. von Widdern, H. Cardinal. "On Cavitation in Centrifugal Pumps." Escher-Wyss News, Jan. - March 1936, P.15.

87. Wislicenus, G. F., Watson, R. M. and Karassik, I. J. "Cavitation Characteristics of Centrifugal Pumps Described by Similarity Considerations." Trans. ASME, Vol. 61, 1939, p. 17.

CHAPTER 5.

88. Tachmindji, A. J. and Morgan, W. B. "The Design and Estimated Performance of a Series of Super-cavitating Propellers." Proc. 2nd ONR Symposium on Naval Hydrodynamics, U.S. Govt. Printing Office, Washington, D.C., 1960.

89. Tachmindji, A. J., Morgan, W. B., Miller, M. L. and Hecker, R. "The Design and Performance of Super-cavitating Propellers." David Taylor Model Basin Report C-807, Washington, D. C., 1957.

90. van Niekirk, C. G. "Ducted Fan Design Theory." Trans. ASME, J. Appl. Mech., Vol. 25, 1958, p. 325.

91. Wu, T. Y. "A Free Streamline Theory for Two-Dimensional Fully Cavitated Hydrofoils." Cal. Inst. of Tech. Hyd. Lab. Report No. 21-17, July, 1955.

92. Plesset, M. S. and Parkin, B. R. "Hydrofoils in Non-cavitating and Cavitating Flow." Proc. N.P.L. Symposium on Cavitation in Hydrodynamics, H.M.S.o., London, 1956.

93. Tulin, M. P. and Burkart, M. P. "Linearized Theory for Flows about Lifting Foils at Zero Cavitation Number." David-Taylor Model Basin Report C-638, Washington, D.C., 1955.

94. Tulin, M. P. "Super-cavitating Flow Past Foils and Struts." Proc. N.P.L. Symposium on Cavitation in Hydrodynamics, H.M.S.O., London, 1956.

95. Stripling, L. B. and Acosta, A. J. "Cavitation in Turbo Pumps - Part I." Trans. ASME, Series D, J. Basic Eng., Vol. 84, 1962, p. 326.

96. Stripling, L. B. "Cavitation in Turbo Pumps - Part II." Trans. ASME, J. Basic Eng., Vol. 84, 1962, p. 339.

97. Dumov, V. I. "Designing Centrifugal Pumps with Boost Impellers to Improve Cavitation Performance." Teploenergetika, 1959, No. 6, p. 35. N.E.L. Translation No. 690.

98. Ross, C. C. and Banerian, G. "Some Aspects of High Suction Specific Speed Pump Inducers." Trans. ASME, Vol. 78, 1956, p. 1715.

99. Norbury, J. F. "The Super-cavitating Axial-Flow Pump - A Preliminary Study." N.E.L. Fluids Note No. 88, 1960.

100. Acosta, A. J. "Experimental Study of Cavitating Inducers." Proc. 2nd ONR Symposium on Naval Hydrodynamics, U.S. Govt. Printing Office, Washington, D.C., 1960.

101. Birkoff, G. and Zarantonello, E. H. "Jets, Wakes and Cavities," Academic Press, New York, 1957.

102. Mullan, J. "An Investigation of Cavitating Inducers." Report No. 53, M.I.T., 1959.

CHAPTER 6.

103. Salemann, V. "Cavitation and N.P.S.H. Requirements of Various Liquids." Trans. ASME, Series D, J. Basic Eng., Vol. 81, 1959, p.167.

104. Stepanoff, A. J. "Cavitation in Centrifugal Pumps with Liquids other than Water." Trans. ASME, Series A, J. Eng. Power, Vol. 83, 1961, p. 79.

105. Grindell, A. G. "Correlation of Cavitation Inception Data for a Centrifugal Pump Operating in Water and in Sodium-Potassium Alloy (Nak)." Trans. ASME, Series D, J. Basic Eng., Vol. 82, 1960, p. 821.

106. Smith, P. G., De Van, J. H. and Grindell, A. G. "Cavitation Damage to Centrifugal Pump Impellers During Operation with Liquid Metals and Molten Salts at 1040-1400°F." ASME Paper No. 62-HYD-2.

107. Silverstein, A. "Researches in Space Flight Technology." J. Roy. Aero. Soc., Vol. 65, Dec. 1961, p. 779.

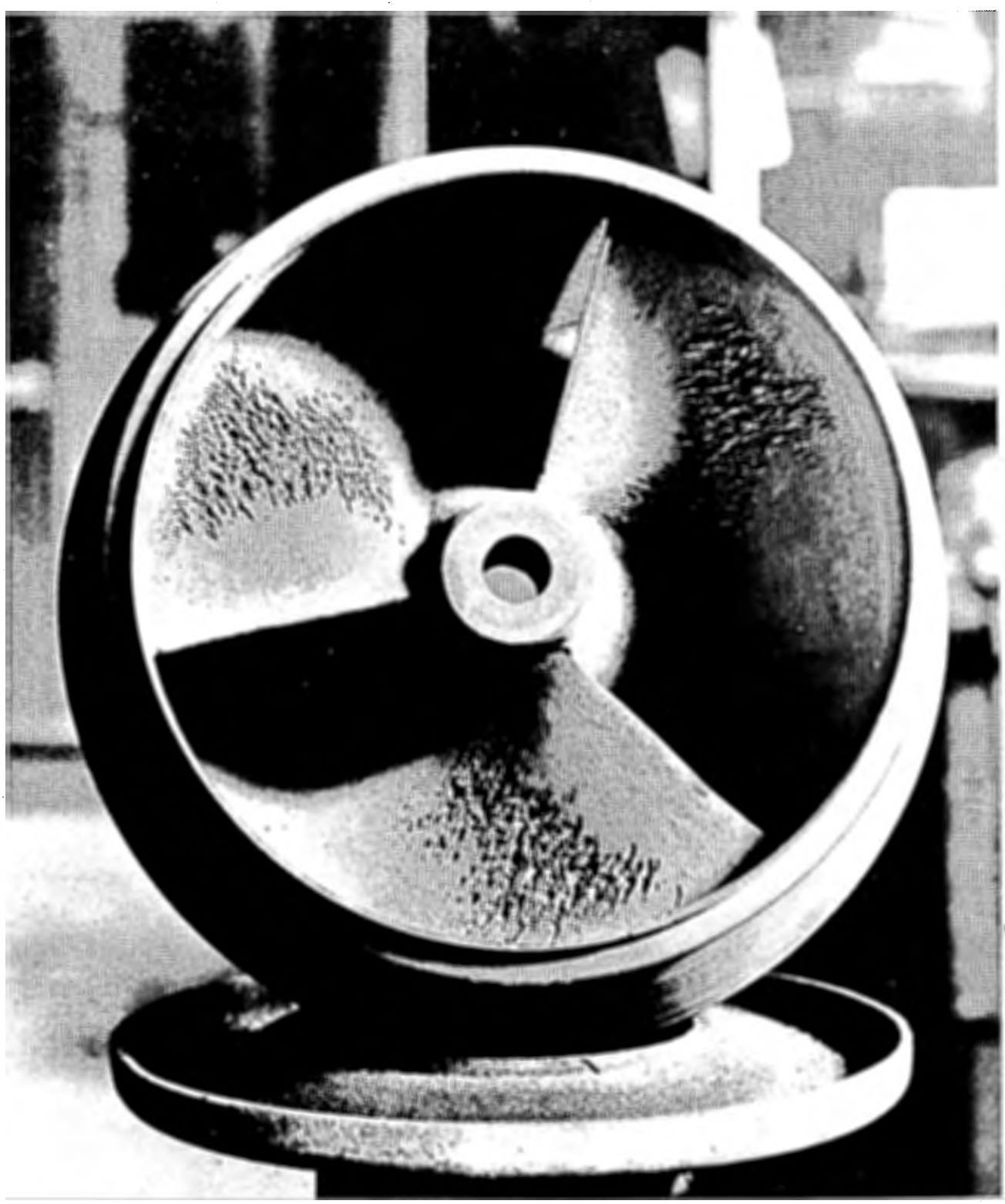

FIG. 1.1. THE EFFECT OF CAVITATION EROSION ON CAST IRON IMPELLER AFTER 100 HOURS IN CLEAN WATER

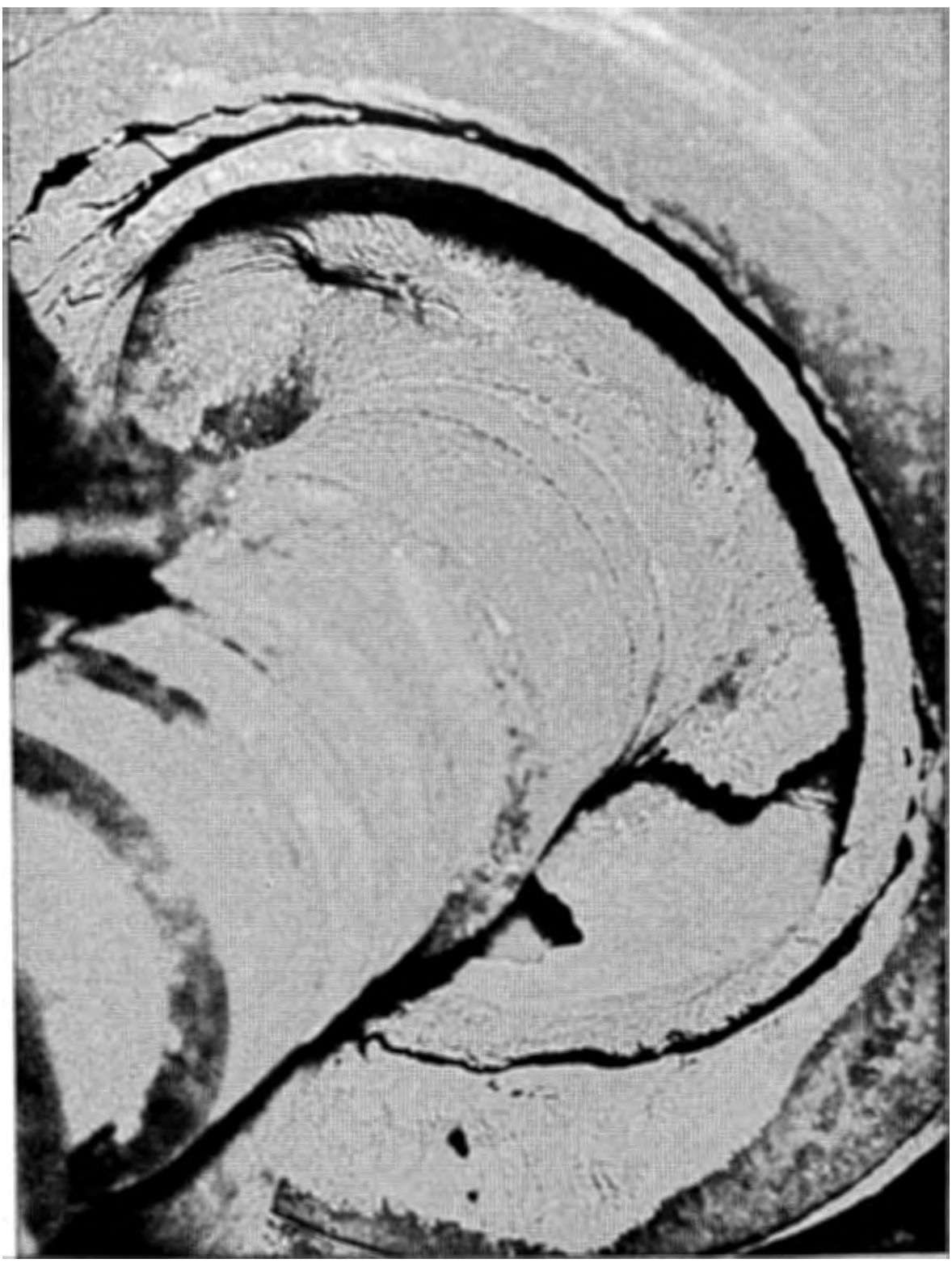

FIG1.2. THE EFFECT OF CAVITATION EROSION AND CORROSION ON BRONZE IMPELLER AFTER 1000 HOURS IN SEA WATER

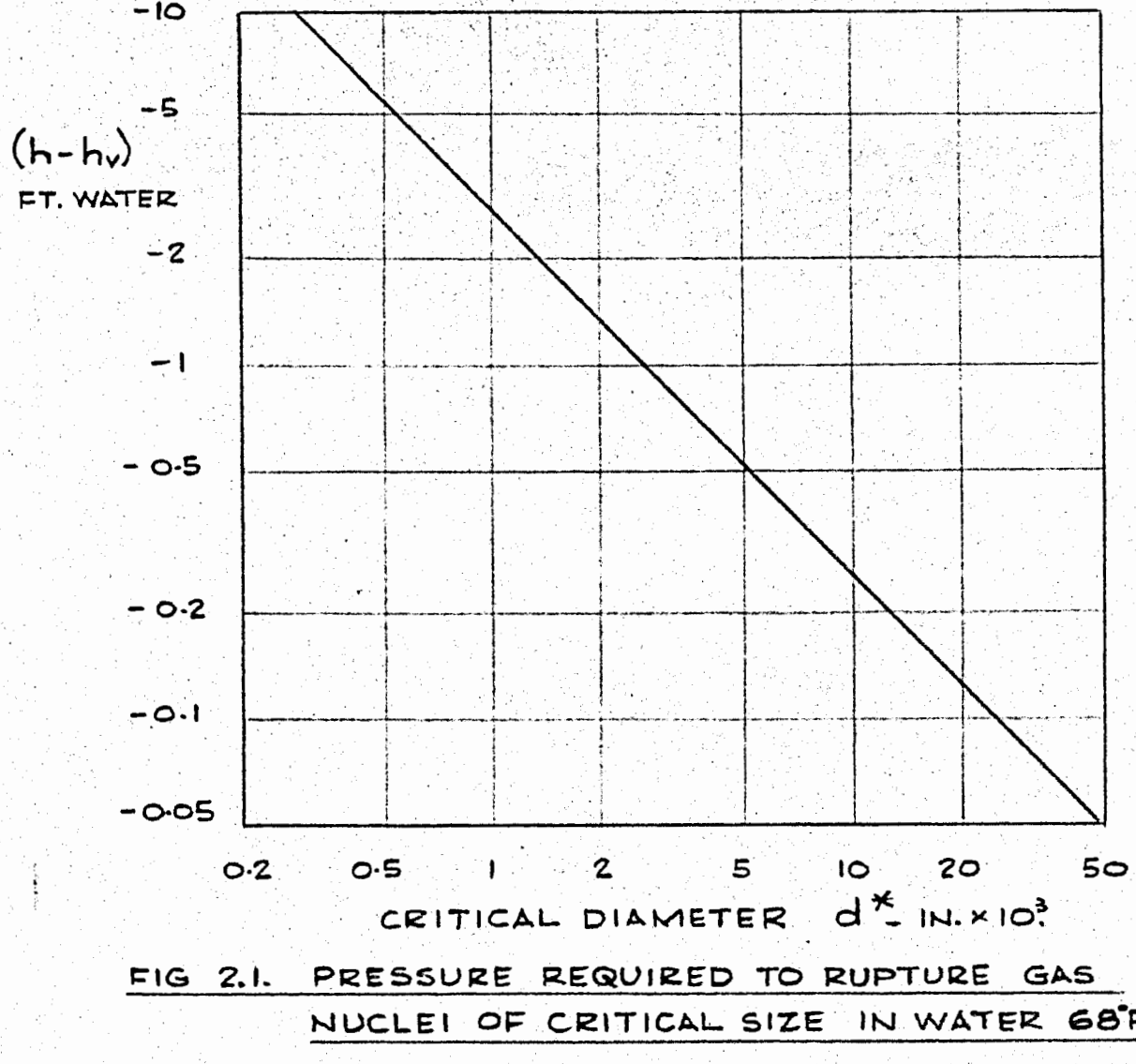

FIG 2.1. PRESSURE REQUIRED TO RUPTURE GAS NUCLEI OF CRITICAL SIZE IN WATER 68°F.

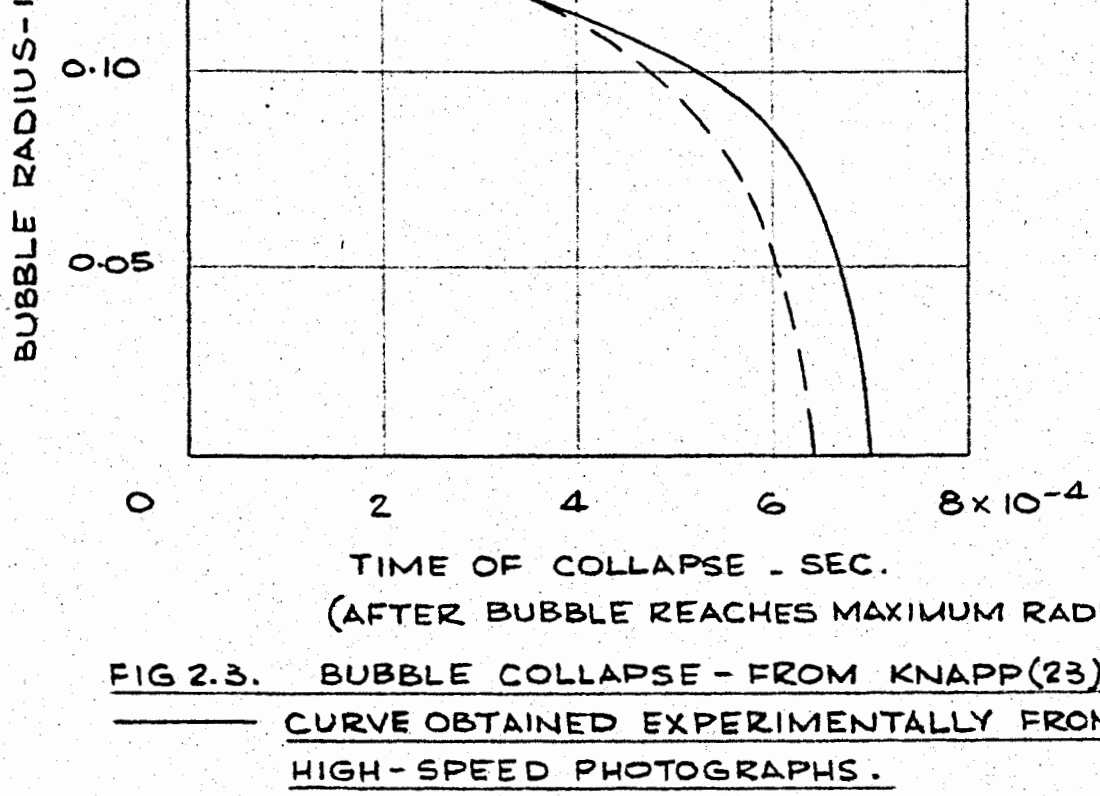

FIG 2.3. BUBBLE COLLAPSE - FROM KNAPP(23).

——— CURVE OBTAINED EXPERIMENTALLY FROM HIGH-SPEED PHOTOGRAPHS.

– – – – RAYLEIGH THEORETICAL CURVE FROM EQUAL MAXIMUM DIAMETER AND PRESSURE DIFFERENCE.

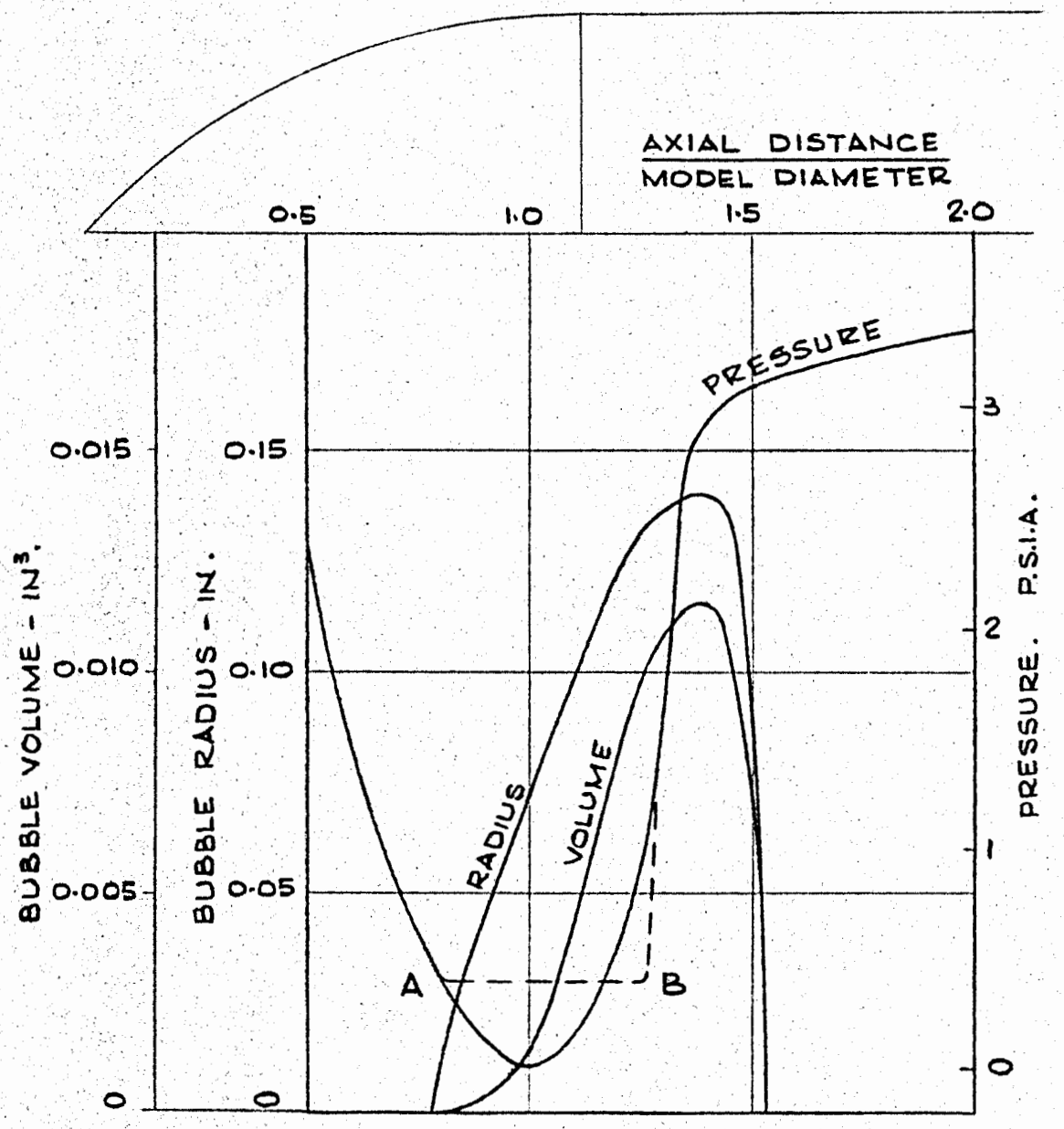

FIG 2.2. RELATION OF BUBBLE GROWTH AND COLLAPSE TO PRESSURE-FROM KNAPP (23).

FIG 3.1. DEFINITION OF NET POSITIVE SUCTION HEAD.

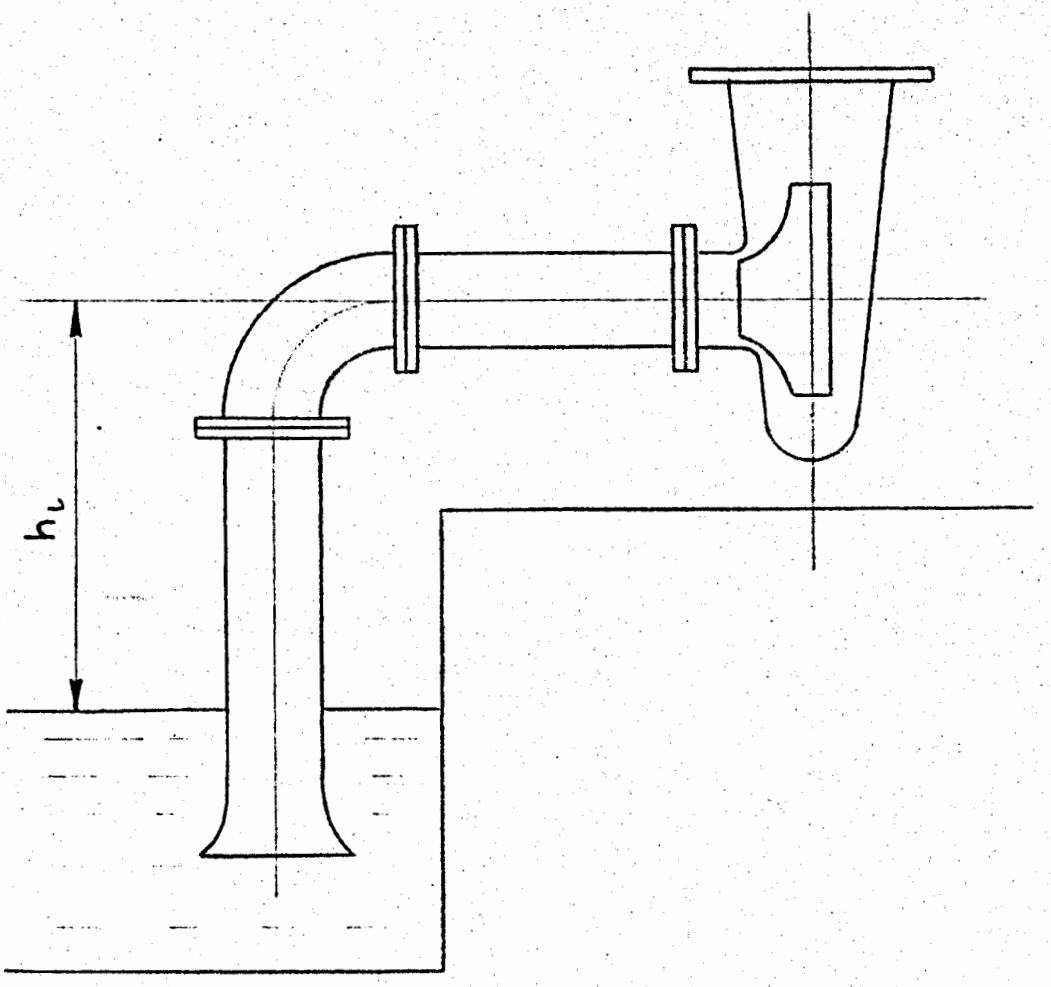

NET POSITIVE SUCTION HEAD (H_{sv}) IS DEFINED AS THE DIFFERENCE BETWEEN THE TOTAL PRESSURE OF THE LIQUID AT THE SUCTION SIDE OF THE RUNNER AND ITS SATURATION PRESSURE.
IN THE CASE OF THE HORIZONTAL PUMP SHOWN ABOVE -

$$H_{sv} = h_a + h_s + \frac{V^2}{2g} - h_v$$

$$h_s = -(h_l + h_f)$$

WHERE h_a = ATMOSPHERIC PRESSURE
h_s = STATIC PRESSURE OF LIQUID AT IMPELLER INLET (ABOVE ATMOS.)
h_v = VAPOUR PRESSURE OF LIQUID AT IMPELLER INLET
h_l = STATIC SUCTION LIFT
h_f = FRICTION LOSS IN SUCTION PIPING
V = VELOCITY OF LIQUID AT IMPELLER INLET.

h_s h_v AND V ARE MEASURED AT A CONVENIENT REFERENCE PLANE, USUALLY PUMP SUCTION FLANGE.

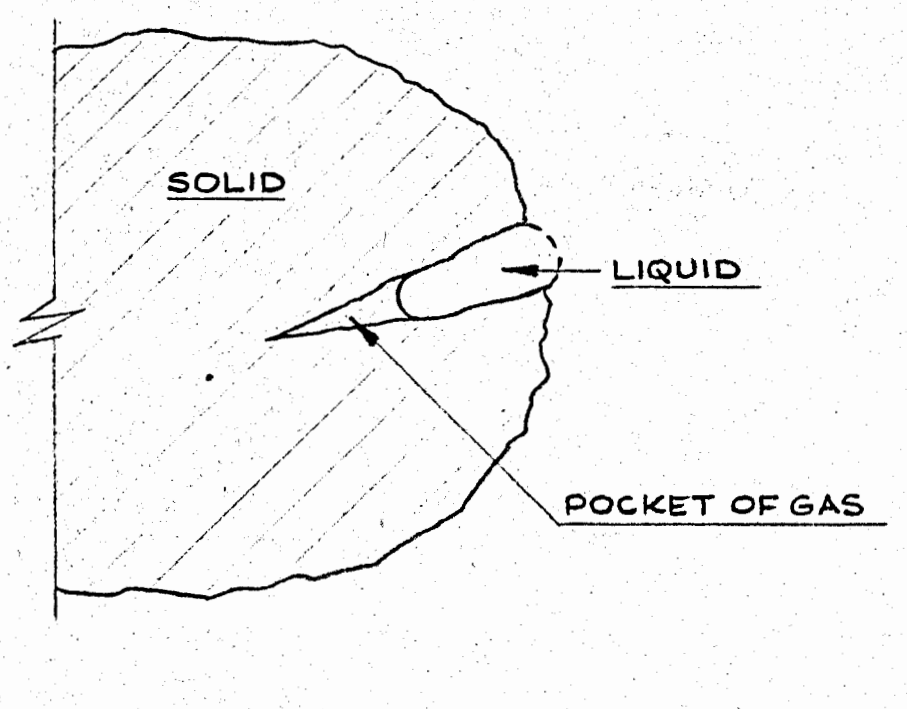

FIG 3.2. SKETCH OF CAVITATION NUCLEUS. (MUCH ENLARGED).

		FORCES AND CHARACTERISTICS	GENERAL SIMILARITY REQUIREMENTS
IDEAL FLOW	1	INERTIA FORCES ONLY (CLASSICAL THEORY)	$\sigma = H_{sv}/H$ = CONSTANT OR $K = (p-p_v)/\frac{1}{2}\rho V^2$ = CONSTANT
HYDRODYNAMIC SCALE EFFECTS ON THE FLUID PRESSURE	2	VISCOUS AND INERTIA FORCES	REYNOLD'S LAW $Re = \frac{VL}{\mu/\rho}$ = CONSTANT
	3	GRAVITY AND INERTIA FORCES	FROUDE'S LAW $Fr = \frac{V}{\sqrt{gL}}$ = CONSTANT
	4	ELASTIC AND INERTIA FORCES (COMPRESSIBILITY)	CONSTANT MACH NUMBER $M = V/a$ = CONSTANT
	5	EFFECTS OF SURFACE IRREGULARITIES	h/L = CONSTANT FOR Re = CONSTANT
THERMO-DYNAMIC SCALE EFFECTS	6	EFFECTS OF VAPOUR PRESSURE	p_v/p = CONSTANT
	7	EFFECTS OF VAPOURIZATION AND HEAT TRANSFER	$\Delta p_v/\frac{1}{2}\rho V^2$ = CONSTANT WHERE $\Delta p_v = \frac{\partial p_v}{\partial t} \cdot \frac{C_Q}{C_H} \cdot \frac{a_v}{a_l} \cdot \frac{v_l}{v_v} \lambda$
MOLECULAR AND OTHER MICROSCOPIC SCALE EFFECTS	8	SURFACE TENSION AND INERTIA FORCES	CONSTANT WEBER NUMBER $W = \frac{\rho V^2 L}{\delta}$ = CONSTANT
	9	SPECTRUM OF NUCLEI	$\sqrt[3]{N} \cdot L$ = CONSTANT $\Delta_{max}/\Delta_{mean}$ = CONSTANT

NOTES:-

(a) ITEMS (6) AND (7) MAY BE NEGLECTED IF p_v/p IS VERY SMALL, E.G. FOR COLD WATER.

(b) THE RELATIONS GIVEN IN ITEM (9) ASSUME THAT ALL NUCLEI ARE POTENTIAL CENTRES OF CAVITATION.

FIG 3.3. REQUIREMENTS FOR SIMILARITY OF CAVITATING FLOWS.

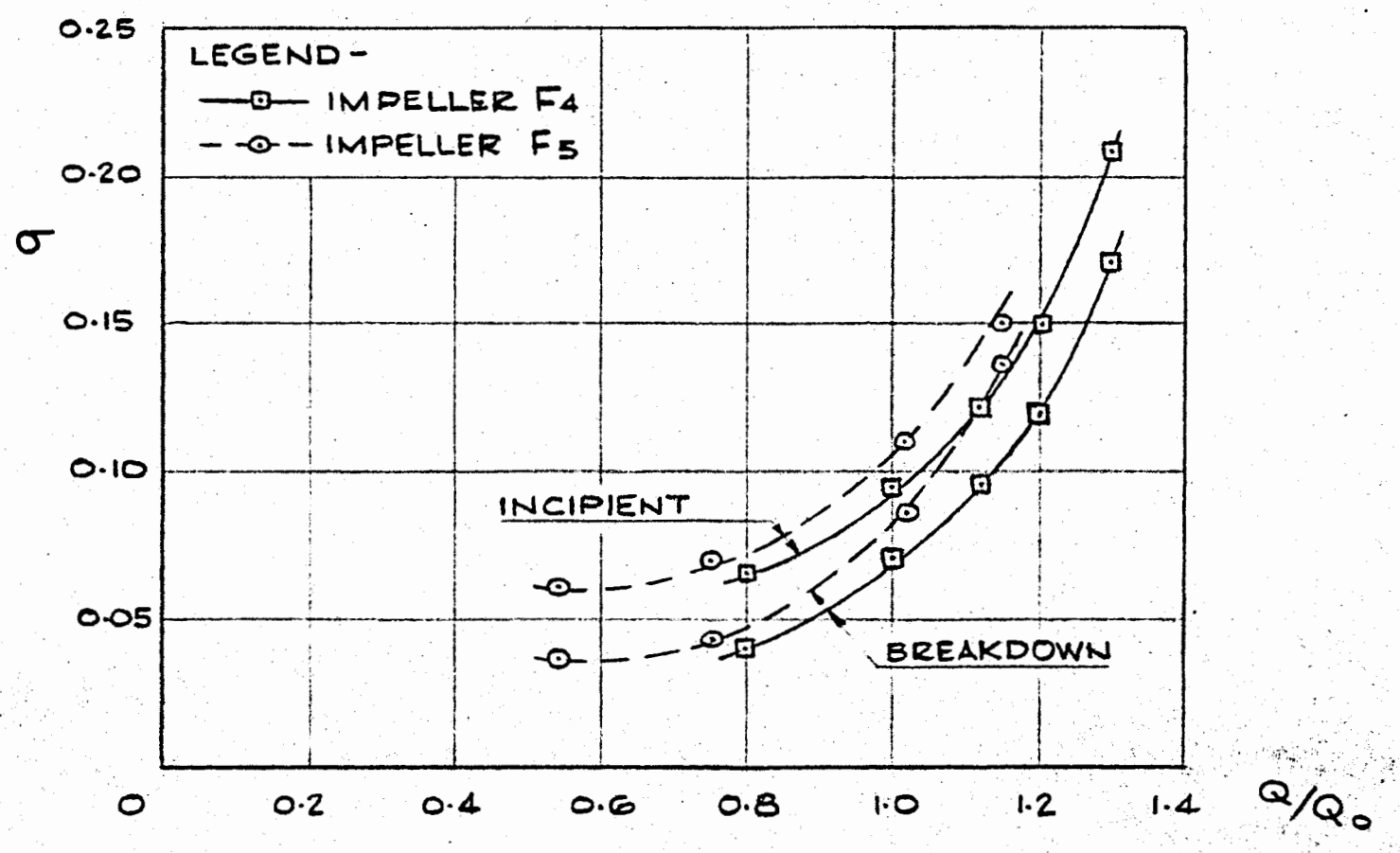

FIG 3.4. RESULTS OF CAVITATION TESTS ON TWO SIMILAR PUMPS. IMPELLER F_4 IS APPROXIMATELY HALF THE SIZE OF IMPELLER F_5.

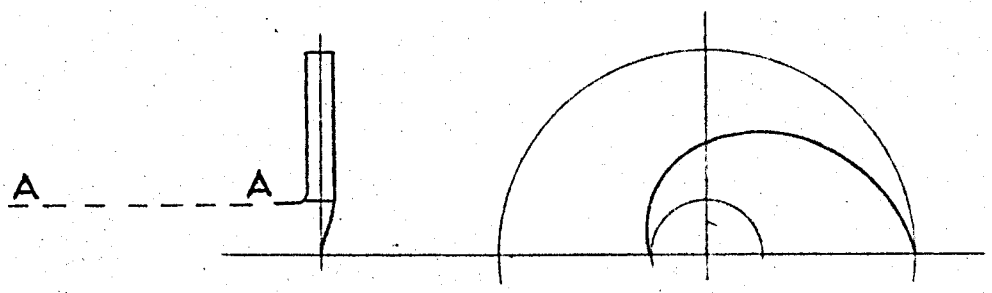

(a) RADIAL

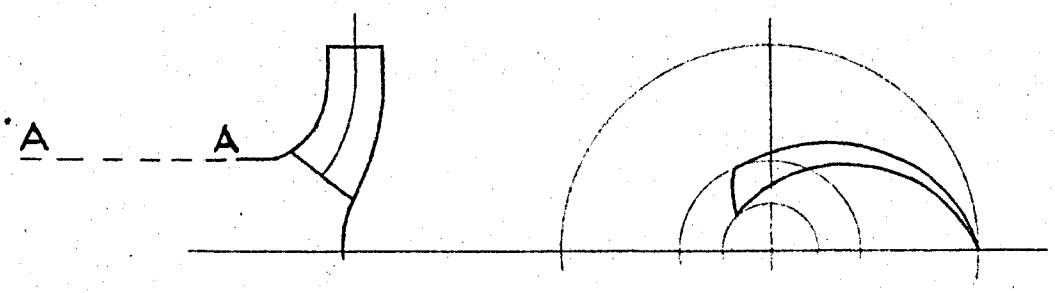

(b) FRANCIS

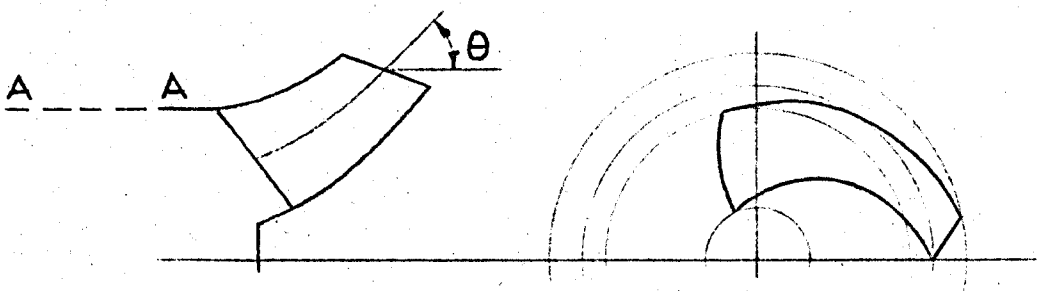

(c) MIXED FLOW

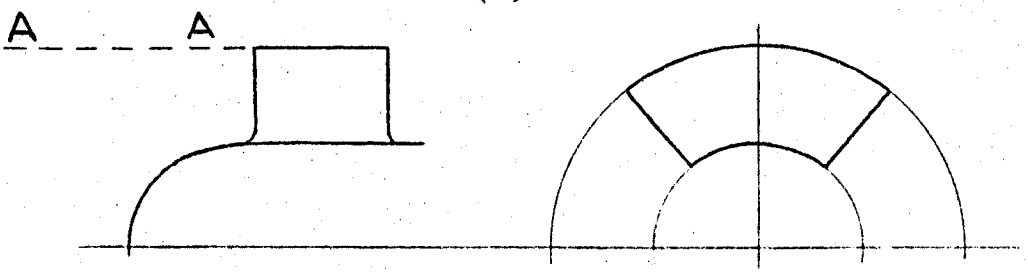

(d) AXIAL FLOW

	CENTRIFUGAL			AXIAL FLOW
	RADIAL	FRANCIS	MIXED FLOW	
BLADE CURVATURE	SINGLE	DOUBLE	DOUBLE	TWISTED BLADES
θ	90°	90°	$0 < \theta < 90°$	0°
SPECIFIC SPEED (APPROX)	< 40	40 - 140	140 - 330	> 330

FIG 4.1. CLASSIFICATION OF PUMP IMPELLERS.

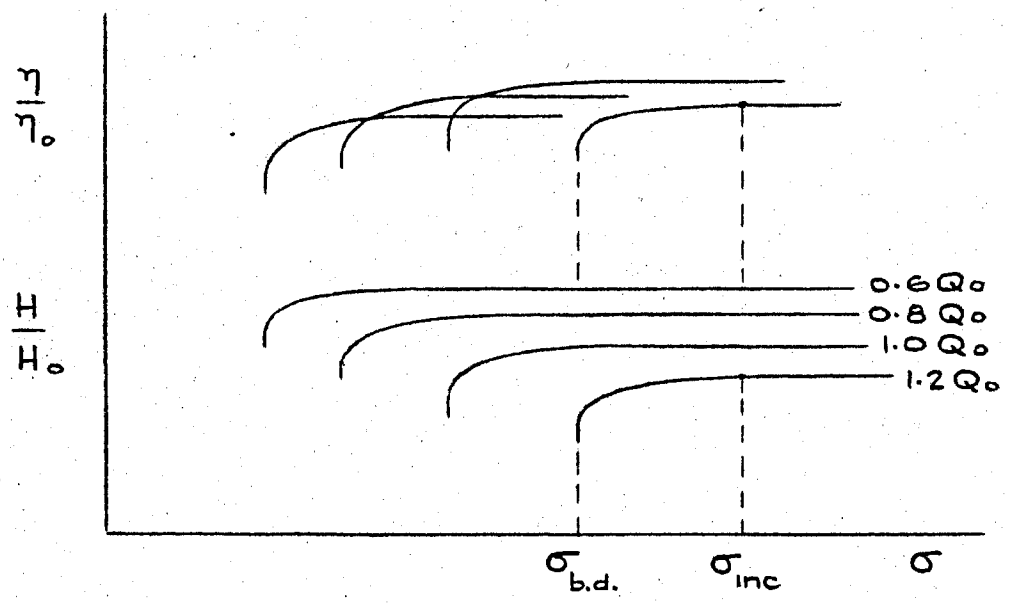

FIG 4.2. RESULTS OF TYPICAL CAVITATION TEST. SUFFIX "o" REFERS TO DESIGN CONDITIONS.

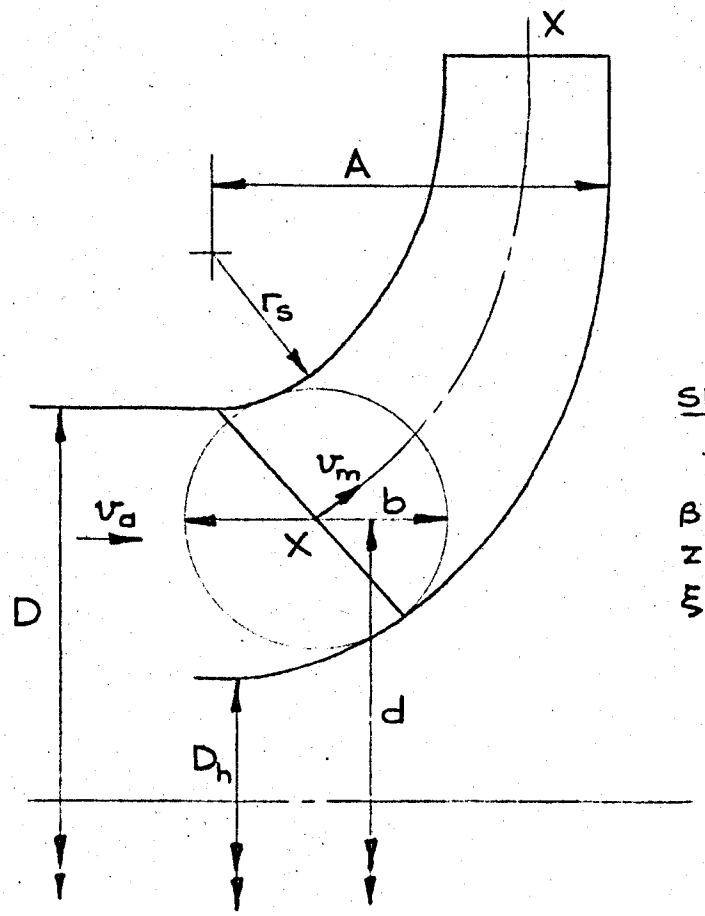

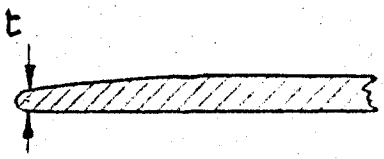

SECTION XX AT BLADE INLET.

β = BLADE ANGLE AT INLET
z = NUMBER OF BLADES
$\xi = D_h/D$

FIG 4.3. IMPELLER INLET. DEFINITION OF SYMBOLS.

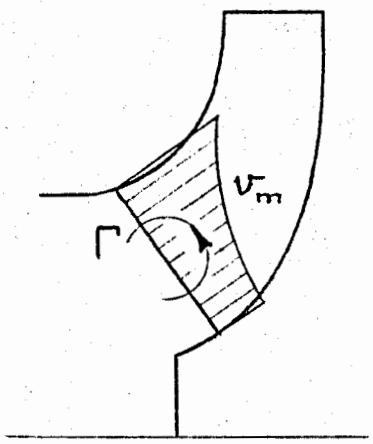

FIG 4.4. INLET VELOCITY DISTRIBUTION.
(METHOD OF PFLEIDERER).

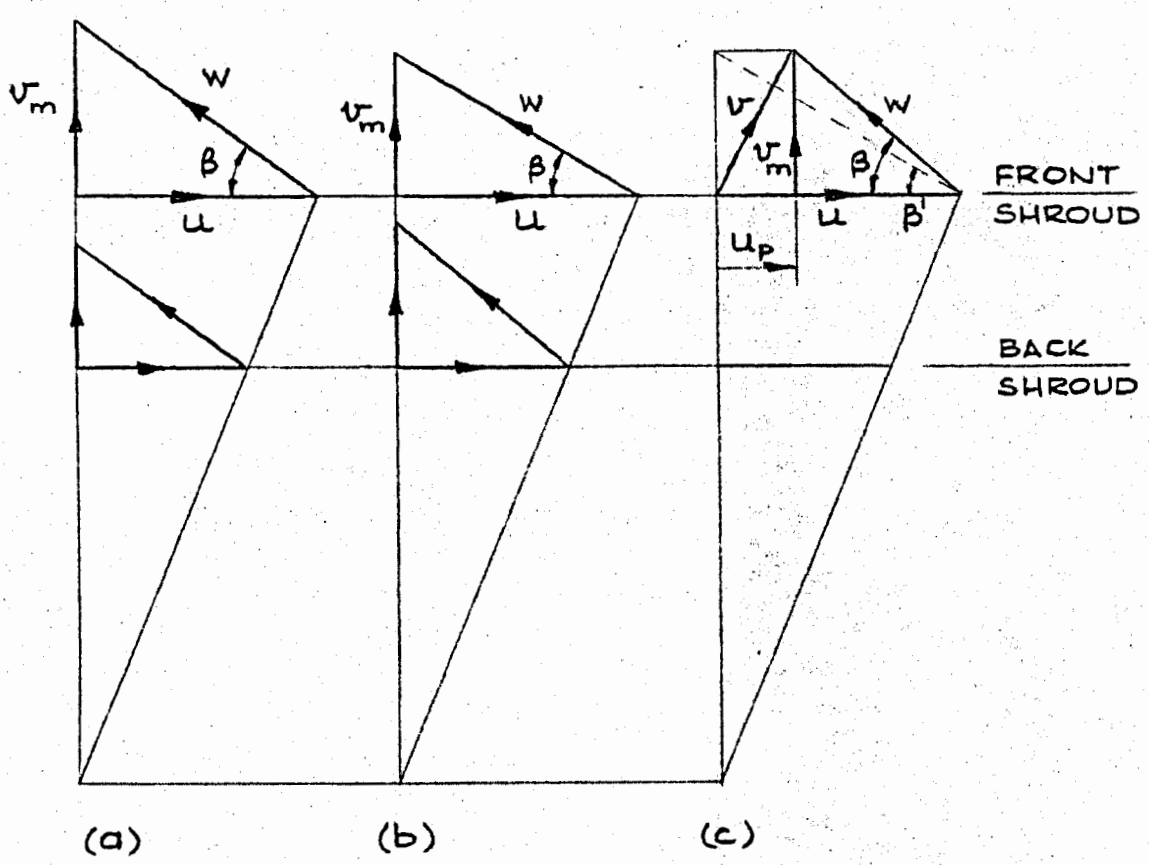

FIG 4.5. INLET VELOCITY DIAGRAMS.
ANGLE OF INCIDENCE $\alpha = 0$.

(a) NO PRE-ROTATION. v_m DISTRIBUTION AS FIG 4.4.

(b) NO PRE-ROTATION. v_m = CONSTANT.

(c) PRE-ROTATION. v_m = CONSTANT.

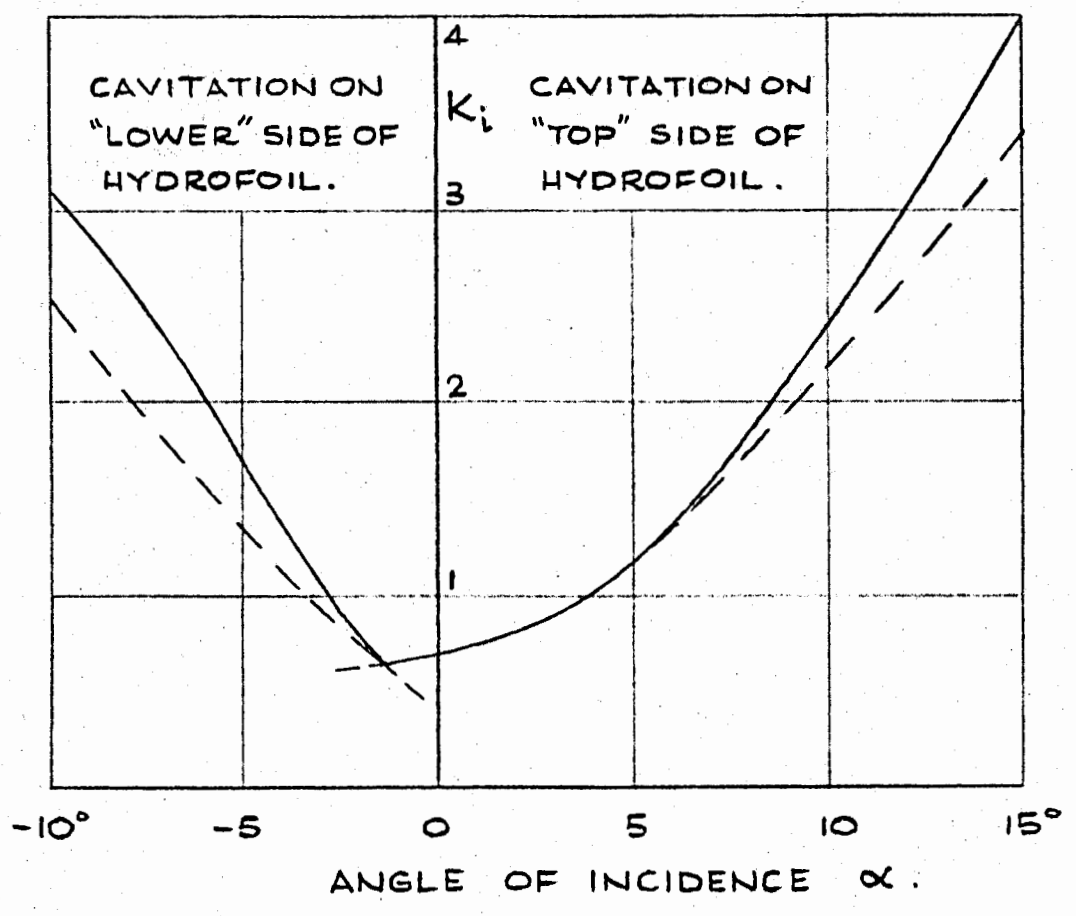

FIG 4.6. CAVITATION CHARACTERISTICS OF HYDROFOIL NACA 4412.
——— K_i FROM WATER TUNNEL TESTS.
– – – – K_i PREDICTED FROM $C_{P\,MIN}$ IN WIND TUNNEL TESTS.
RESULTS TAKEN FROM DAILY (21) AND ARE FOR TWO-DIMENSIONAL FLOW.

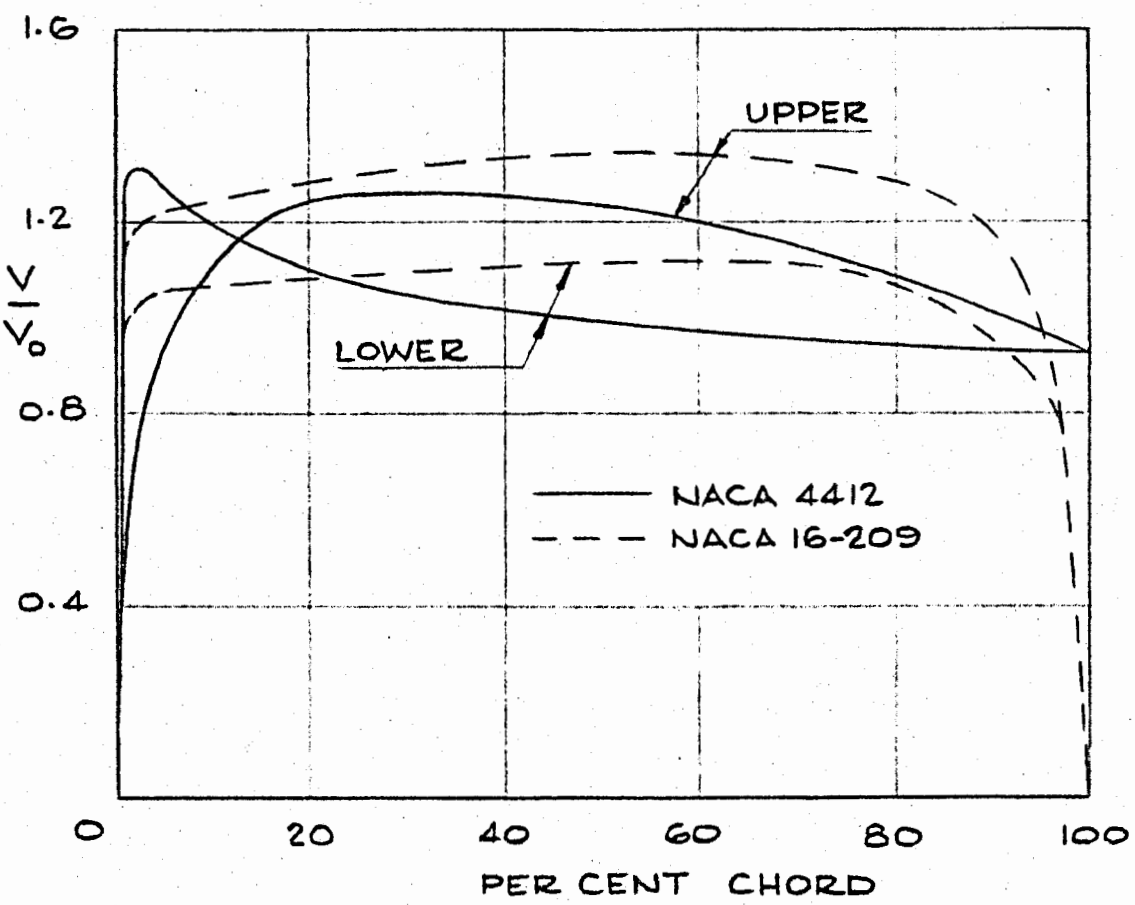

FIG 4.7. COMPARISON OF VELOCITY DISTRIBUTIONS. NACA 4412 AND 16-209 AEROFOILS AT C_L=0·2.

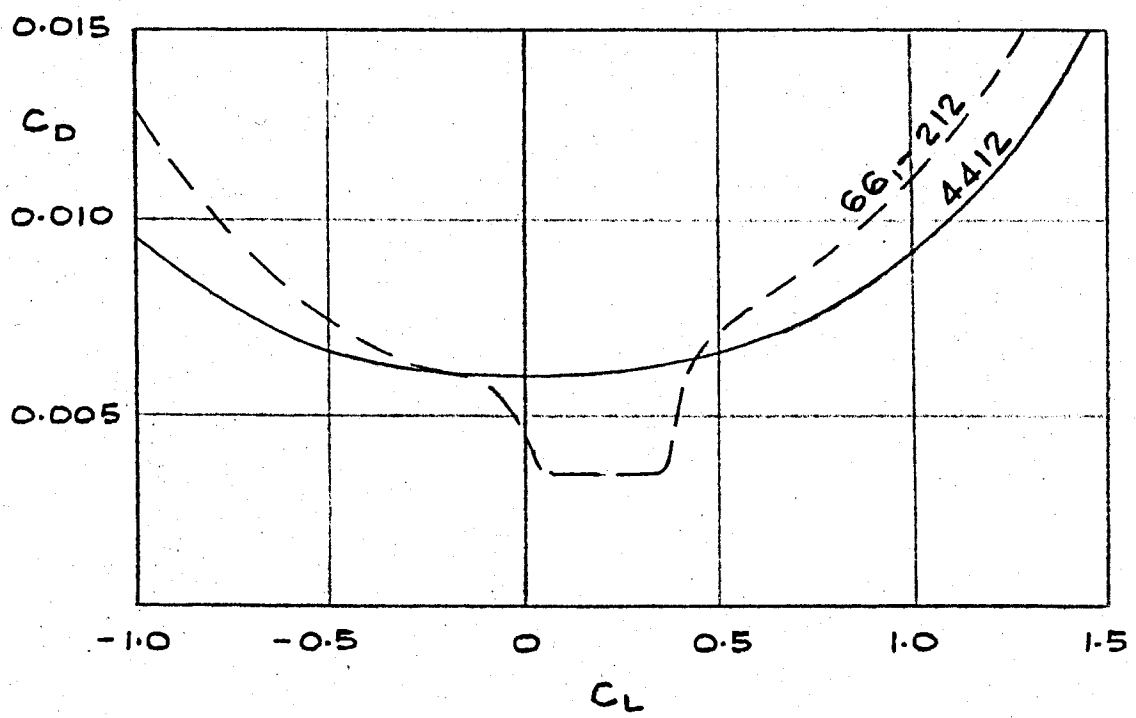

FIG 4.B. COMPARISON OF DRAG COEFFICIENTS. NACA 4412 AND 66_1-212 AEROFOILS.

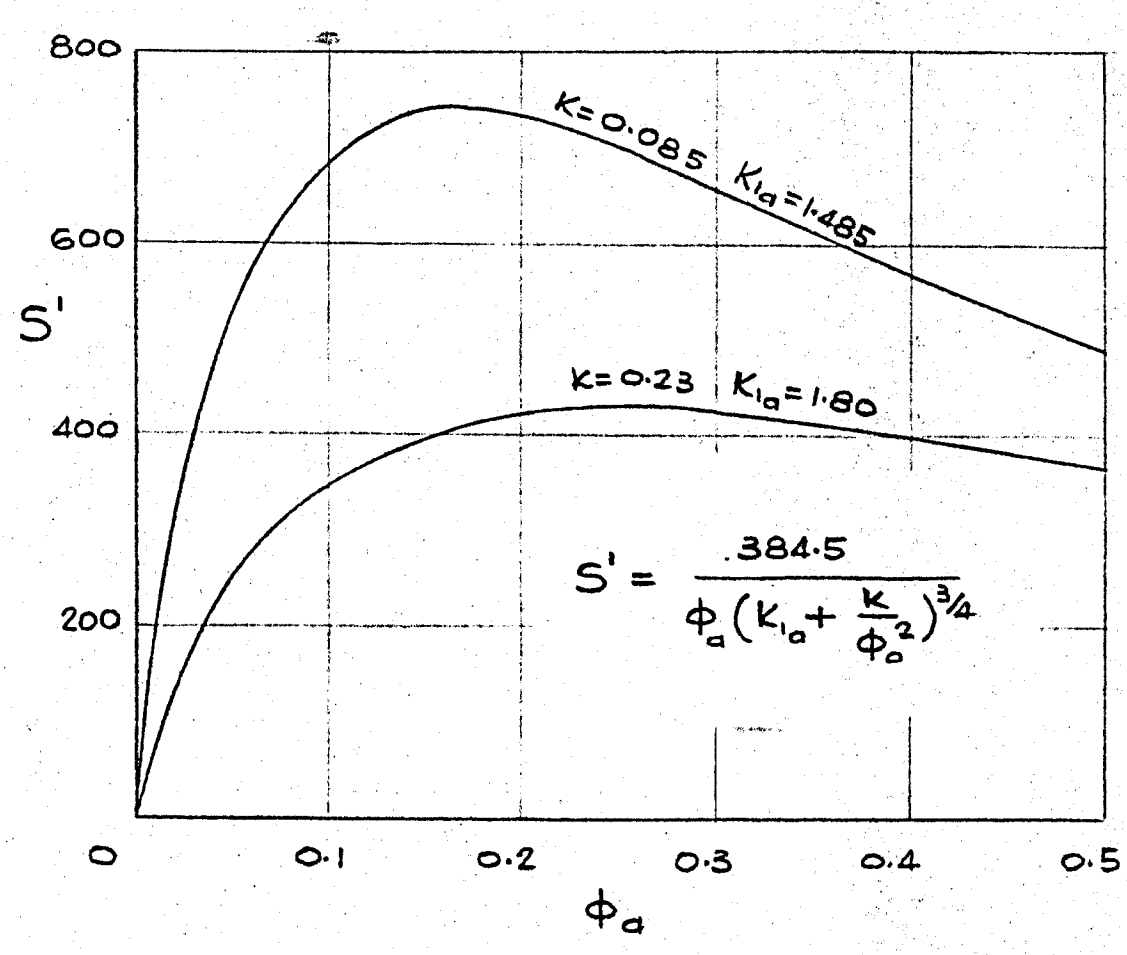

FIG 4.9. S' VS. Φ_a.

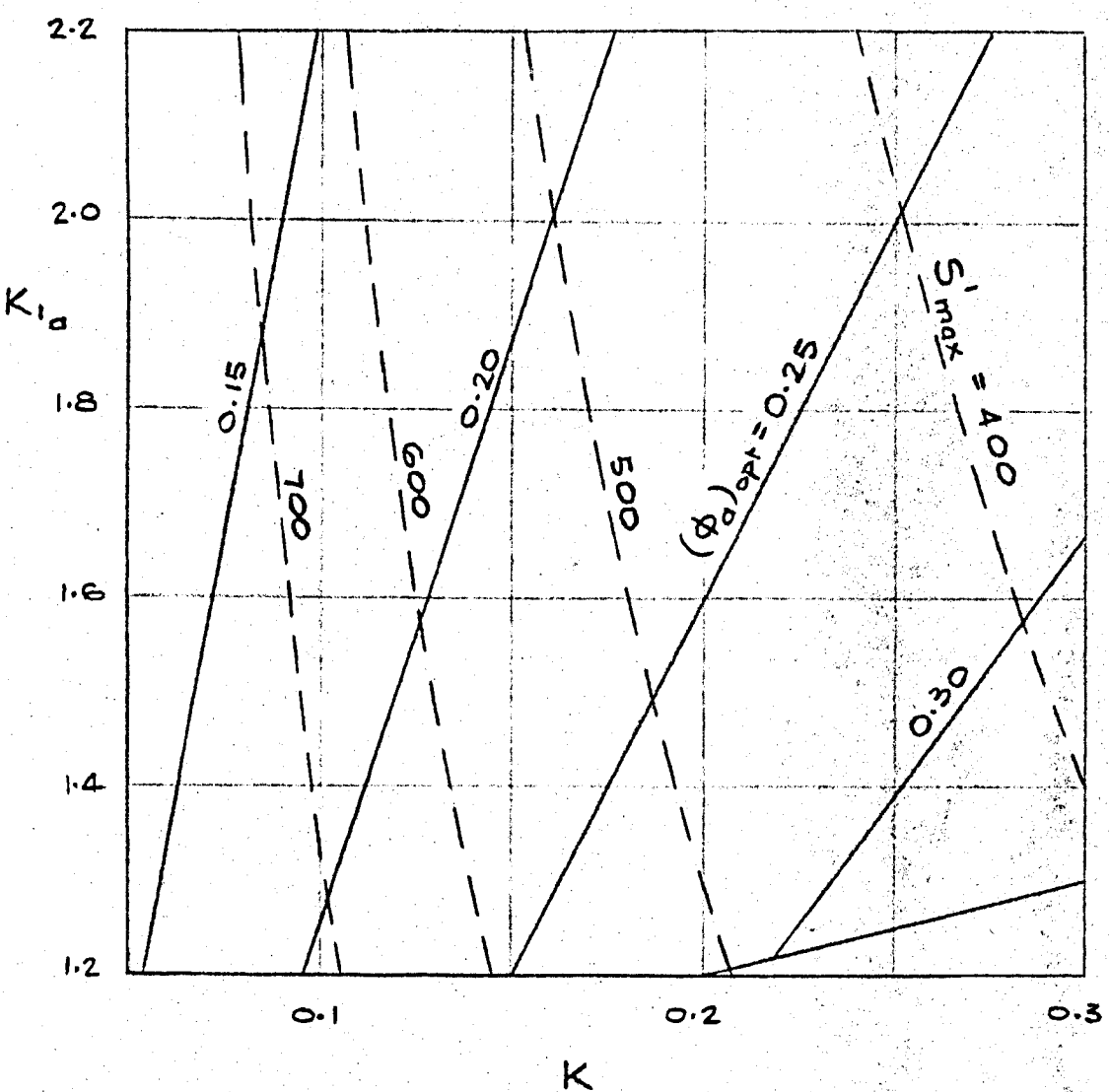

FIG 4.10. S'_{max} AND $(\Phi_a)_{opt}$ VS K AND K_{1a}.

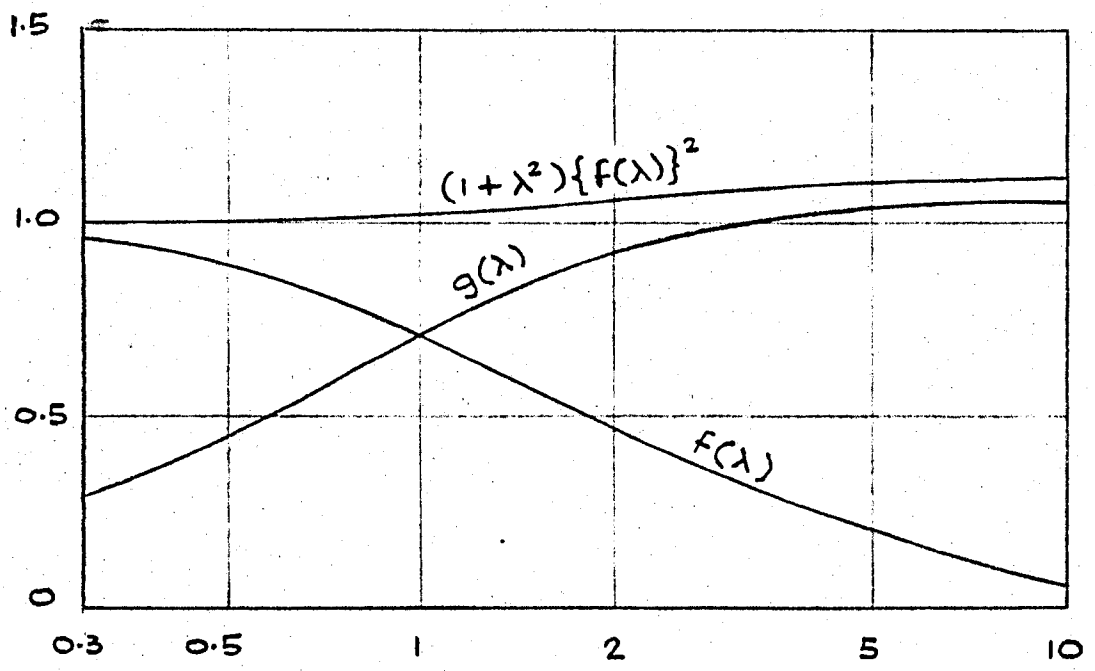

FIG 4.11. $f(\lambda)$, $g(\lambda)$, $(1+\lambda^2)\{f(\lambda)\}^2$ vs. λ.

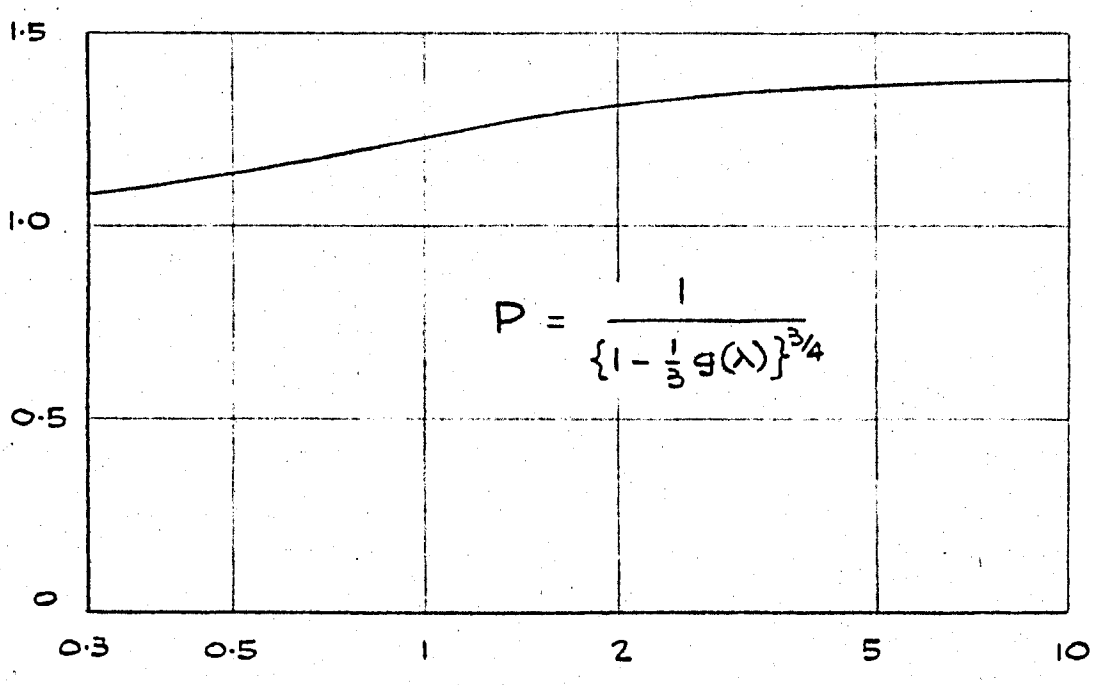

FIG 4.12. P vs. λ.

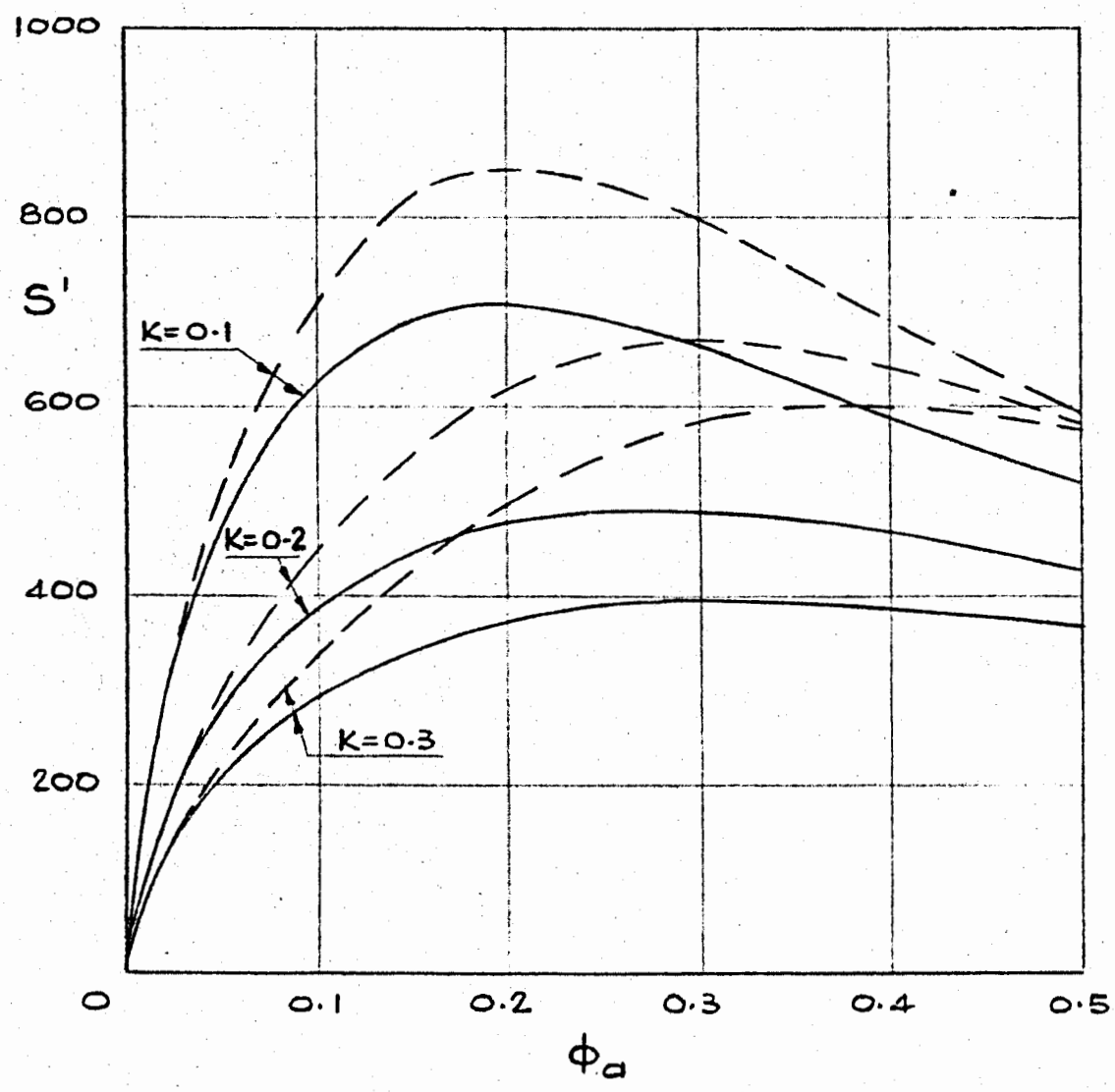

FIG 4.13. S' VS. ϕ_a FOR VARIOUS K, K_{1a} AND λ.

$K = 0.1, 0.2, 0.3.$

$K_{1a} = 1.2 + K.$

$\lambda = 0$ SHOWN BY FULL LINE.

$\lambda = 2$ SHOWN BY DOTTED LINE.

NOTE:

FOR CONVENTIONAL DESIGNS MAXIMUM $S' = 400$.
FOR SPECIAL DESIGNS MAXIMUM $S' = 640$.
S' CAN BE HIGHER THAN 640 FOR CONDENSATE EXTRACTION PUMPS AND FOR SOME REFINERY AND PROCESS DUTIES WHERE OPERATION UNDER PARTIALLY CAVITATING CONDITIONS IS PERMISSIBLE.

SUCTION TANK.
THIS TANK IS PARTLY FILLED WITH WATER. THE PUMP INLET PRESSURE IS CONTROLLED BY VARYING THE PRESSURE OF THE AIR ABOVE THE WATER IN THIS TANK.

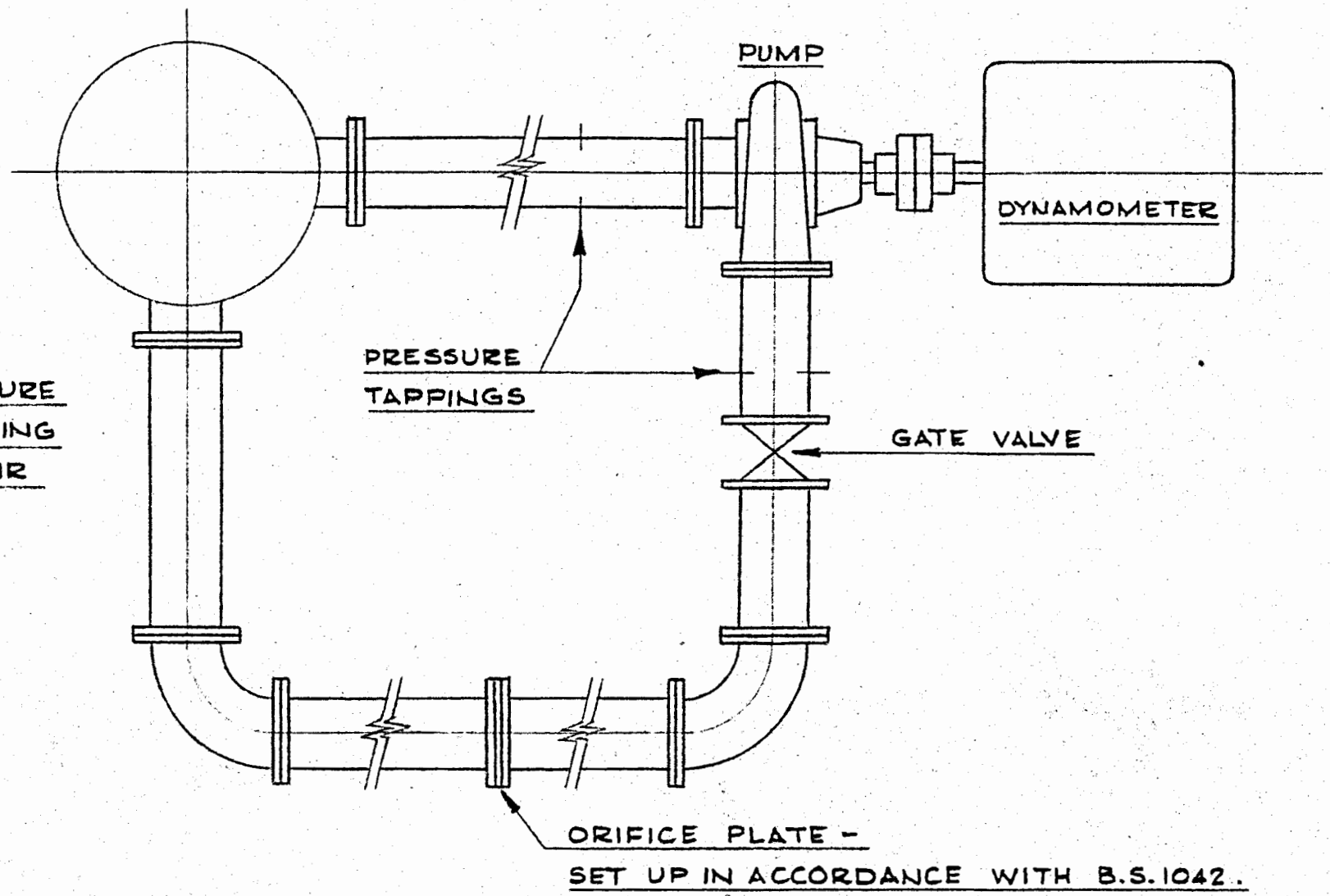

FIG 4.14. PLAN VIEW OF LABORATORY RIG FOR PUMP CAVITATION TESTS.

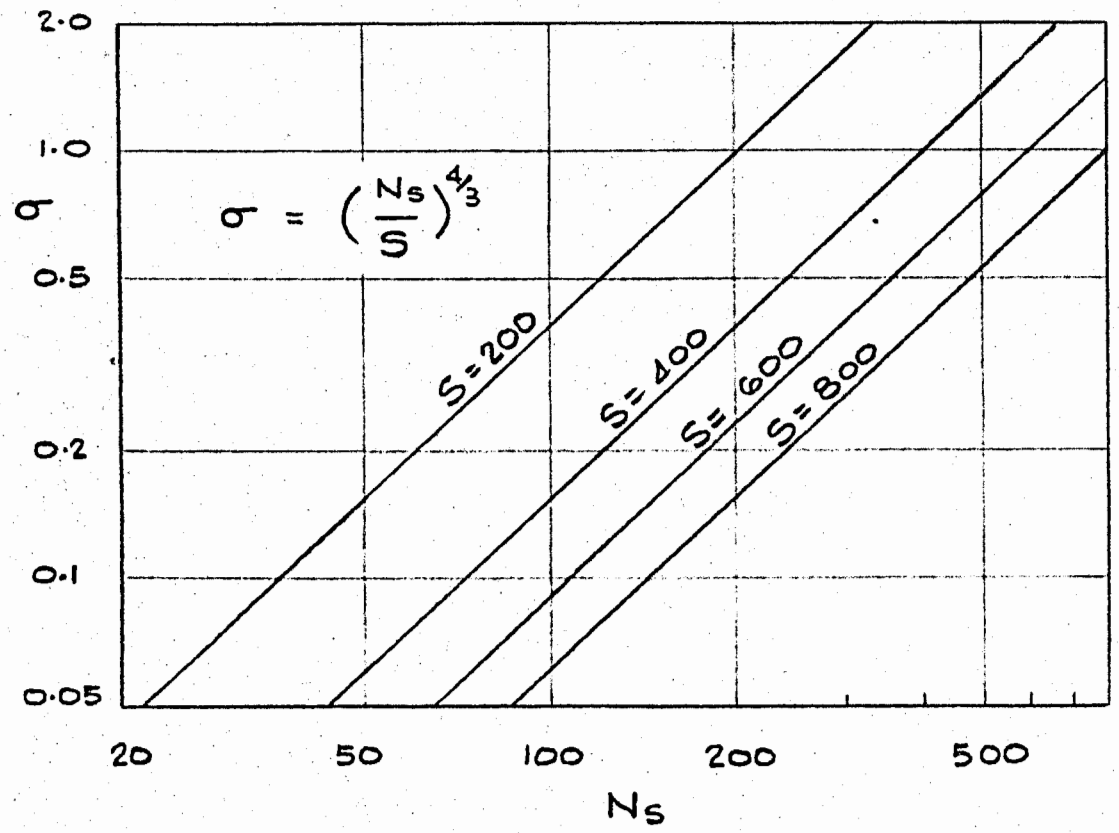

FIG. 4.15. σ VS N_s FOR VARIOUS S.

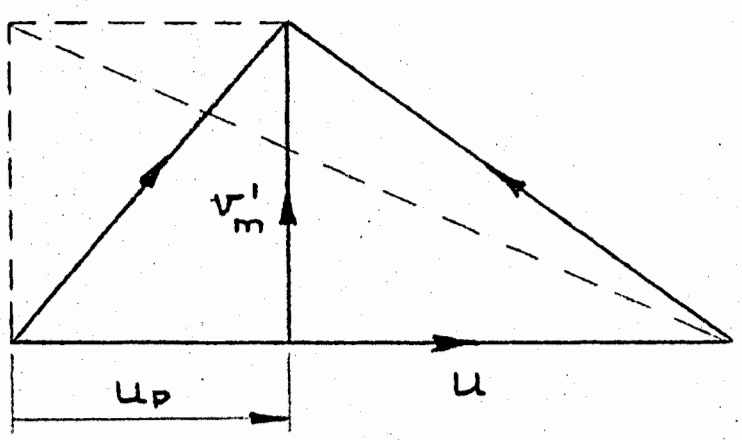

FIG. 4.16. INLET VELOCITY DIAGRAM.

THIS DIAGRAM HAS BEEN DRAWN USING A MERIDIONAL VELOCITY v_m'.

$v_m' = \frac{Q}{\pi d b}$. $\tan\beta = R\frac{v_m'}{u}$.

SYMBOLS ARE DEFINED IN TEXT.

SEE ALSO FIG 4.3.

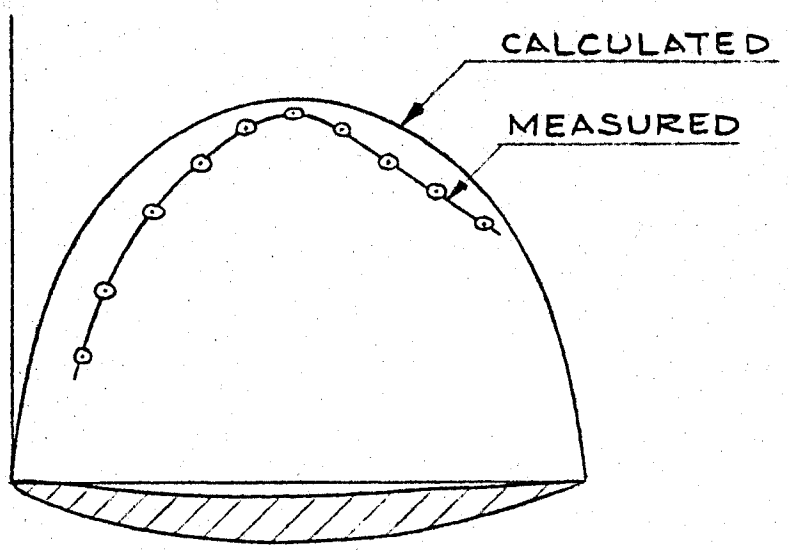

FIG 4.17. COMPARISON OF CALCULATED AND MEASURED DIFFERENTIAL PRESSURE ACROSS BLADE OF AXIAL-FLOW PUMP. THESE CURVES HAVE BEEN TAKEN FROM MORELLI AND BOWERMAN (80). THEY APPLY FOR DESIGN FLOW CONDITIONS AT A RADIAL STATION 73% OF THE OUTER RADIUS.

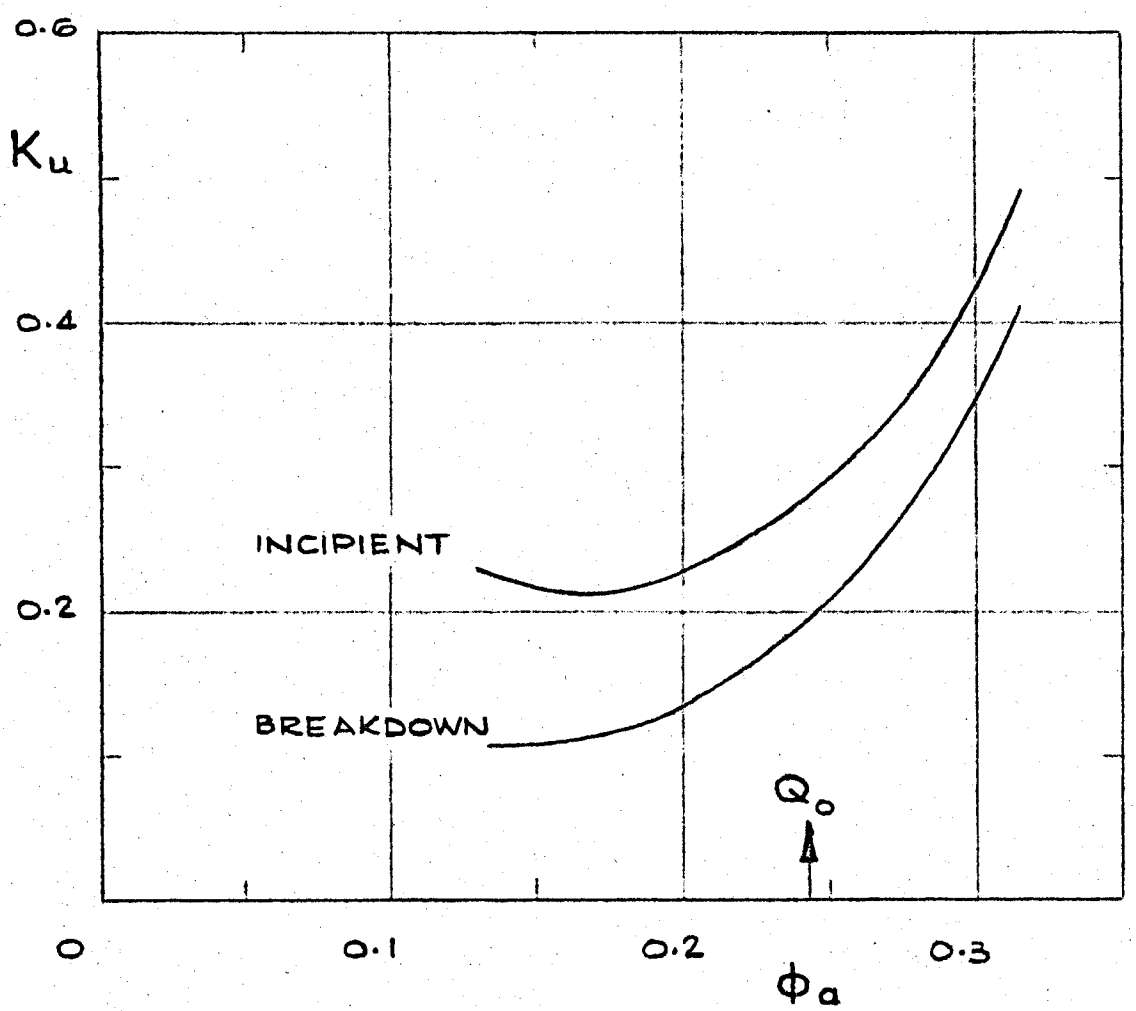

FIG. 4.18. K_u VS ϕ_a - IMPELLER F_4.

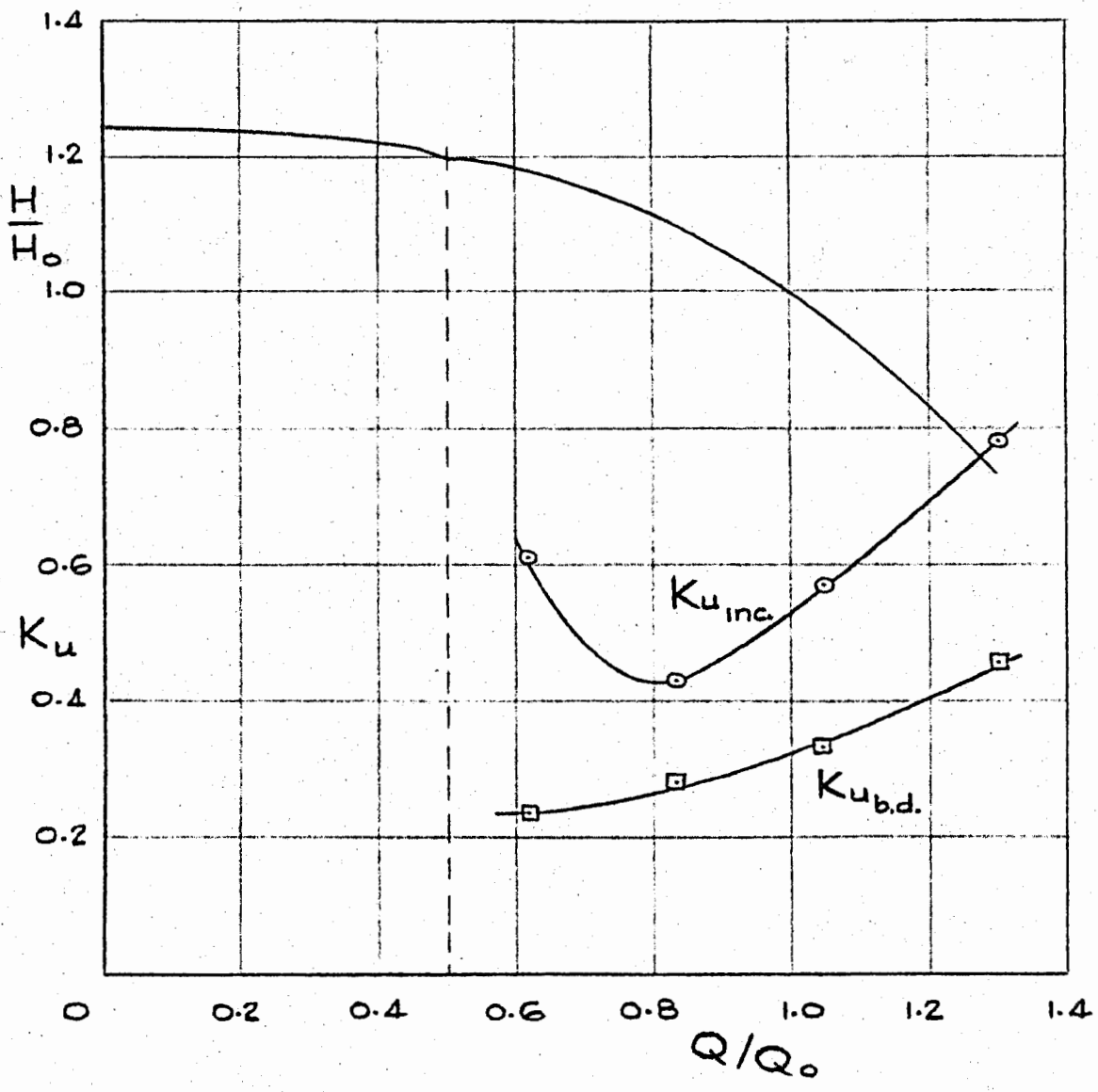

FIG 4.19. PERFORMANCE AT OFF-DESIGN CONDITIONS - FRANCIS IMPELLER.

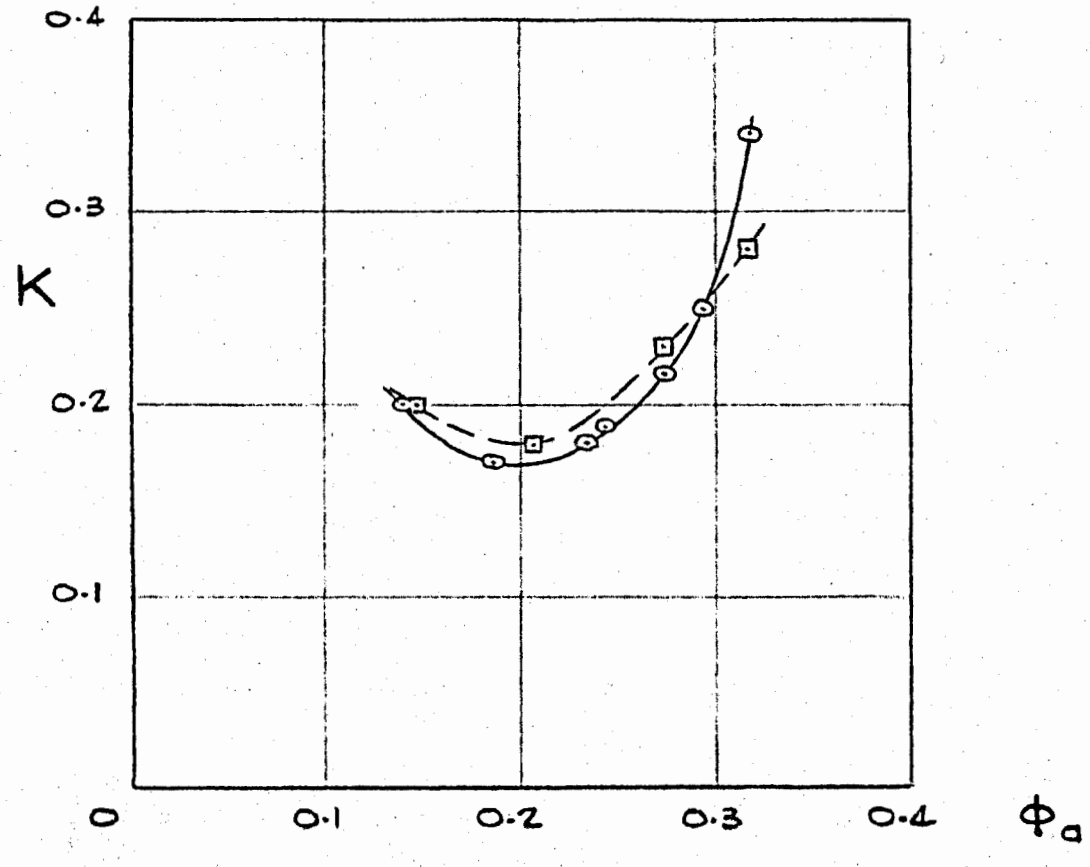

FIG 4.20. K VS. ϕ_a

—o— IMPELLER F4.

– –□– – IMPELLER F5.

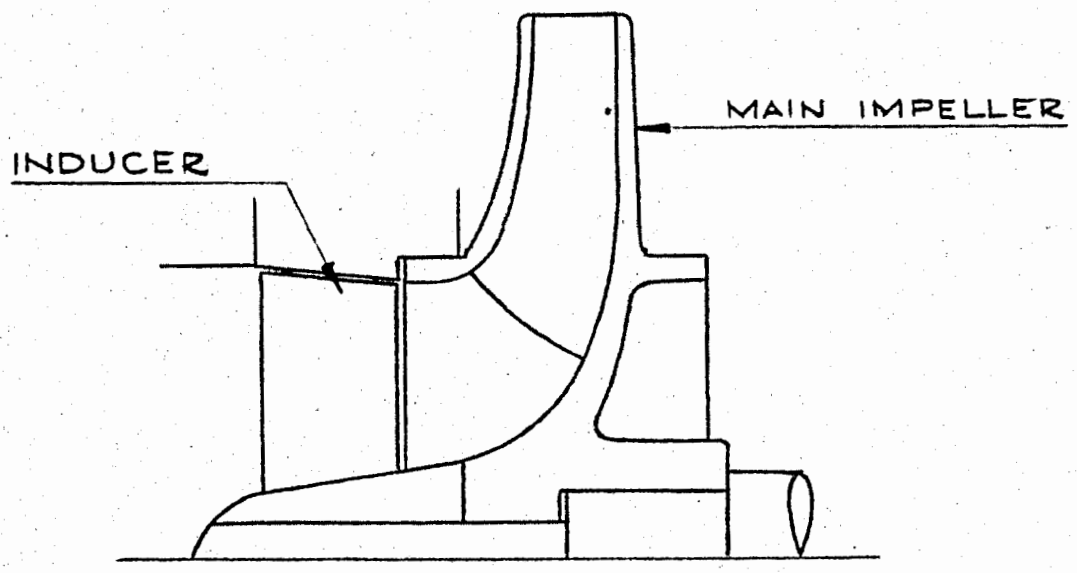

FIG 5.1. CROSS-SECTION OF TYPICAL PUMP-INDUCER COMBINATION.

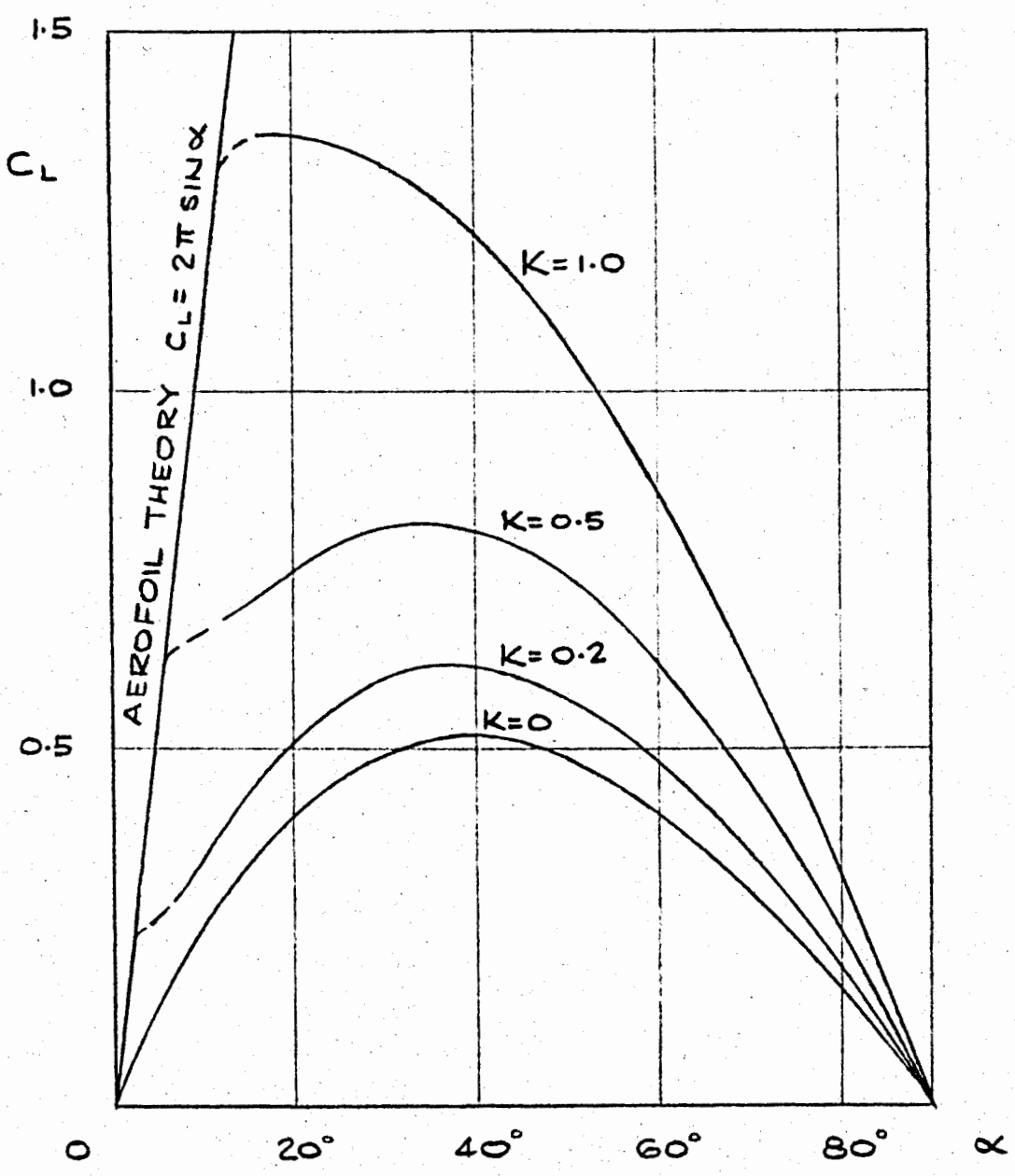

FIG 5.2. C_L VS α . THIN FLAT PLATE IN TWO-DIMENSIONAL SUPER-CAVITATING FLOW. (FROM STREETER (36))

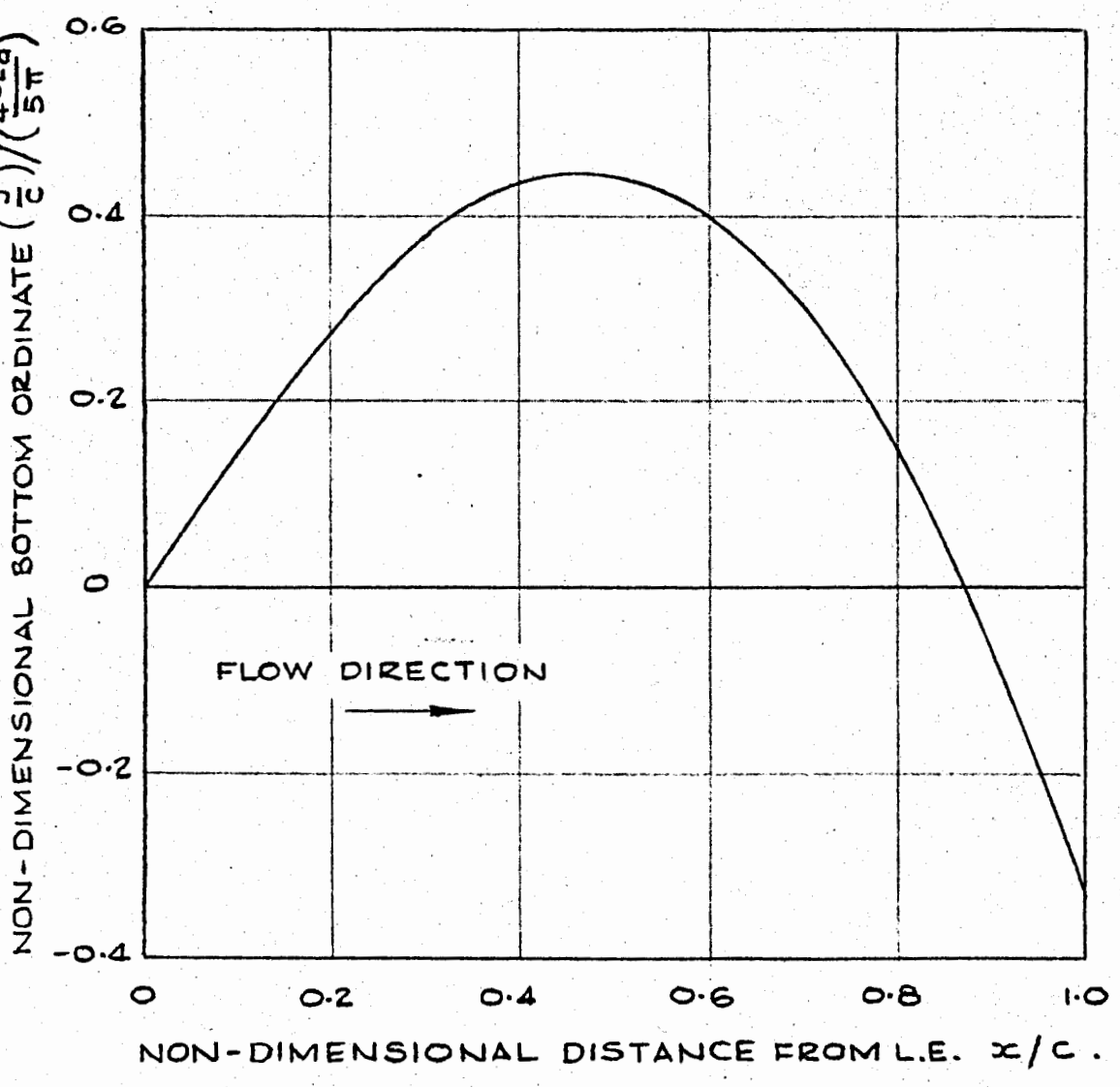

FIG 5.3. NON-DIMENSIONAL BOTTOM ORDINATES OF A LOW-DRAG SUPER-CAVITATING HYDROFOIL - REFERENCE (93).

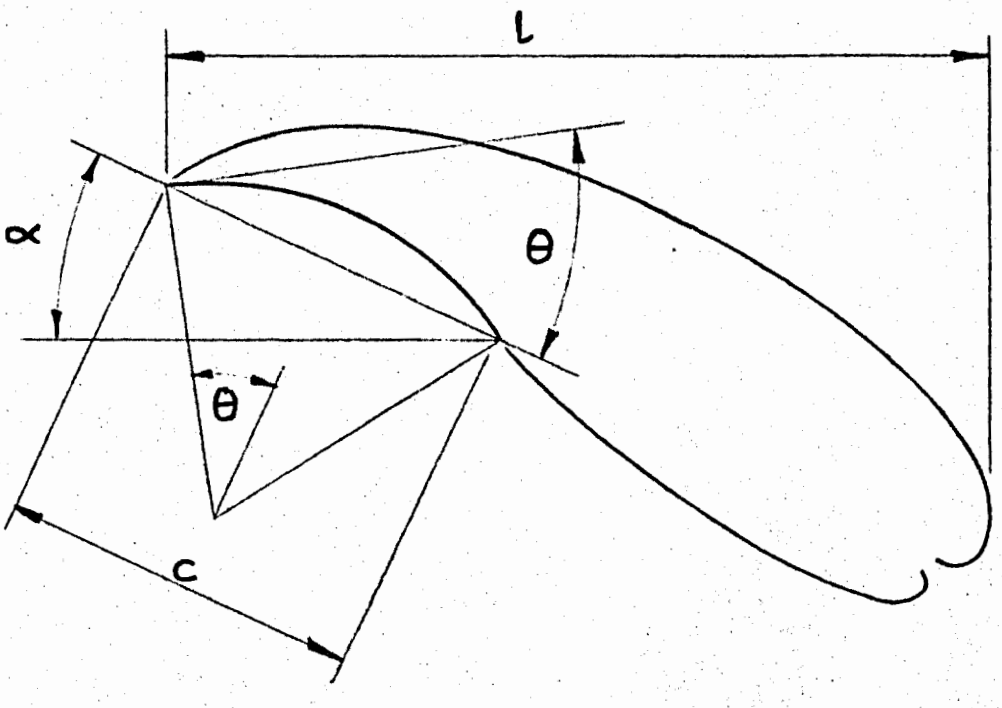

FIG 5.5. DEFINITION OF SYMBOLS - CIRCULAR ARC HYDROFOIL IN SUPER-CAVITATING FLOW.

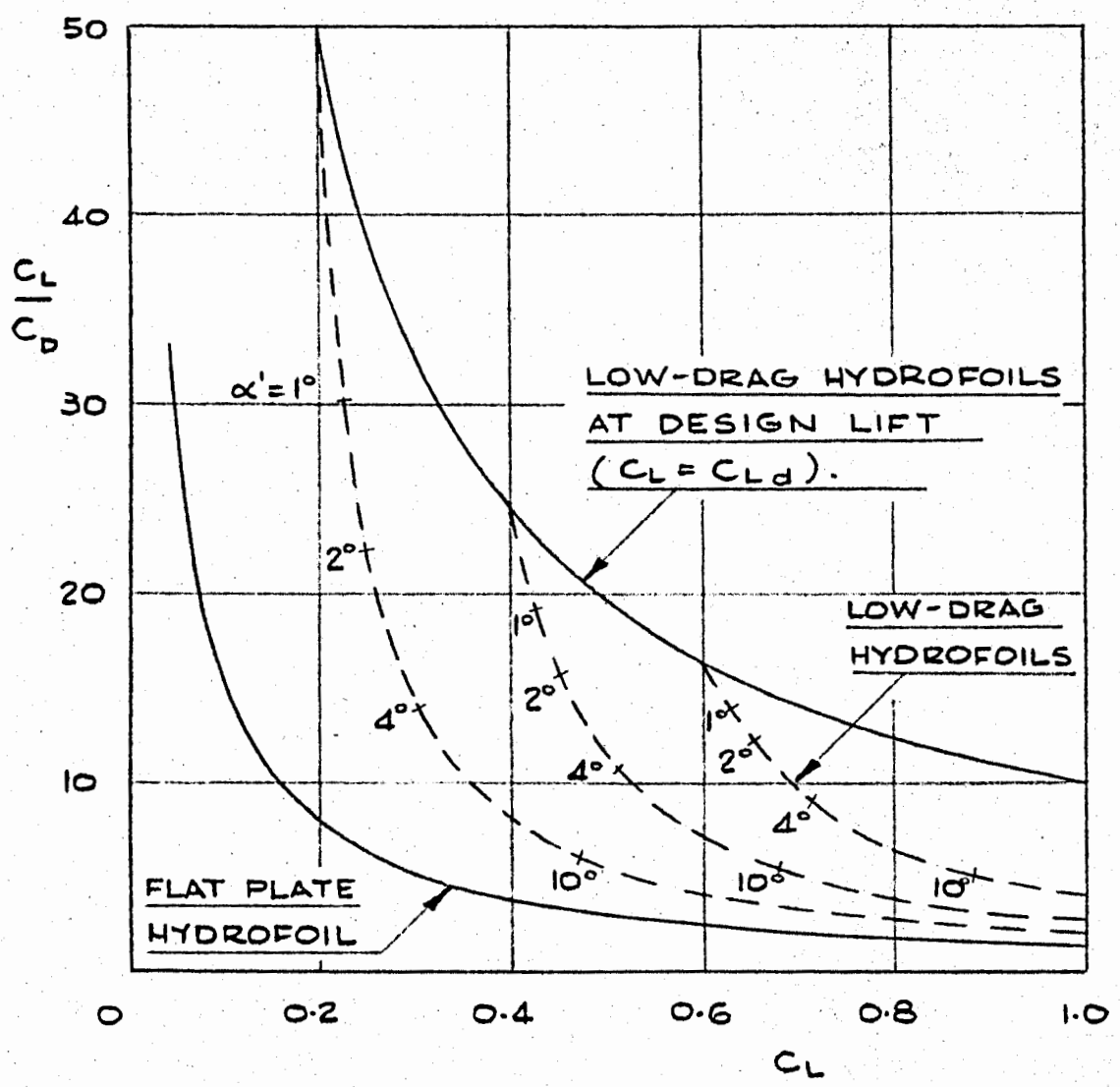

FIG 5.4. LIFT-DRAG RATIOS OF A FAMILY OF LOW-DRAG SUPER-CAVITATING HYDROFOILS FOR K=0. REFERENCE (93).

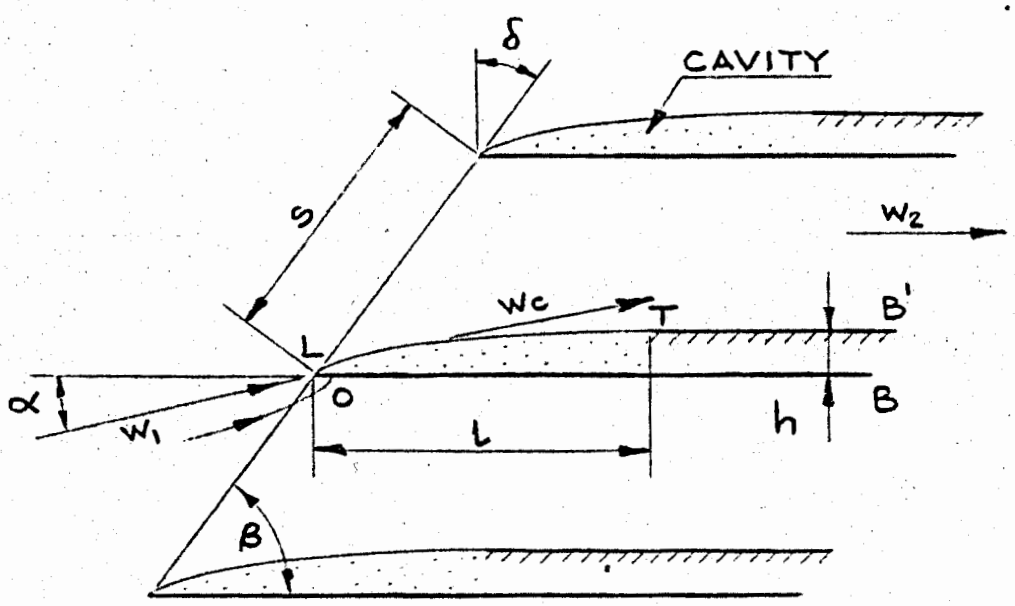

FIG 5.6. SKETCH OF PARTIALLY CAVITATING CASCADE.

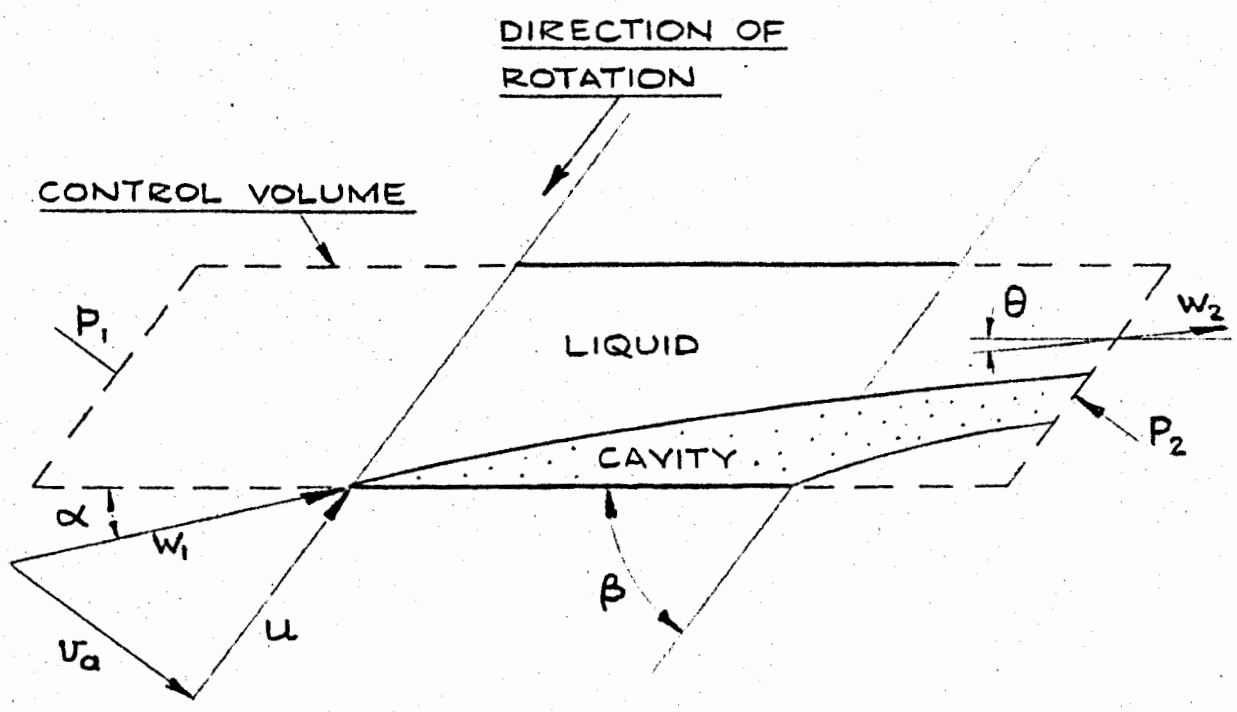

FIG 5.7. SKETCH OF SUPER-CAVITATING CASCADE.

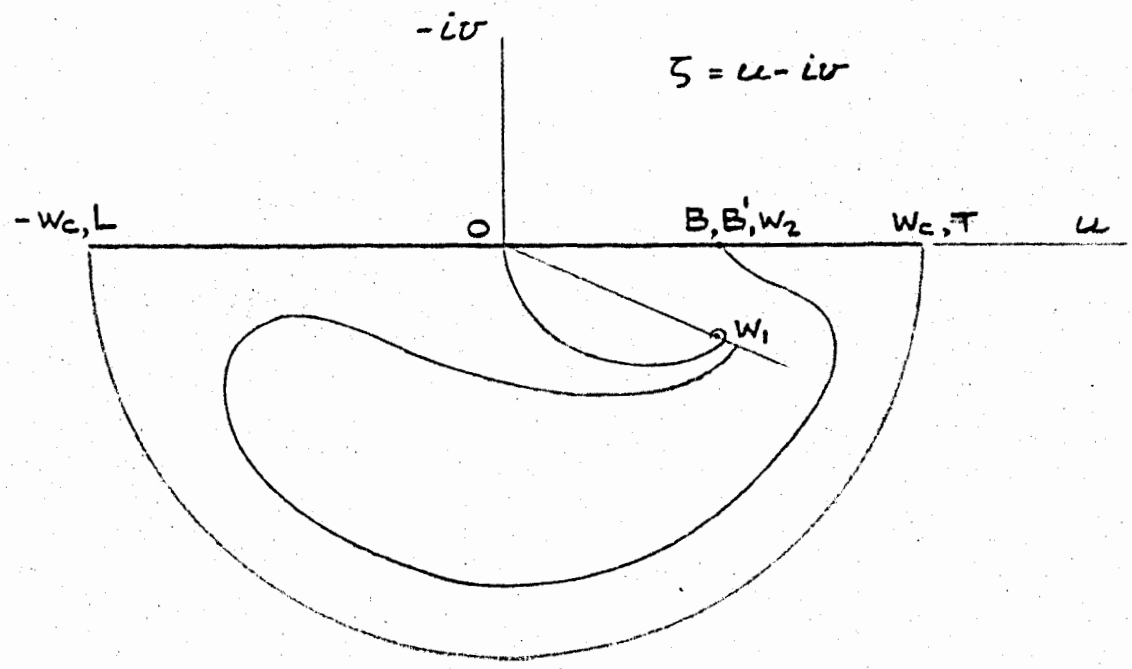

FIG 5.8. HODOGRAPH OF FLOW IN PARTIALLY CAVITATING CASCADE (REFER FIG 5.6). IT IS ASSUMED THAT THE BLADE CHORD IS INFINITELY LONG.

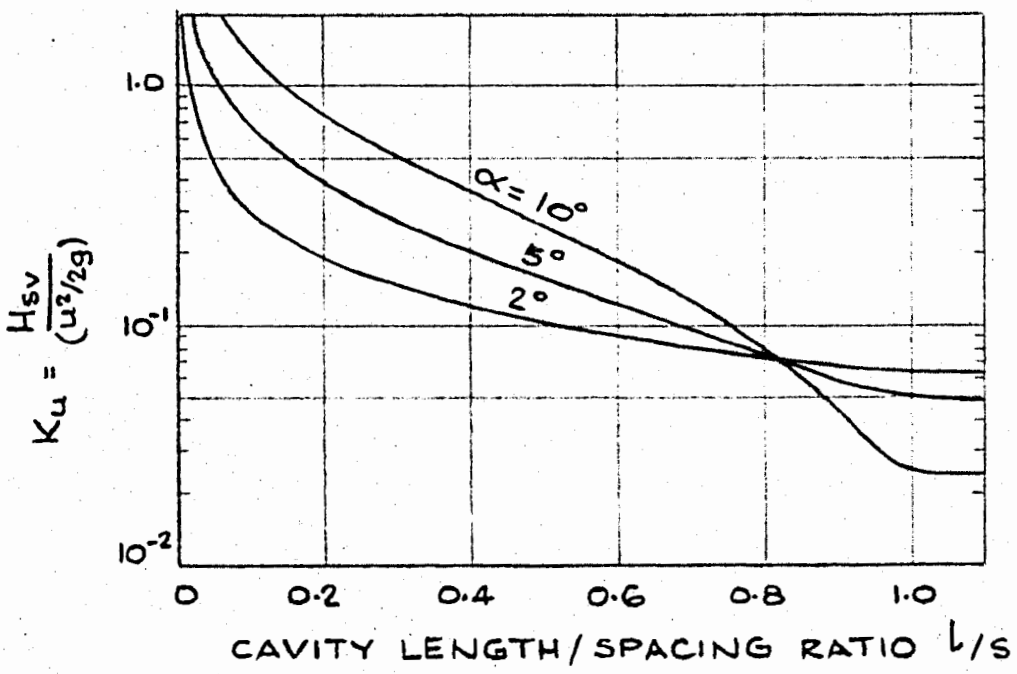

FIG 5.9. K_u vs. l/s.
IDEAL SUPER-CAVITATING CASCADE, $\beta = 15°$ - FROM REFERENCE (95).

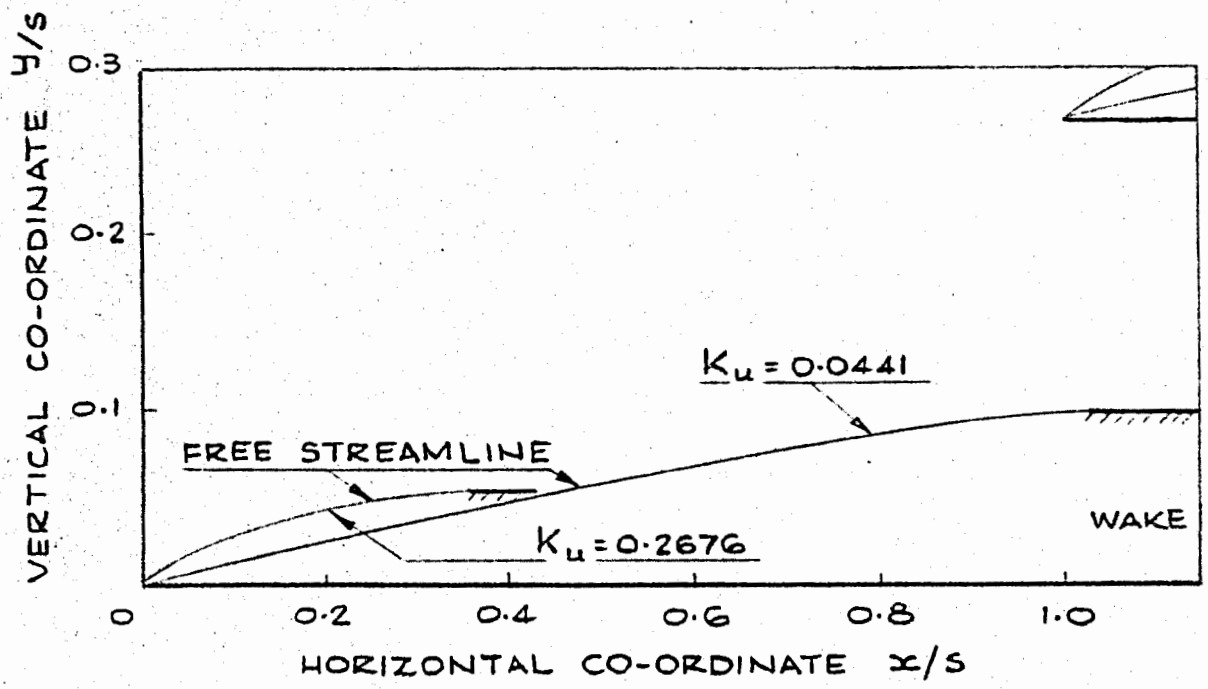

FIG 5.10. CAVITY SHAPE - IDEAL SUPER-CAVITATING CASCADE, $\beta = 15°$ $\alpha = 6°$.
NOTE DISTORTED SCALE.
FROM REFERENCE (95).

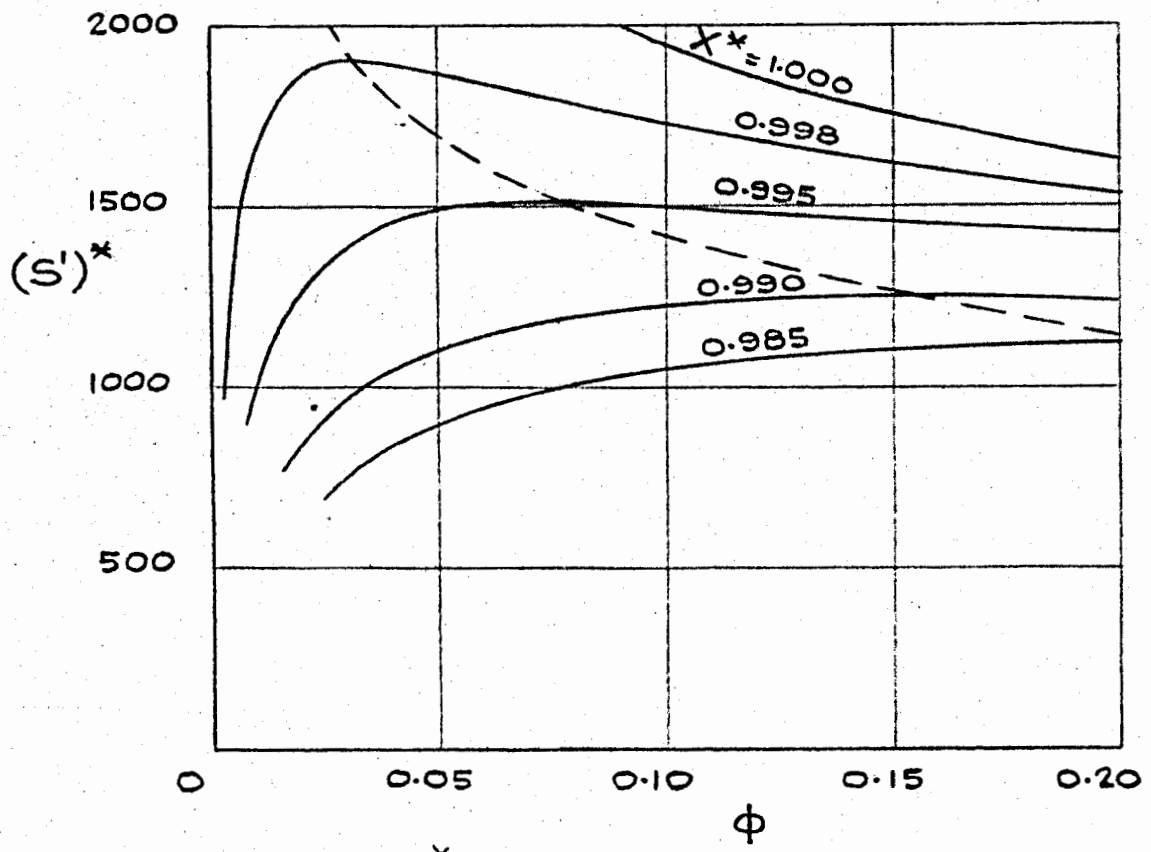

FIG 5.11. $(S')^*$ VS ϕ.
EQUATION (5.23) WITH $\beta = 14°$.

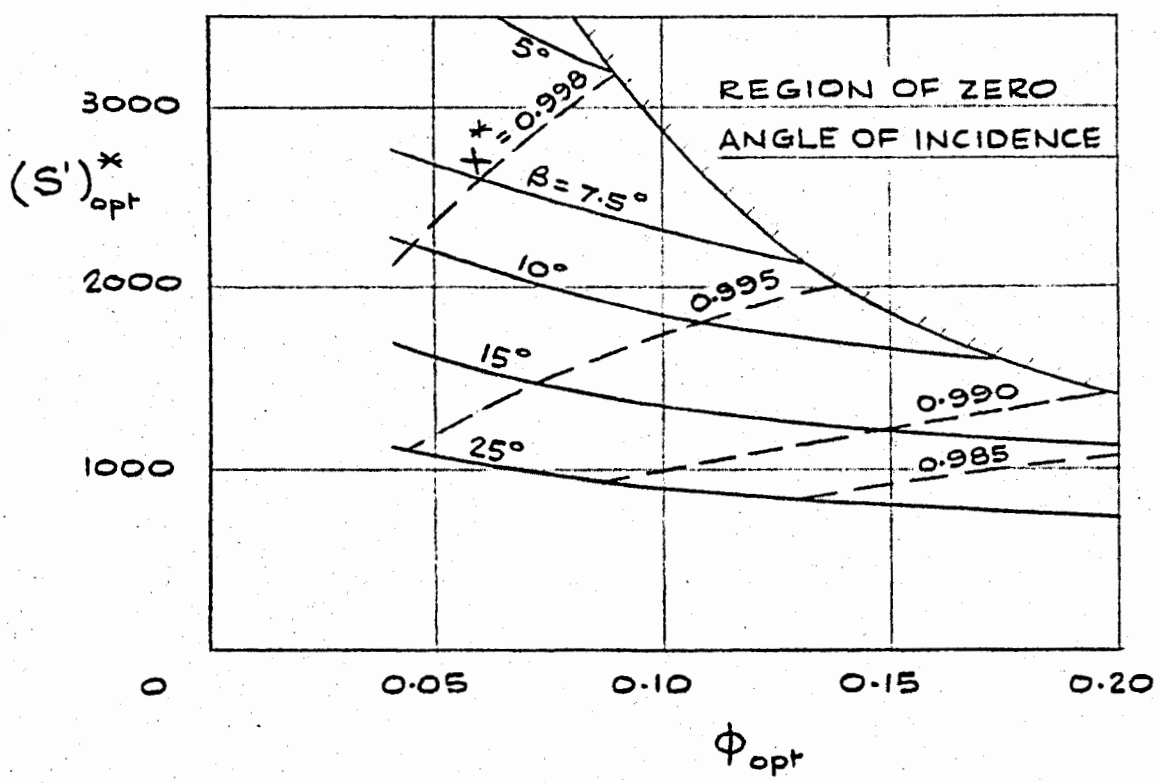

FIG 5.12. $(S')^*_{opt}$ VS ϕ_{opt}. EQUATION (5.26)

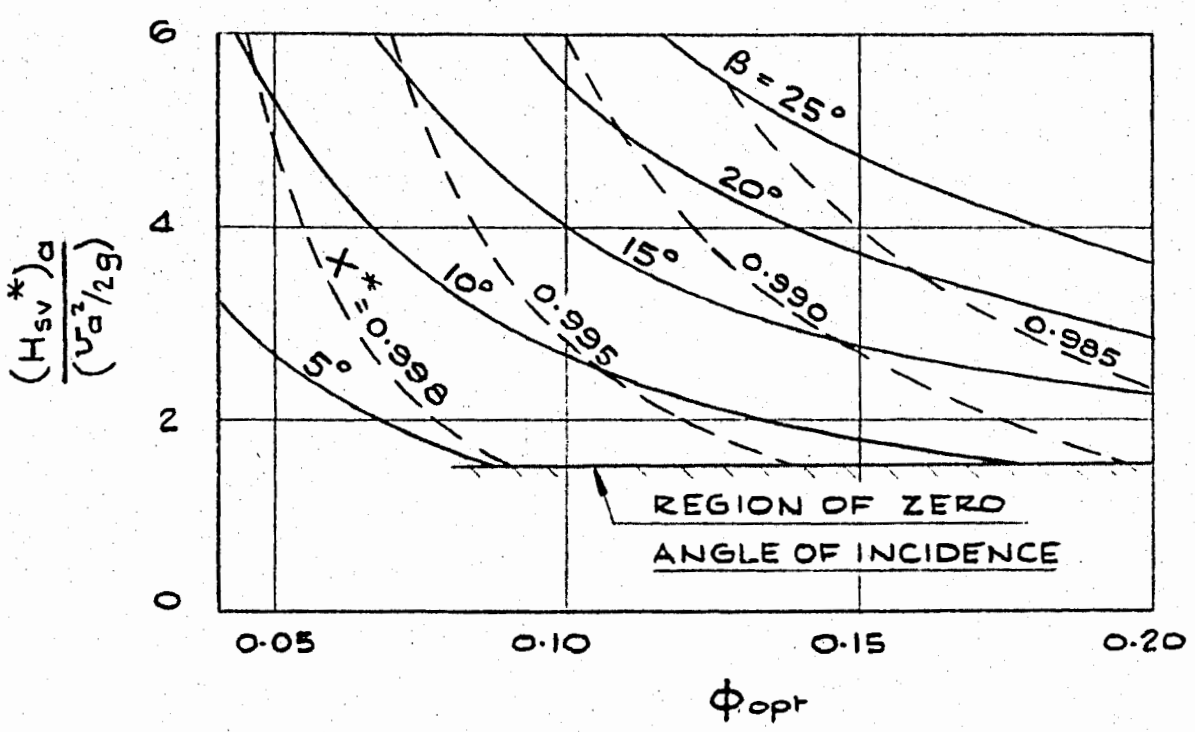

FIG 5.13. INDUCER INLET COEFFICIENT VERSUS ϕ_{opt}.
EQUATION (5.27).

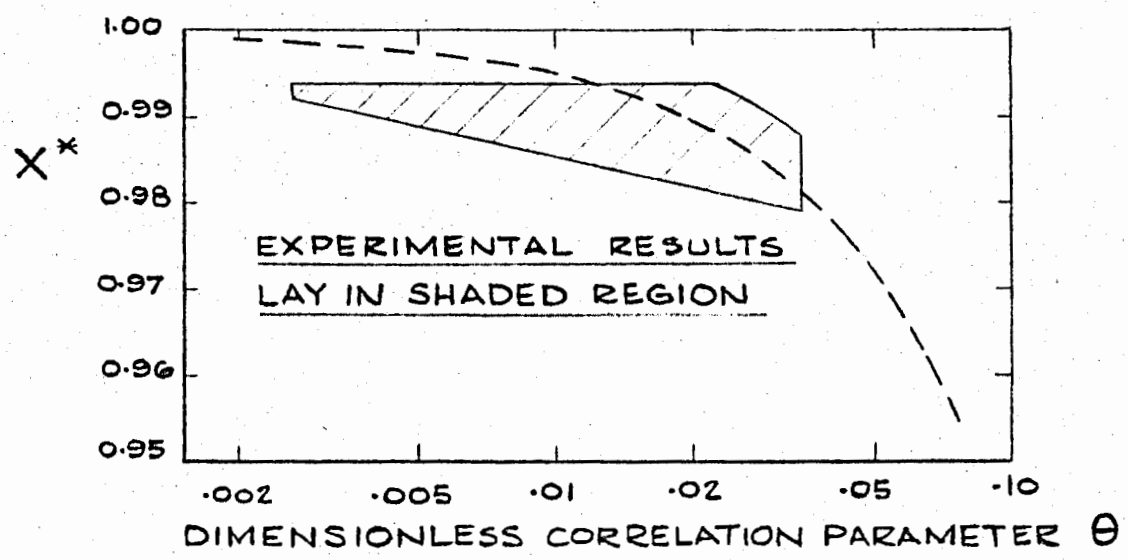

FIG 5.14. X^* VERSUS θ.
INDUCER CORRECTION COEFFICIENT FOR CAVITATION HEAD BREAKDOWN.
COMPARISON OF EXPERIMENTAL RESULTS WITH EQUATION (5.30).
FROM REFERENCE (96).

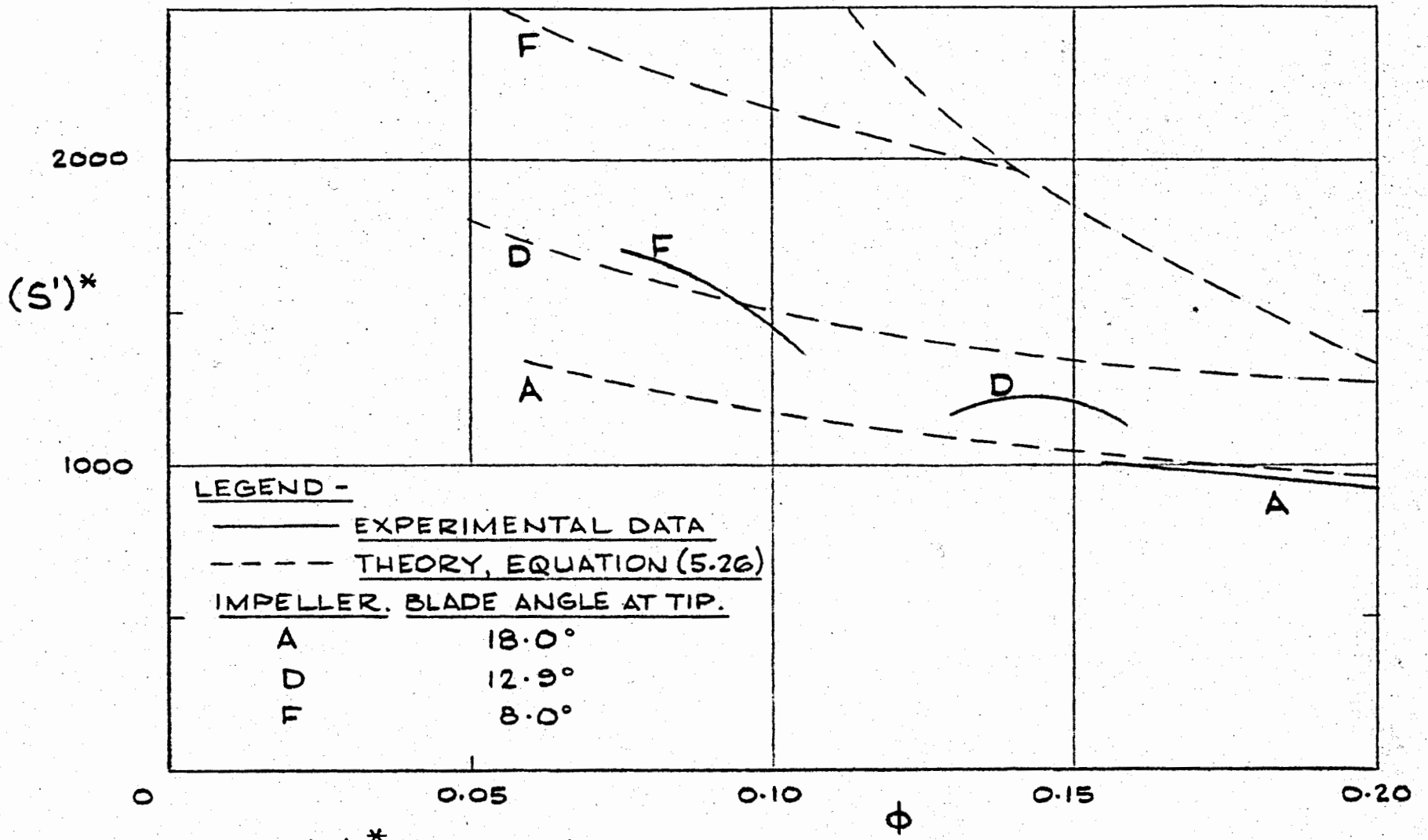

FIG 5.15. $(S')^*$ VERSUS ϕ . SUCTION SPECIFIC SPEED PERFORMANCE AT COMPLETE HEAD BREAKDOWN. THESE CURVES ARE TAKEN FROM FIG (12) OF REFERENCE (96).

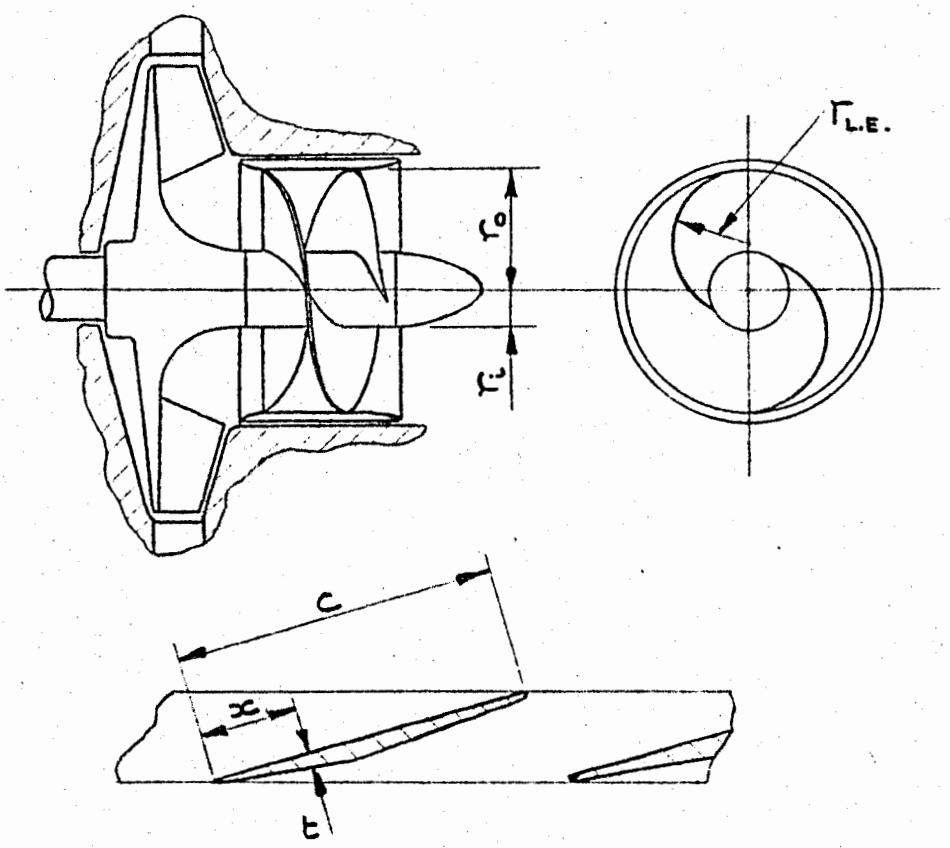

FIG 5.16. CAVITATION INDUCER FOR CENTRIFUGAL PUMP, AFTER DUMOV (97).

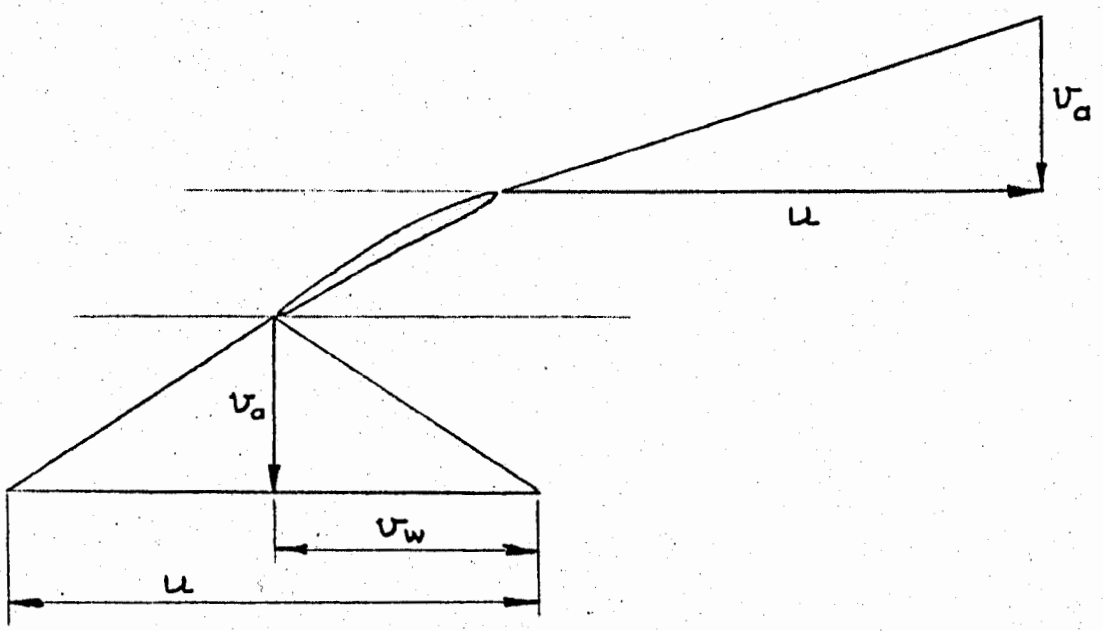

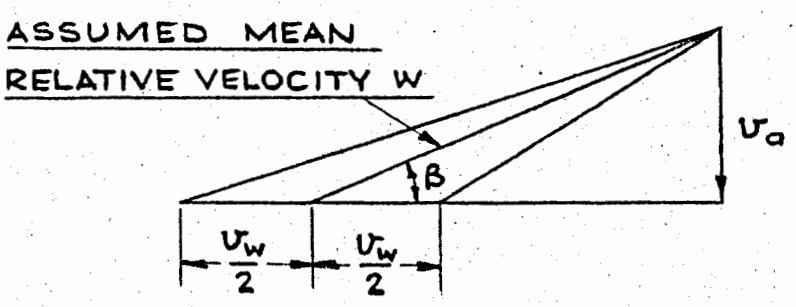

FIG 5.17. VELOCITY TRIANGLES FOR BLADE ELEMENT OF AXIAL-FLOW PUMP.

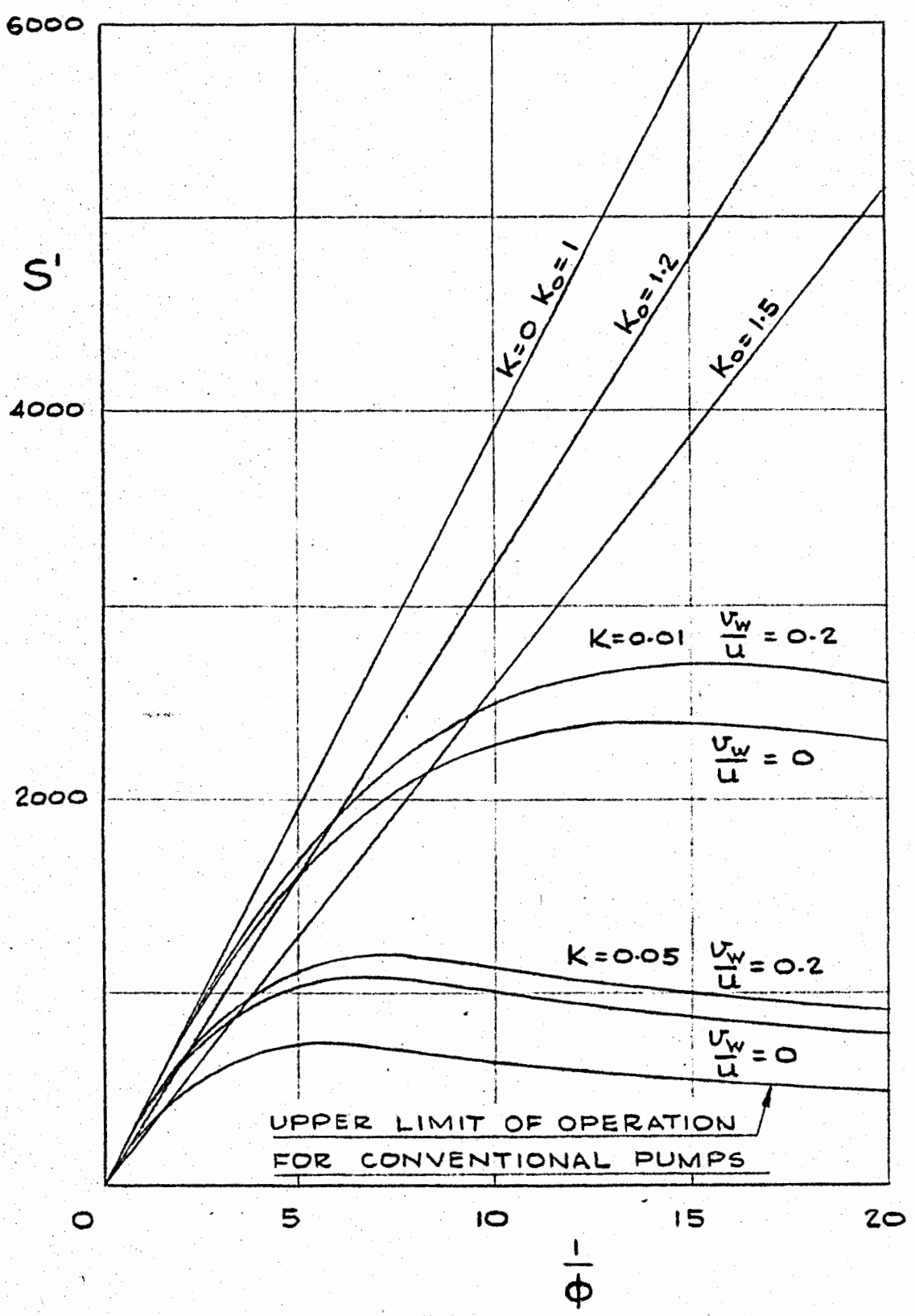

FIG 5.18. S' VERSUS $\frac{1}{\Phi}$.
SUPER-CAVITATING AXIAL-FLOW PUMPS.

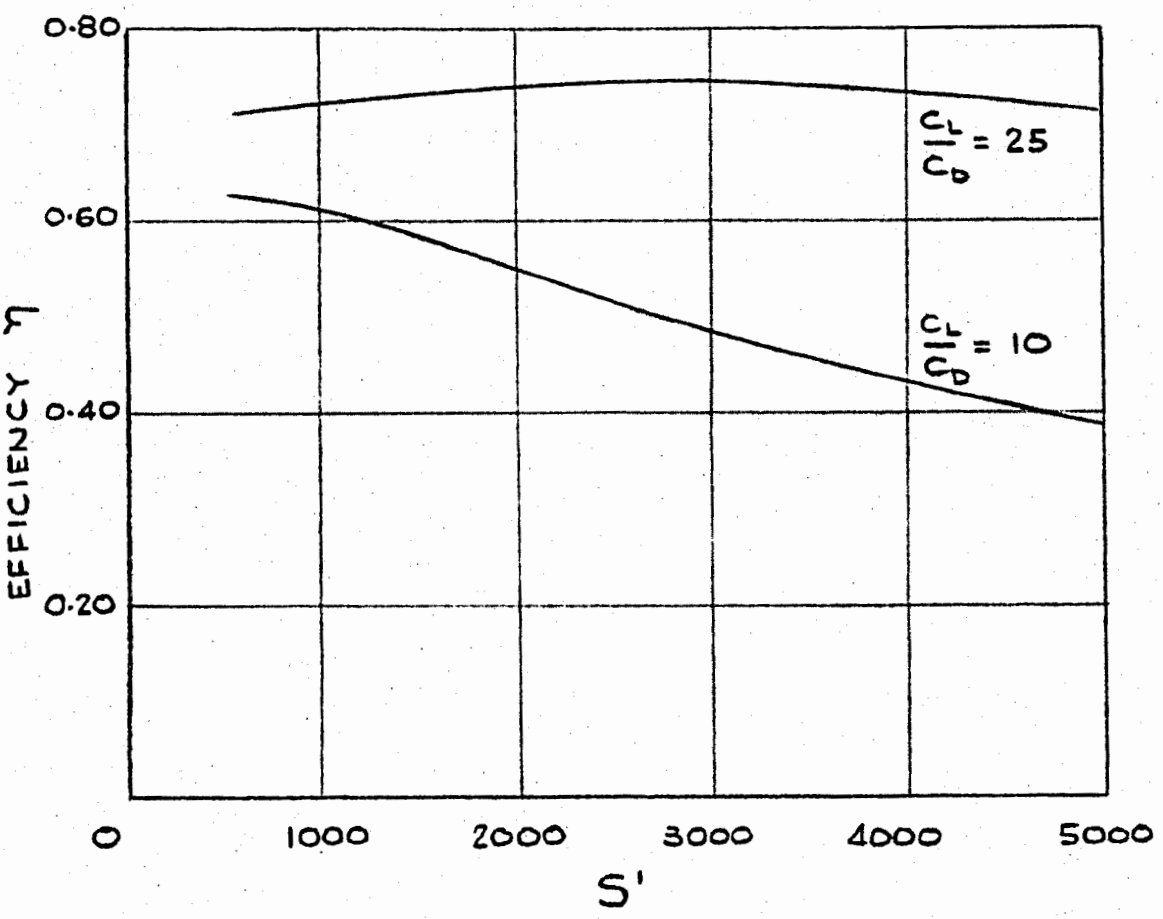

FIG 5.19. η VERSUS S'.
PREDICTED EFFICIENCIES OF SUPER-CAVITATING AXIAL-FLOW PUMPS. AFTER NORBURY (99).

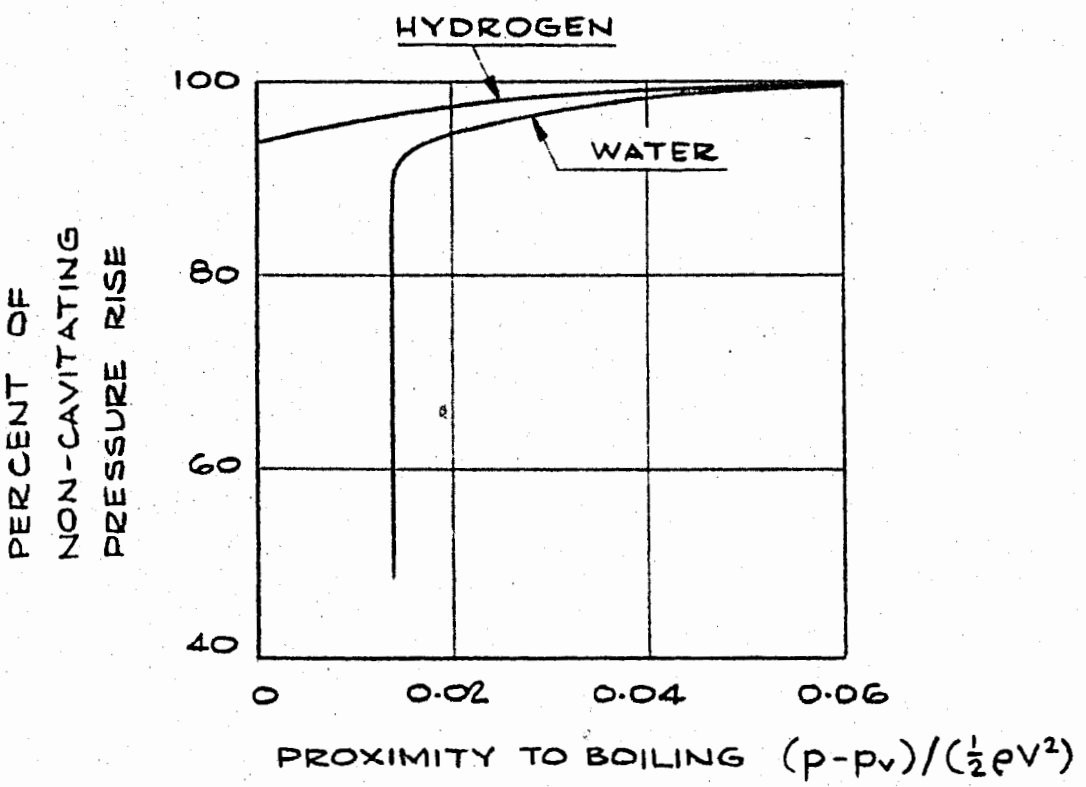

FIG 6.1. EFFECT OF CAVITATION ON PERFORMANCE OF INDUCER PUMP. FROM REFERENCE (107).